QUINONE –BASED ORGANIC REDOX COMPOUNDS FOR ELECTROCHEMICAL ENERGY STORAGE DEVICES

A thesis submitted in fulfilment of the requirements

for the award of the degree of

DOCTOR OF PHILOSOPHY

From

AUTONOMOUS UNIVERSITY OF MADRID

by

SUHEDA ISIKLI, B. Sc., M. Sc.

INSTITUTE OF IMDEA ENERGY, ELECTROCHEMICAL PROCESSES UNIT

September, 2013

CERTIFICATION

I, Suheda Isikli, declare that this thesis, submitted in fulfilment of the requirements for the award of Doctor of Philosophy, in the Department of Organic Chemistry, Faculty of Science, Autonomous University of Madrid, comprises only my original work unless otherwise referenced.

Suheda Isikli

September 2, 2013

Madrid

DEDICATION

To Francisco

ACKNOWLEGMENTS

I would like to thank my supervisor Dr. Raúl Díaz and my Ph.D. tutor Prof. Carmen Carreño for their valuable advice, help, encouragement and support during my doctoral study.

I would like to give my special thanks to all group members in Electrochemical Processes Unit of IMDEA Energy Institute for helping me whenever I need and sharing their knowledge. Our group leader Prof. Marc Anderson is especially acknowledged and for his inspiring and encouraging way to guide us to a deeper understanding of research, and his invaluable comments during this doctoral work. I also want to thank Dr. Jesus Palma and Dr. Rebeca Marcilla and Dr. Chandrasekaran Ramasamy for their priceless help and understanding.

I would like to offer my special thanks to my other Ph.D. colleagues; Susana Vaquero, Teresa González de Chavez and Laura Sanz, for being my family in Spain and best friends that I have ever had in my entire life. I will keep all those unforgettable memories in the depth of my heart.

This work would be very difficult without the technical assistance from people at IMDEA Energy Institute, such as María Eugenia di Falco (BET, Chemicals, Installation and many others), Dr. Fernando Picó(FE-SEM, AFM) and Pablo Matatagui (Informatics). Kind help of PhD colleagues such as Jorn Gruber (Matlab), Tokhir Gafurov (Matlab), Alfonso Carrillo (TGA, Mendeley), Alicia Bayón (TGA and MASS), Julio Núñez (FTIR and origin), Dr. Prabhas Jana (FT-IR and Raman), Cristina Ochoa, Laura Collado, Antonio Berenguer and Dr. Javier Fermoso for using some instruments, techniques and software is also highly appreciated. I also owe my very special thanks to all above mentioned people for their encouragement, care and life-long friendship.

I would like to thank to the research group of Prof. Carmen Carreño in Autonomous University of Madrid for their collaboration in organic synthesis part. My special thanks go to María Ribagorda and Mercedes Lecea from this group.

I want to thank Prof. Patrick Unwin from Warwick University for giving me the opportunity to extend my knowledge on Scanning Electrochemical Microscopy during my internship from June 2012 to September 2012. People from Unwin's group, such as Robert Lazenby and Dr. Aleix Güell are also acknowledged.

Financial support provided by Comunidad de Madrid and European Social Fund to the SOLGEMAC Project through the Programme of Activities between Research Groups (S2009/ENE-1617) is gratefully acknowledged.

Lastly, I owe my loving thanks to my parents, my brother and my sister for their love and care. My special thanks go to my partner, Francisco Puche. Without his support, it would have been impossible to complete this work.

TABLE OF CONTENTS

LIST OF FIGURES and TABLES

RESUMEN

El futuro de la integración de las energías renovables en la producción energética mundial depende en gran medida del desarrollo de dispositivos de almacenamiento de energía adecuados. De entre ellos, los dispositivos electroquímicos son los más prometedores para muchas aplicaciones, pero se requiere desarrollar dispositivos con altas densidades de energía y de potencia lo que, entre otros desafíos, requiere mejorar los actuales materiales activos de electrodo. En este sentido, los carbones son materiales de electrodo particularmente interesantes por sus características, entre las que se encuentran una alta área superficial, una buena conductividad eléctrica, o un coste competitivo.

De entre los posibles dispositivos de almacenamiento electroquímico de energía los supercondensadores son interesantes por características como sus altas densidades de potencia y largas vidas útiles. El almacenamiento de energía en los supercondensadores tiene lugar gracias a la acumulación electrostática de cargas en la doble capa electroquímica, para lo que se suelen usar carbones de alta área superficial como materiales activos de electrodo.

El principal inconveniente para la aplicación comercial de los supercondensadores son sus bajas densidades de energía, por lo que la investigación en este campo explora distintas estrategias para acercar las densidades de energía de estos dispositivos a las de las baterías, y una de estas estrategias es el uso de materiales activos de electrodo pseudocapacitivos, que almacenan energía mediante reacciones redox que tienen lugar en su superficie.

De entre las especies que presentan pseudocapacitancias las quinonas, compuestos orgánicos que presentan transferencias electrónicas múltiples y reversibles, son de las más estudiadas entre otras razones porque algunos carbones las presentan de manera natural en su superficie, por lo que se está tratando de optimizar la presencia de estos compuestos en la superficie de distintos carbones mediante diferentes estrategias, entre las que se encuentran métodos de adición que puedan resultar comercialmente competitivos.

La reducción homogénea de sales de diazonio es la metodología más estudiada para la adición covalente de compuestos quinónicos a la superficie de carbones. Este método siempre presenta procesos de fisisorción paralelos, por lo que uno de los objetivos del presente trabajo doctoral fue el estudio de estos procesos de fisisorción. Para ello se ha usado la impregnación, que es una alternativa más simple y barata que el uso de la química de diazonio. Se ha estudiado la adición de dos diferentes quinonas: para-benzoquinona (p-BQ) y antracentetraona (AT) en dos tipos diferentes y representativos de carbón y se ha llevado a cabo una completa caracterización estructural, físicoquímica y electroquímica para evaluar los cambios y su influencia en el rendimiento de los diferentes obtenidos como materiales activos de electrodo en supercondensadores.

La adsorción de moléculas de AT en un carbón de alta área superficial (Pica) y un carbón negro (Vulcan) da lugar a diferencias en las propiedades electroquímicas y en el rendimiento como electrodos de supercondensadores que se pueden correlacionar con la diferente naturaleza de los carbones usados. Por ejemplo, aunque la adición de AT mejora significativamente la capacitancia tanto del carbono Pica como del Vulcan, la quinona es más estable en el primero, entre otras razones debido a su estructura microporosa y su superficie funcionalizada.

Para estudiar el efecto de la molécula de quinona añadida se impregnó el Pica también con p-BQ. Con esta molécula se puede añadir una mucha mayor cantidad de quinonas sobre el carbón que con AT, y con la cantidad óptima de p-BQ añadida (30 % en peso) sobre la superficie del carbono Pica la capacitancia alcanza valores de 350 Fg^{-1} a 10 mVs^{-1}, mucho mayor que la del carbono no modificado o la del modificado con AT, y además con una menor pérdida de rendimiento a altas velocidades y con una pérdida de rendimiento después de 5000 ciclos de carga/descarga a 1.5 Ag^{-1} de solo el 6.5%, similar a la del carbón sin modificar.

Aunque los métodos de modificación no covalente resultan en importantes incrementos de la densidad de energía, la pérdida en densidad de potencia justifica la exploración de estrategias de adición covalente. Dadas las limitaciones que presenta la química del diazonio, en este trabajo se ha explorado

la adición de quinonas a carbones mediante reacciones de *Friedel-Crafts* como posible metodología alternativa, dadas sus potenciales ventajas.

Las reacciones de Friedel-Crafts son estrategias muy eficientes para la formación de enlaces C-C a través de reacciones de sustitución aromática electrofílica que en nuestro caso tienen lugar entre los anillos aromáticos del carbón y la quinona, como se prueba mediante la caracterización presentada. El resultado más sorprendente del uso de esta estrategia de adición es un crecimiento anómalo del volumen y superficie de microporos respecto al volumen y superficie totales después de la adición, y eso a pesar del decrecimiento del volumen y la superficie total de poro. Además, se observa un decrecimiento homogéneo del tamaño de poro desde un valor inicial de 1.4 nm a un valor de 0.86 nm después de la adición de la quinona.

La caracterización electroquímica muestra un aumento sustancial de la capacitancia específica después de la adición de la quinona que se mantiene incluso después de ciclados largos a altas velocidades. Este importante aumento de la capacitancia gravimétrica no proviene únicamente de las reacciones pseudocapacitivas de la p-BQ añadida sino también de una mayor capacitancia de doble capa, y ello a pesar de una menor superficie específica. Este aumento de la capacitancia de doble capa es probablemente debido al pequeño tamaño promedio de poro (0.86 nm) y su equivalencia con el tamaño de los iones del electrolito (el tamaño de los iones SO_4^{2-} hidratados es de unos 0.76 nm).

En este trabajo también se muestra la potencialidad del uso de compuestos quinónicos como pares redox en baterías de flujo, uno de los principales puntos débiles que impiden la comercialización de estos dispositivos. En este sentido, aunque las quinonas presentan propiedades electroquímicas prometedoras, su baja solubilidad acuosa es su principal obstáculo para su aplicación en estos dispositivos, ya que la concentración del par redox activo determina la densidad de energía alcanzable.

En este trabajo se propone la adición de compuestos polihidroxilados a quinonas como estrategia para aumentar sus solubilidades acuosas preservando sus propiedades electroquímicas. Para la prueba de

concepto se ha usado la juglona (5-hidroxi-1,4-naftoquinona). La adición covalente de un compuesto polihidroxilado a la misma resulta en una solubilidad acuosa mejorada 200 veces que no afecta significativamente a las propiedades electroquímicas de la juglona. Esta estrategia se ha usado para el diseño de *"moléculas modelo"* para la selección de compuestos quinónicos naturales como pares redox activos de baterías de flujo.

Por último también se han realizado estudios con una serie de quinonas que incluye compuestos modelo ampliamente estudiados como la p-BQ y la AQ junto con compuestos enantioméricos y sus mezclas racémicas para la comprensión de los fenómenos cinéticos implicados en la transferencia electrónica que tiene lugar en las reacciones redox de los compuestos quinónicos. Los análisis se han realizado usando microscopía de sonda próxima electroquímica ultramicroelectrodos de oro y fibra de carbón en electrolitos apróticos porque en ellos los radicales productos de la reacción redox son estables y se puede estudiar la transferencia monoelectrónica de las quinonas al anión radical.

Los resultados muestran diferencias en la velocidad de transferencia electrónica entre enantiómeros tanto sobre ultramicroelectrodos de oro como de fibra de carbón que se pueden atrubuir a las distintas orientaciones de los enantiómeros sobre la superficie de los electrodos. También se observa por primera vez un "fouling" de la superficie del electrodo con las quinonas en electrolitos apróticos. El grado de este "fouling" depende tanto del material de electrodo como de la quinona.

SUMMARY

The future of renewable energies for the integration into the world`s energy production is highly dependent on the development of efficient energy storage devices, representing both high energy and high power densities, and carbons are the widely studied electrode materials in many electrochemical energy storage devices due to their unique features such as high surface area, good electrical conductivity and low cost

Supercapacitors (SCs) are electrochemical energy storage devices which became the research focus and commercial interest for diverse applications due to their high power density and long cycling life. Charge storage in supercapacitors occurs through the electrostatic charge separation at the electrode-electrolyte interface, so called "*double layer"* region, typically by using high surface area carbon-based electrodes. However, relatively low energy density compared to batteries is a challenging issue preventing their widespread applications. Therefore, different strategies have been proposed in order to achieve energy density values closer to batteries, and among them, employing pseudocapacitive materials emerged as a powerful concept to overcome this issue.

In general, activated carbon surface has naturally existing redox functionalities which undergo Faradaic-type reactions. Quinone bearing functionalities have been confirmed as effective pseudocapacitive source thanks to their multiple and reversible electron transfer mechanism. Accordingly, further attempts have been done to attach these molecules onto carbon surfaces by simple and cost affordable processes.

Homogeneous reduction of diazonium salts is the most studied methodology for the covalent derivatization of carbon powder with quinone type compounds. During the process of the covalent attachment, there is always a parallel physisorption process, contributing a significant level of active material loading. As impregnation is a cheaper and simpler alternative to the reduction of diazonium

salts, in this thesis work, solution impregnation of para-benzoquinone (p-BQ) and anthracenetetraone (AT) molecules onto the carbon-based electrodes has been studied.

A complete electrochemical, structural, and physicochemical characterization has been carried out, in order to have a clear understanding of physisorption processes on the properties of carbon electrodes and on the performance of SC device.

Adsorption of AT molecules on a high surface area carbon (Pica) and carbon black (Vulcan) electrodes were achieved. Different electrochemical properties of AT was associated with the different nature of the carbon substrate. Besides, the relation between the carbon substrate type and performance of SC device was successfully analysed. AT modification brings about a substantial improvement of the specific capacitance for both Pica and Vulcan modified electrodes. A stable grafting was detected for Pica carbon whereas; Vulcan carbon gives rise to unstable grafting due to its mesoporous structure and non-functionalized surface, both playing a prominent role on carbon-quinone interaction and thereby, on non-covalent functionalization.

Impregnation with p-BQ at an optimum loading ratios (30 wt.%) on the surface of Pica activated carbon electrode resulted in a maximum capacitance of 350 Fg^{-1} at 10 mVs^{-1} which is a significant increase of capacitance compared to unmodified carbon, especially taking into account that the loss of performance at high rates is low. Extended charge/discharge cycling behavior shows a loss of 6.5% of total capacity for p-BQ modified Pica after 5000 cycles at 1.5 Ag^{-1}, which is similar to the one of unmodified carbon electrodes.

Even though non-covalent methods result in an important increment in energy density of SC, low power density at high current loadings brings up the necessity of covalent strategies. Therefore, an organic covalent strategy was tested as an alternative approach for modification of carbon substrate in order to increase energy density without deteriorating power performance of electrochemical SCs.

This was attained through the direct covalent attachment of quinone species to the carbon structure via *Friedel-Crafts* reaction. This highly effective C-C bond-forming occurs through the electrophilic aromatic substitution reaction, taking place between the aromatic rings of Pica carbon and benzoquinone. Several characterization techniques confirmed the successful covalent bond formation between carbon particles and p-BQ units with the presence of the non-oxidized hydroquinone species. The most striking finding regarding this grafting technique is the anomalous increase of the micropore volume and surface ratio to total volume or surface despite an overall decrease in both pore volume and surface. Micro-pore size reduced from 1.4nm to 0.86 nm homogenously after grafting and the unusual increase of the micropore volume and surface are ratio to total volume or surface area was reported. Electrochemical characterization exhibits a substantial increase in the specific capacitance with respect to unmodified electrodes even after 2500 consecutive cycling. This important increment in gravimetric capacitance does not only arise from the pseudocapacitive p-BQ reactions but also an increased electrochemical double layer capacitance upon grafting. This unexpected increase in the double layer capacitance is most probably due to a better matching of newly created carbon pore size (0.86nm) with the size of electrolyte ions (the size of SO_4^{2-} ions: 0.76nm).

The use of quinone-based redox compounds was also demonstrated as electrolyte active units for Redox Flow Batteries (RFBs). Although quinones present promising electrochemical properties, their low solubility builds up an obstacle to the widespread applications in RFB applications since, they require highly soluble electrolyte materials to achieve the relevant energy density values for practical applications.

Studies performed on the water solubility of quinones led us to conclude that the addition of a polyhyroxy compound to the quinones can promise a bright future to boost the aqueous solubility. A novel organic synthesis method developed in this doctoral work is the covalent attachment of polyhydroxy compounds to the quinonoid structures to increase the water solubility significantly.

The target molecule was successfully synthesized through the addition of a polyhydroxy compound, i.e. sugar, to Juglone molecule (5-hydroxy-1,4-naphthoquinone). Juglone molecule was selected as the starting compound due to highly reversible kinetics and very stable redox potential then, a polyhdroxy compound was covalently attached via organic synthesis. This strategy resulted in a compound with 200 times better water solubility comparing to that obtained with juglone compound. Water solubility of functionalized quinones was highly affected by both quinonoid base and the type of polyhydroxylated unit. Other key benefit of this modification route is that the desired electrochemical features of Juglone were outstandingly preserved in the functionalized compound. This strategy was confirmed as a novel approach to design *"model molecules"* for selection of the natural quinone compounds as electrolyte materials in RFB systems.

Lastly, complementary studies were focused on the understanding of the kinetic phenomenon of quinone electron reduction. Demonstrated results give valuable information for ET kinetics of a quinone family (including widely-studied compounds such as p-BQ and AQ combined with the enantiomeric compounds and their racemic mixtures) studied at gold (Au) and carbon fibre (CF) ultramicro-electrodes (UMEs) in an aprotic media since stabilization of the radicalic species takes place and a single-step one ET of quinones to anion radical can be easily studied.

Electrode surface fouling was verified for the first time in an aprotic media for all studied quinonoid compounds. Different degree of surface fouling was reported depending both on the electrode material and the nature of the quinone compound.

Rate constants via steady state cyclic voltammetries (CVs) are calculated at Au electrode and compared with the previously reported literature content. Scanning electrochemical microscopy (SECM) technique was successfully employed for Au UME on flat gold substrate by employing positive feedback method. Higher rate constants with respect to steady-state results were reported by implementation of SECM technique due to higher mass transport rates. Non-steady-state voltammetry was successfully implemented for the rate constant analysis of all compounds at CF

micro-electrode since high degree of electrode fouling was prevented by increasing the scan rates beyond the traditional potential scan rate values.

Chapter 1: Introduction

1.1 General Background

Today`s energy consumption without a doubt depends on the fossil fuels such as oil, coal and natural gas (Fig.1.1a). Even though there has been a significant effort to integrate renewable sources into the energy production, the predictions for the energy consumption/ production for the near future does not really seem to change in a drastic way (Fig.1.1b).

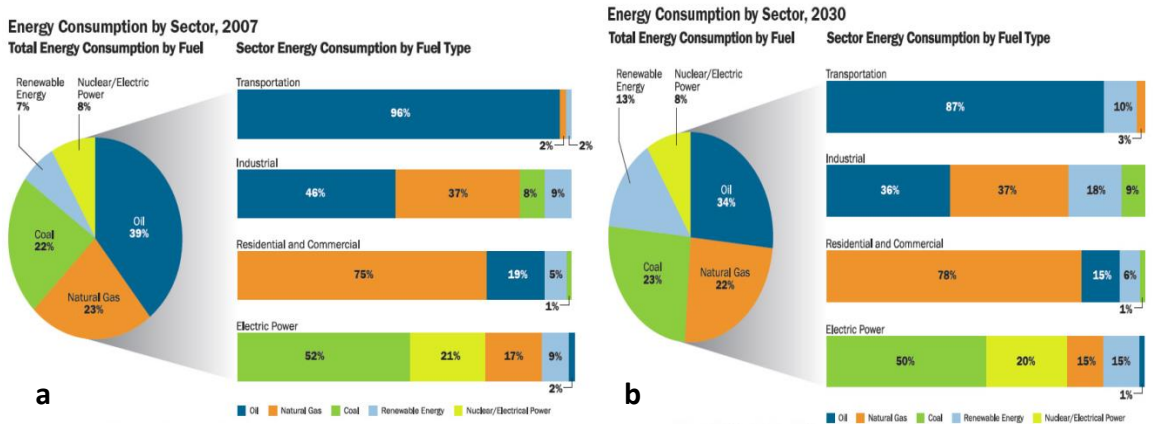

Figure 1.1. Energy consumption by sector in 2007(a) and in 2030(b)[1]

It is known that Renewable Energy Sources have indeed technical issues limiting their application such as intermittency, fluctuation and unpredictability which indeed make them unreliable for the future energy demand. However, new technological developments in "*energy storage*" are promising a bright future for the integration of renewable sources into the world energy consumption.

Especially when our oil dependency for the transportation systems is taken into consideration, electrochemical energy storage technologies turn to a serious challenge to change the present situation. Advances in these technologies will definitely mark the future of electric vehicles (EVs).

Electrochemical energy storage and conversion systems basically include batteries, fuel cells, and electrochemical capacitors or supercapacitors (SCs). Although the energy storage and conversion

mechanisms are different, they present some common features. One of the key similarity is the charge storage process occurs at the phase boundary of the electrode/electrolyte interface. [2]

In batteries and fuel cells, electrical energy is generated by conversion of chemical energy via redox reactions at the anode and cathode that makes the device kinetically limited to the rate of these processes. On the other hand, charge storage in a SC occurs through the physical separation of charged species in the electrode-electrolyte interface. These features determine the device application for a particular purpose. For instance, Li-ion batteries display very high energy density [3] but low power capability which restricts their use in high power applications. On the contrary, SCs deliver the stored energy very quickly, nevertheless they are able to store relatively small amount of energy comparing to batteries. Thus for the applications requiring both high power and energy, i.e. EVs, the combination of both technologies have been proposed. [4] The combination of batteries and SCs enables to achieve high power and energy densities. However, the main limitation is the poor performance of both technologies[5, 6]which is not satisfying the requirements to replace today`s combustion engine technology in EVs.

Another important type of energy storage devices are Redox Flow Batteries (RFBs). A flow battery is best described as a secondary battery that converts the chemical energy in the electro-active materials (generally stored externally in an electrolyte) directly to electrical energy. Current applications of redox flow cells have been widened in several different areas such as energy generation and storage purposes including: generation, transmission and distribution. However, disadvantages of flow batteries such as their more complicated system and relatively higher cost limit their widespread applications.

All type of electrochemical energy storage devices consist of two electrodes in contact with an electrolyte. Here the key aspects to improve the performance of such devices are the novel electrode or electrolyte materials. The electrodes are the places where the electrochemical reactions occur. The electrons flow through the external circuit outside the batteries or the SCs, while the ions carried by electrolyte flow inside the electrode material to allow the electrochemical reactions to

take place. Therefore, properties of both electrodes and electrolyte play a critical role in the electrochemical performance.

The purpose of this doctoral work is to discuss possible ways to improve performance of activated carbon-based SC electrodes by providing different grafting strategies and the development of highly water soluble organic species for redox flow battery (RFB) applications.

1.2 Statement of Problem

1.2.1 Supercapacitors

Electrochemical double layer capacitors (EDLCs), also known as supercapacitors or ultracapacitors, are energy storage devices with very high specific power and long durability upon hundreds of thousands of cycles without significant deterioration. The early commercialization of capacitors for memory back-up in consumer electronics and storage systems for micro solar power generators is expected to be broadened to high power/energy applications, such as hybrid and electric vehicles, power quality systems and smart grids, but higher energy densities are needed to achieve this goal.[7]

The charge storage mechanism of EDLCs consists of electrostatic charge separation at extremely small distances within the electrical double layer at the electrode/electrolyte interface; hence their capacitance is mainly governed by the surface area of the electrodes. Carbons are widely studied electrode materials in these devices due to their high surface area, suitable electric conductivity, and low cost.[8]

The materials for SCs can be classified into two different types: electrochemical double layer and pseudo-capacitive materials. The double layer materials store charge via non-faradaic electrostatic processes based on reversible adsorption/desorption phenomenon of ions in the electrolyte onto the active materials, whereas the pseudo-capacitive materials utilize a reversible faradaic redox reaction on the surface of the electrode materials.[9]

1.2.1.1 Electrochemical double-layer materials

The key aspect for obtaining high capacity is using high surface area and highly conductive electrode materials. Graphitic carbons satisfy all the requirements for this application, including high conductivity, electrochemical stability and open porosity.[10]

Many different carbons have been tested for SC applications. Among them, activated, templated and carbide-derived carbons [11], carbon fabrics, fibres, nanotubes[12], onions [13] and nanohorns [14] have been tested for EDLC applications.

Activated carbons are the most widely used materials today, because of their high surface area, suitable conductivity and moderate cost. However, a major concern with these materials is that the entire surface area is not accessible by an electrolyte. [15] This effect has been attributed to the following facts: (i) microporous structure with pore size smaller than 2nm leads to the low rate of molecular or ionic transport through the pores, and (ii) a hydrophobic character of graphite-like surface provides a low coverage of ions for the formation of a double layer. Therefore electrochemical double layer materials are not satisfying the performance requirements and these drawbacks restrict the applications of carbon as electrode materials in SCs.[16]

1.2.1.2 Pseudo-capacitive materials

Implementation of the redox active materials such as metal oxides [17] and conducting polymers[18] as electrodes materials for SC result in even higher capacitance than activated carbon materials.[19] Pseudocapacitive charge storage occurs through a highly reversible redox processes. This phenomenon is also known as “pseudocapacitance”. As mentioned before, there are two types of well-known pseudo-capacitive materials: The first one are conducting polymers. Among different materials, high pseudocapacitances have been reported mainly for thiophene-based polymers. [20] Cell voltage can be increased while using n- and p-doped polymers at the negative and positive electrode respectively. [18] However, they demonstrate poor cycling stability and relatively low capacitance. The

others are transition metal oxides, which are widely studied due to the fast and reversible redox reactions taking place at the electrode surface.

Among these metal oxides, RuOx shows the best performance. Hydrous ruthenium oxides (RuO_2 $0.5H_2O$) have been intensively studied for pseudocapacitors because of their high theoretical specific capacitance (1358 F g^{-1}) and high electrical conductivity (3×102 Ω^{-1} cm^{-1}).[21] However, the high toxicity, high cost and poor power performance of RuO_2 have limited its industrial application. Researchers are also looking for alternative materials such as V_2O_5, $Co(OH)_2$, MnO_2 [22] or organic redox-carbon composite materials which demonstrate a promising future. [23] The problem is that the real specific capacitance is far from the theoretical specific capacitance. It is evident that the capacitance strongly depends on the morphology and surface area. The performance will be further improved via changing the morphology of metal oxides and the surface area of carbon composite materials.

1.2.2 Redox Flow Batteries

A RFB is an electrochemical system which stores energy in two solutions consisting of different redox couples at different redox potentials.[24]

Among several types of RFB systems, the vanadium flow battery is the most well-known type in which energy can be stored chemically in different ionic forms of vanadium in a dilute sulphuric acid electrolyte. The electrolyte is pumped from separate storage tanks into cells across a proton exchange membrane where one form of electrolyte is electrochemically oxidized and the other is reduced. This process creates a current that is collected by electrodes and flow through an external circuit. The reaction is reversible allowing the battery to be charged and discharged repetitively.[25]

RFBs can have a huge impact on the storage of energy from renewable sources. They can for example be used for the stabilization and smooth output of renewable energy. Performance of such devices depends on the type of the membranes, electrode, and electrolyte materials, but the cost of

vanadium electrolytes and the membranes used are the most critical factors to achieve commercial competiveness.

1.2.2.1 Different electrolyte active materials

The criterion for the selection of the supporting electrolyte is based on electrochemical kinetics of the active species at the electrode−electrolyte interface, the electrolyte solubility, and minimal cross-contamination of the active electrolytes.[26]

In general, vanadium RFB technology has obtained substantial progress recently. However, there still exist some problematic issues including high cost of the raw material and hazardous nature of the electrolyte compounds which should be solved.[27]Therefore, novel approaches are a must for developing a low cost, high-efficiency and environmentally friendly large-scale RFB.

1.3 Importance of Research Field

In this doctoral work, studies were carried out with the aim of developing SCs based on carbon-organic redox composite materials and looking for alternative electrolytes for RFB, especially based on water-soluble organic materials. Quinone type redox species were chosen because of their well-known electrochemistry, high reversibility, fast electrochemical kinetics, abundance and low cost.

For SCs and RFBs, the use of carbon-quinone combination is expected to have several benefits to the performance of the electrodes:

(1) *Important enhancement of specific capacitance*: Both specific capacitance and energy density of the SCs were improved since quinonoid species give and uptake two electrons in the electrode-electrolyte interface contributing to the pseudocapacitance substantially.

(2) *Taking advantage of adsorption process*: Quinones can be adsorbed on the surface of carbon type molecules because of some strong interactions either with carbon skeleton or naturally existing carbon functionality.[28] Adsorption species can also considerably contribute to the increment in the total capacitance acting as a pseudocapacitive source.

(3) *Alternative grafting techniques*: Alternative grafting strategies of carbons with different quinone-type organic compounds were proposed. These new strategies enable to study the influence of the grafting of several compounds on the carbon structure and the performance of SCs constructed by these composite electrodes.

(4) *Power capability and cycle life*: quinone grafting makes an important improvement in specific energy without losing power capability and cycle stability of the SC device.

(5) *Highly soluble organic species for RFB electrolyte*: As mentioned before, one of the important criteria that a redox couple should have in order to be applied as electrolyte active species in RFB systems is high solubility. In this sense, one of the main disadvantages of quinone-type organic compound is their low water solubility. Water solubility of quinone compounds can be enhanced by addition of suitable functionality via organic synthesis methods.

(6) *Kinetic properties and stability of redox species*: It is previously known that the functionality has an important influence on the electrochemical properties of quinone redox species. [29] So the kinetic properties were demonstrated to be highly related with the structure of the molecule, type of functional groups and their attachment side to the molecule.

It is also necessary to investigate the mechanism and understand how fast are the electron transfer kinetics for quinone species. The rate of electron transfer influences the electrochemical performance of both SCs and RFBs. Although basic components (electrolyte, electrode, binder etc.) of the electrochemical storage devices have been the main focus of the electrochemical energy storage field, combination of different materials and organic novel approaches are also important to improve the performance of both SCs and RFB. Therefore, in this doctoral work, it has been of the utmost importance to carry out these investigations for the development of novel, cheap, environmentally friendly and organic alternatives as electrode or electrolyte active materials.

1.4 Objectives of Study

The driving questions behind this doctoral work are how the performance of supercapacitors can be improved when composite carbon-quinone electrodes are used, what alternative strategies can be proposed for quinone grafting/adsorption on carbon and how the aqueous solubility of quinone kind molecules can be increased in order to make them suitable candidates for RFB applications. Once the grafting/adsorption strategy and water-soluble quinone redox couple are identified as the potential candidates for the use as electrode/electrolyte materials for supercapacitors and RFBs, the next step would be the further performance improvement for these different applications. In this present thesis work, this was done by means of designing of the supercapacitor cells for boosting the overall performance (for SC) and redesigning the model quinone molecule in order to increase the water solubility without loss of the good kinetic properties (for RFB).

In general, the objectives of this doctoral work are to determine an effective quinone adsorption route, synthesize different carbon-quinone composite SC electrode materials and synthesize the proper water soluble model compound for RFB applications. All of these concepts were supported with the supplementary work based on the understanding of the kinetic phenomenon of quinone species at different electrode materials. Additionally, strong emphasis was given to characterize the physical, structural and electrochemical changes of the materials upon different strategies for a better comprehension of performance behaviour.

Some of the scope of the research which is presented in this doctoral thesis is briefly outlined as follows:

(1) A thorough literature review of current state-of-the-art SCs and RFBs technologies, especially with emphasis of composite pseudocapacitive materials and possible alternative strategies for the synthesis of such organic materials.

(2) Synthesis of carbon-quinone composite materials via simple adsorption and different organic grafting techniques, including Friedel Crafts reactions (Chapter 4 and 5).

(3) Utilizing instrumental analysis techniques to better understanding of composite formation and modifications of carbon physical and chemical properties. These techniques include thermogravimetric analysis (TGA) coupled mass spectroscopy, Brunauer-Emmett-Teller (BET) specific surface area measurements, Raman spectroscopy, Fourier transform infrared (FT-IR) spectroscopy, Ultraviolet-Visible (UV-VIS) Spectroscopy and Solid State Nuclear Magnetic Resonance Spectroscopy (Solid-NMR) (Chapter 3).

(4) Application and characterization of these composite carbon materials as electrode materials for use in SCs via cyclic voltammetry (CV), galvanostatic charge-discharge cycling, and also electrochemical impedance spectroscopy (EIS).

(5) Construction of different SC cell configurations in order to further enhance the performance of the systems (Chapter 4 and 5).

(6) Investigation of a new type of organic-based electrolyte for RFB applications (Chapter 6). Enhancement of water solubility is the primary scope in order to integrate those compounds into desired aqueous battery system and acquire high energy density values. Herein organic synthesis gives edge to synthesize the most proper compound due to the combination of high water solubility and excellent electrochemical properties (Chapter 6).

(7) Study of the electron transfer kinetics and surface passivation processes of a quinone family at different types of electrode materials by using scanning electrochemical microscopy (SECM) and fast scan cyclic voltammetry techniques (FSCV) (Chapter 7).

(8) Determination of kinetic differences between well-studied quinone compounds and model enantiomers with their racemic forms (Chapter 7).

(9) Finally, summarizing the overall doctoral work and providing some suggestions for further research work related to these composite materials and model redox couple as electrolyte for RFBs (Chapter 8).

References

1. Annual Energy Outlook Tables A1 A2 A17, 2009.
2. M. Winter and R. J. Brodd, *Chemical Reviews*, 2004, **104**, 4245–69.
3. M. Armand and J.-M. Tarascon, *Nature*, 2008, **451**, 652–7.
4. D. Cericola and R. Kötz, *Electrochimica Acta*, 2012, 1–17.
5. Y. Zhu, S. Murali, M. D. Stoller, K. J. Ganesh, W. Cai, P. J. Ferreira, A. Pirkle, R. M. Wallace, K. A. Cychosz, M. Thommes, D. Su, E. A. Stach, and R. S. Ruoff, *Science (New York, N.Y.)*, 2011, **332**, 1537–41.
6. R. J. Brodd, K. R. Bullock, R. a. Leising, R. L. Middaugh, J. R. Miller, and E. Takeuchi, *Journal of The Electrochemical Society*, 2004, **151**, 151.
7. M. Conte, *Fuel Cells*, 2010, **10**, 806–818.
8. V. Khomenko, E. Raymundo-Piñero, and F. Béguin, *Journal of Power Sources*, 2008, **177**, 643–651.
9. P. Simon and Y. Gogotsi, *Nature Materials*, 2008, **7**, 845–54.
10. Y. Gogotsi, *Carbon Nanomaterials*, CRC, 2006.
11. Y. Kyotani, T., Chmiola, J. & Gogotsi, *in Carbon Materials for Electrochemical Energy Storage Systems,eds Beguin, F. & Frackowiak, E., Ch. 13 CRC/Taylor and Francis*.
12. D. N. Futaba, *Nature Materials*, 2006, **5**, 987–994.
13. C. Portet, J. Chmiola, Y. Gogotsi, S. Park, and K. Lian, *Electrochimica Acta*, 2008, 7675–7680.
14. C. M. Yang, Y. J. Kim, M. Endo, H. Kanoh, M. Yudasaka, S. Iijima, and K. Kaneko, *Journal of American Chemical Society*, 2007, **129**, 20–21.
15. K. Kinoshita, *Carbon: Electrochemical and Physicochemical Properties*, John Wiley & Sons, New York, 1998.
16. C.-T. Hsieh, S.-M. Hsu, J.-Y. Lin, and H. Teng, *The Journal of Physical Chemistry C*, 2011, **115**, 12367–12374.

17. T. Brezesinski, J. Wang, S. H. Tolbert, and B. Dunn, *Journal of Sol-Gel Science and Technology*, 2010, **57**, 330–335.

18. M. Mastragostino, C. Arbizzani, and F. Soavi, *Solid State Ionics*, 2002, **148**, 493–498.

19. P. S. Katsuhiko Naol, *The Electrochemical Society Interfce*, 2008, 34.

20. H. Jung, N. Venugopal, B. Scrosati, and Y. Sun, *Journal of Power Sources*, 2013, **221**, 266–271.

21. H. Kim and B. N. Popov, *Journal of Power Sources*, 2002, **104**, 52–61.

22. C. P. C. S. Sarangapani, B. V. Tilak, *Journal of Electrochemical Society*, 1996, 3791.

23. M. Ghanem, I. Kocak, A. Al-Mayouf, M. AlHoshan, and P. N. Bartlett, *Electrochimica Acta*, 2012, **68**, 74–80.

24. M. Skyllas-Kazacos, G. Kazacos, G. Poon, and H. Verseema, *International Journal of Energy Research*, 2010, 182.

25. C. Ding, H. Zhang, X. Li, T. Liu, and F. Xing, *Physical Chemistry Letters*, 2013, 1282–1294.

26. M. Chakrabarti, R. Dryfe, and E. Roberts, *Electrochimica Acta Acta*, 2007, 2189–2195.

27. W. Wang, Q. Luo, B. Li, X. Wei, L. Li, and Z. Yang, *Advanced Functional Materials*, 2012, 1–17.

28. L. Madec, A. Bouvrée, P. Blanchard, C. Cougnon, T. Brousse, B. Lestriez, D. Guyomard, and J. Gaubicher, *Energy & Environmental Science*, 2012, **5**, 5379.

29. C. Frontana, A. Vázquez-Mayagoitia, J. Garza, R. Vargas, and I. González, *The Journal of Physical Chemistry A*, 2006, **110**, 9411–9.

Chapter 2: Literature Review

Development of energy storage devices has become a "*hot topic*" of research due to the increasing demand and growing concerns for energy requirement and global warming.[1]

However, ideal energy storage device and methods are not so far available to satisfy all technical and economical requirements from a growing variety of applications. Electrochemical batteries, supercapacitors (SCs), superconducting magnetic energy storage, pumped hydro, flywheels, compressed air energy storage and hydrogen storage are alternative solutions for energy storage.[2]

Reliable energy storage is very essential for using renewable energy in remote area and its integration into the electric system. Electrochemical energy storage systems offer a promising future regarding renewable energy storage. The key storage technologies can be sorted into two groups: the electrochemical capacitors (ECs) and the rechargeable batteries. Improvement of these devices not only has an impact on renewable energy storage, but also has a direct influence on the portable electronics and transport systems.

The lack of alternative reliable technologies in transport systems is the major cause of greenhouse gas emissions and fossil-fuel consumption. This fact has actually stimulated the growing demand for electric vehicles (EVs) or hybrid electric vehicles (HEVs) technologies which has a great potential to minimize the consumption of fossil fuels and reduce the global warming. For such applications, the electric energy storage system requires high energy density, high power density, long cycle life, and most importantly safety. Nevertheless, the current technologies (rechargeable lithium-ion batteries) do not completely satisfy all the needs required for the replacement of internal combustion engine technology. However, a plausible alternative solution proposed is to design a new type of energy storage device which combines a high energy density battery and a high power SC.[3]

Recently, great efforts have been dedicated to the performance improvement of such devices in order to reach requirements of EVs.

Figure 2.1 shows a comparison of the power and energy capabilities for different electrochemical energy storage technologies and combustion engine .[4] This graph is also known as "*Ragone plot*", which exhibits that batteries and fuel cells are high energy density devices upon comparing to SCs. SCs can be operated at high charge/discharge rates and thus, they are more suitable for high power applications. Combination of these two technologies can serve as a promising approach to reach the profile of combustion engine.

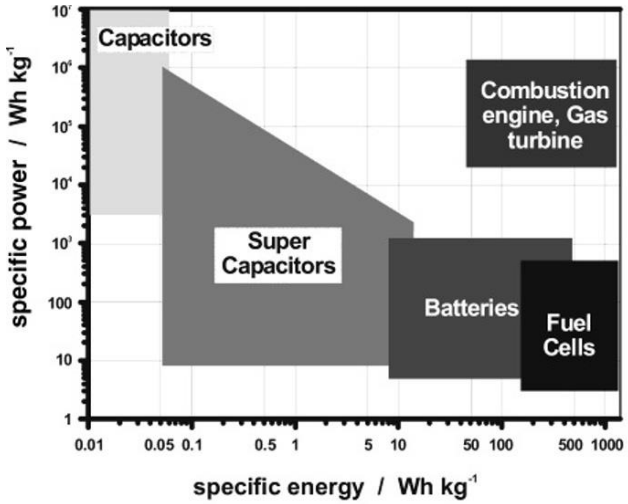

Figure 2.1 A basic Ragone plot of the energy storage domains for the various electrochemical energy conversion systems compared to an internal combustion engine and turbines and conventional capacitors.[4]

In this doctoral work, a detailed study of carbon-quinone composite electrodes for SC and alternative organic electrolytes for RFBs will be presented.

2.1 Supercapacitors

Electrochemical double layer capacitors (EDLCs), also called ultracapacitors or supercapacitors are electrochemical energy storage devices with very high specific power and long durability upon many cycles. [5,6] Unlike batteries, they are capable of undergo hundreds of thousands of cycles at high

discharge rates without significant loss in performance. They can reach capacitances several orders of magnitude higher than conventional capacitors. However, they are not as good as batteries in terms of energy density. In Ragone plot, they fill the gap between conventional capacitors and batteries (Fig 1).

The most important advantages of SC which make them attractive electrochemical storage technologies are high power density due to extremely fast adsorption/desorption processes during charge/discharge, superior stability upon cycling, low self-discharge, safety and relatively low cost. Nonetheless, low energy storage capability limits their widespread application.

2.1.1 History and Development of Supercapacitors

The concept of the SC technology is based on the work of Hermann von Helmholtz [7], who first in 1853 discovered that electrical charge separation could be occurred not only on the surface of a conductor but also at the 'double-layer' interface between an electrode and an electrolyte.

Subsequently, the first electrical device using the double-layer charge storage phenomenon was patented by H.I. Becker (General Electric in 1957).[8] This work was based on the charge storage in the electrode-electrolyte interface by applying a direct current to the porous carbon electrodes in an aqueous electrolyte. At the time of the discovery in General Electrics, in 1957, it was believed that the energy was stored in the carbon pores and it displayed "extraordinarily high capacitance", though the real mechanism was unknown at that time. General Electric did not immediately follow up on this work, and the modern version of the devices were eventually developed by researchers at Standard Oil of Ohio in 1966 (SOHIO), after they accidentally re-discovered the effect while working on experimental fuel cell design. Their cell design was composed of two layers of activated charcoal separated by a thin porous insulator, and this basic mechanical design remained as the basis of most electric double-layer capacitors.

SOHIO also failed to commercialize their invention, licensing the technology to Nippon Electric Company (NEC), who finally marketed the results as “supercapacitors” in 1978, to provide backup power for maintaining computer memory. The term supercapacitor was also given by NEC in 1978.

In figure 2.2, development of SC was demonstrated from conventional electrostatic capacitors to EDLCs. Basic capacitors are known as electrostatic in which charge creation occurs around the dielectric media. This type is not used for energy storage but it is used in electrical and electronics; for filter, tuner and LCR circuit devices due to their low capacitance which in the range of few pico-farad (pF) to few microfarad (µF). In electrolytic capacitors, the metal on which the aluminum oxide (Al_2O_3) film is formed serves as the anode or positive terminal, the oxide film acts as the dielectric, and a conducting liquid or gel acts as the cathode or negative terminal. Capacitances range from about 0.001 µF to 1 F for this type of capacitors. Finally, EDLC or SCs can store energy through reversible ion adsorption onto active materials that have high specific surface area.[9] These systems play an important role in electrical energy storage due to high charge storage capacity which is several hundred of magnitudes more than the electrolytic capacitor.

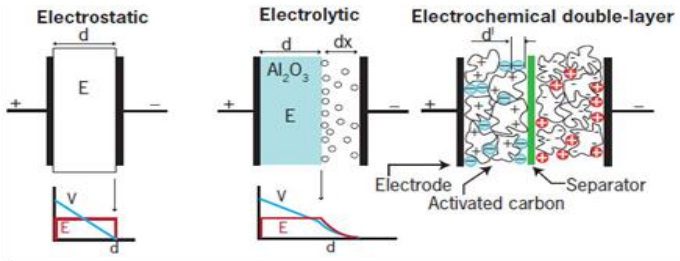

Figure 2.2 Development of capacitors; from conventional to EDLC.[10]

2.1.2 Classification of Supercapacitors

All the existing commercial and developing SC technologies can be summarized into three different categories which are (i) symmetric SC, (ii) asymmetric SC and (iii) hybrid SC. These categorization depends on the cell design, electrode materials and operating principles.[2]

Figure 2.3 illustrates these three main groups along with their sub-categories. In the following parts, SC types which are closely related to the focus of this doctoral work will be explained in detail.

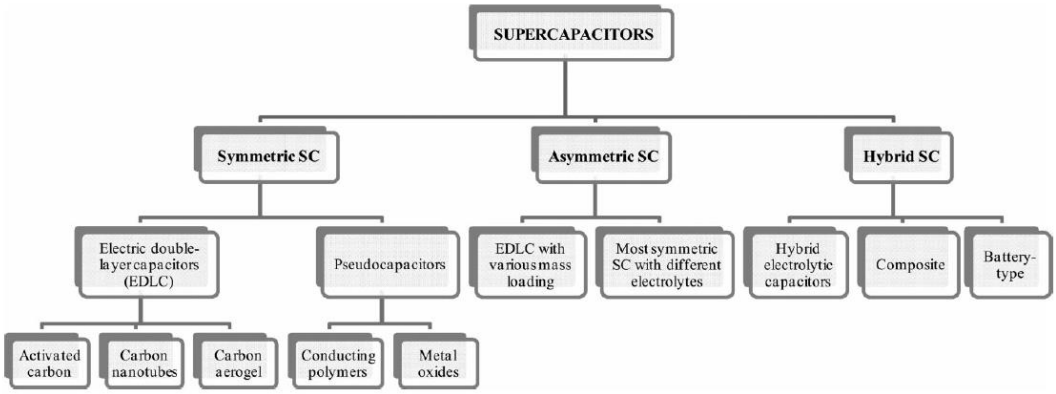

Figure 2.3 A general classification of supercapacitors [2].

2.1.2.1 Symmetric supercapacitors

Symmetric SCs are best described as the devices constructed by the same electrode material at practically equal mass loadings with the same design. For being categorized as symmetric cells, the principle charge storage mechanism should be the same at both sides of the SC cell. This concept can be divided into two categories: electrochemical double layer capacitance and pseudocapacitance.

Electrochemical Double Layer Capacitance:

In EDLC, the fundamental charge storage mechanism is based on the fast adsorption-desorption of the ions from the electrolyte towards the electrodes. EDLCs are able to store more energy than conventional capacitors due to a larger interfacial area between electrode and electrolyte.

Helmholtz explained that the adsorption of oppositely charged ions takes place from solution towards the electrode surface with an excess or deficiency of charge, [7]accordingly he first defined the term “double layer”.[11] The solution side of the double layer is thought to be composed up of several "layers." The inner layer contains solvent molecules and sometimes other species which are thought to be specifically adsorbed (Fig. 2.4). This inner layer is also called the compact, Helmholtz, or Stern layer. The distance (x_1) between the electrical centers of the specifically adsorbed ions is called the inner Helmholtz plane (IHP)

Solvated ions can approach to the surface of metal at a distance x_2; this layer is called the outer Helmholtz plane (OHP). This model assumes that the interaction of the solvated ions with the charged metal occurs by only long-range electrostatic forces, thus, the interaction between charged ions are only electrostatic and independent of the chemical properties of the ions. The three dimensional region extending from OHP into the bulk of the solution is called the diffuse layer. Because of thermal fluctuation in the solution, an ionic-charge density due to the non-specifically adsorbed ions can be created in the bulk of the solution.[12]

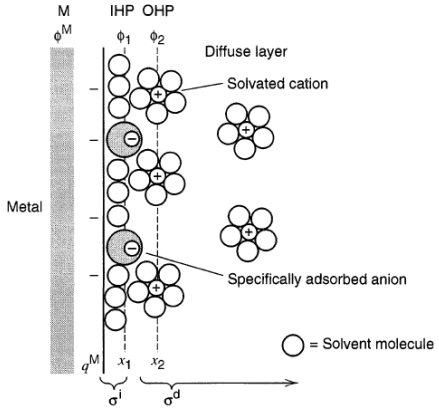

Figure 2.3. Proposed model of the double-layer region[13]

Helmholtz double layer capacitance (C_H) can be calculated just like the capacitance of the parallel-plate capacitor by equation 2.1: [14]

$$C_H = \frac{\varepsilon_0 \varepsilon_r A}{d} \qquad \textbf{(2.1)}$$

where ε_r is the electrolyte dielectric constant, ε_0 is the permittivity of vacuum, A is the ion-accessible specific surface area of the electrode and d is the effective thickness of the double layer.

During the charging process, the electrolyte at the boundary of the electrode is reorganized to counterbalance the electrostatic charge on the electrode surface and this charge separation in the double layer region occurs within extremely small time interval ($\approx 10^{-8}$ s) [15]

Unlike proper metals, carbon materials are considered as semiconductors due to their low density of charge carriers. The density of charge carriers is the highest in the vicinity of the electrode and follows a descending pattern towards the bulk of the solution away from the electrode surface. This region is also known as space charge region and was demonstrated in figure 2.5.

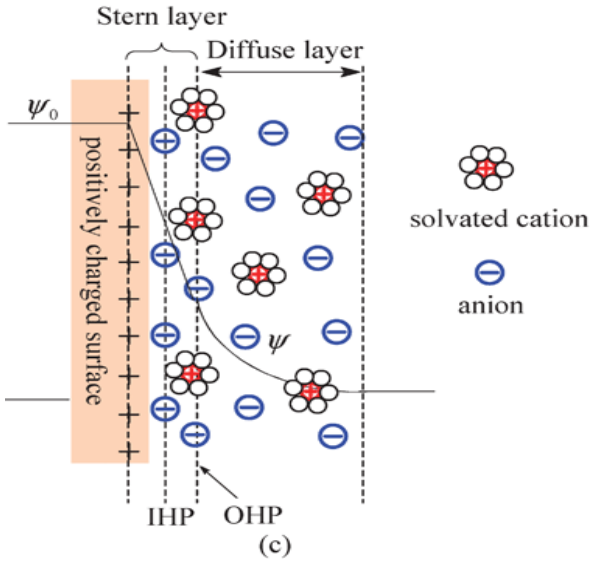

Figure 2.4 A demonstration of double-layer with formation of the space- charge region, Helmholtz layer and diffuse layer.[16]

Upon an applied electric field, a Helmholtz layer forms at the close proximity to the electrode and for counterbalancing the charge in the compact layer, a diffuse layer forms. Due to the formation of the double layer on the electrode surface, a space charge capacitance takes place. The overall capacitance of the electrode can be expressed in equation 2.2.

$$\frac{1}{C_{dl}} = \frac{1}{C_c} + \frac{1}{C_H} + \frac{1}{C_{diff}} \qquad \textbf{(2.2)}$$

where C_{dl} is the overall double layer capacitance of the electrode, C_c is the space charge capacitance and C_H and C_{diff} are the capacitances which comes from the Helmholtz layer and the diffuse layer respectively.[17, 18]

Typically double later capacitance of metals and carbons is in the range of 10-50 μF cm^{-2} in aqueous electrolytes and less in non-aqueous solvents.[19] So, high specific capacitance values can be obtained by application of high surface area carbon electrodes (≈150Fg^{-1}).

Pseudocapacitance:

In pseudo-capacitors energy storage is governed by the fast and reversible faradaic type reactions occurring on the electrode-electrolyte interface.[20] Here, some examples of pseudocapacitive processes are presented.

(i) two-dimensional depositions of adatom arrays on electrode surfaces, e.g. H or Cu on Pt, Pb on Au, Bi on Au, Bi on Ag, H on Rh or Pt.

(ii) redox processes in liquid or solid solutions.

(iii) chemisorption of anions at electrode interface.[19]

As discussed earlier, pseudocapacitive and double layer non-faradaic charging generally overlap[21] so, precise numerical calculation of these different charging becomes complicated.

The pseudo-capacitance charging can be expressed by the equation 2.3:

$$C_p = \frac{Q_{tot}}{V_{tot}} \qquad \textbf{(2.3)}$$

where Q_{tot} and V_{tot} expresses the total charge and the working potential of the electrode respectively.

2.1.2.2 Asymmetric Supercapacitors:

Asymmetric configuration refers to the SCs constructed by two different electrode materials or the same electrode material with different mass loadings. This configuration has been employed in many studies to increase the working potential of SCs working with aqueous electrolytes.[22,23]

Additionally, asymmetric configuration was confirmed as a performance boosting approach for the SCs made by using only activated at different mass loadings. [24]

2.1.2.3 Hybrid Supercapacitors:

Hybrid systems combine capacitor-like (high power) and battery-like (high energy) electrodes in the same cell, offering the advantages of both technologies. A proper hybrid configuration can increase the cell voltage, energy and power density at the same time. Some of the important configurations classified as hybrid systems are pseudo-capacitive metal oxides with a capacitive carbon electrode and lithium-insertion electrodes with a capacitive carbon electrode.[1] The latter also known as lithium ion capacitors (LIC). LIC technology combines activated carbon (from EDCL) and lithium intercalation material (from lithium ion battery) as a positive and a negative electrode respectively. These devices are capable of storing approximately 5–10 times more energy than conventional EDLCs and also have advantages such as high power and long cycle-life.[25,26]

2.1.3 Basic parameters for performance evaluation

Specific Capacitance:

Specific capacitance (C_s in Fg^{-1}) can be calculated from different techniques such as cyclic voltammetry, charge discharge curves and electrochemical impedance spectroscopy (EIS).

From CV experiments, it can be expressed by applying equation 2.4;

$$C_s = \frac{I}{m*v} \qquad \textbf{(2.4)}$$

where I (A) is the current applied to the system, m (g) is the active electrode material weight, and v ($\Delta V/\Delta t$) is the scan rate in V s^{-1}. The specific capacitance calculated by CV curves is the capacitance value expressed for a single electrode.

From CD curves, specific capacitance can be calculated from equation 2.5;

$$C_s = \frac{I}{dV/dt*m_{tot}} \qquad \textbf{(2.5)}$$

where I (A) is the current applied, m_{tot} (g) is the total weight of the both electrodes and dV/dt(V/s) is the slope of the discharge curve. However, this formula gives the capacitance value for the whole system (by 2-electrode CD technique) which can be converted to a single electrode specific capacitance multiplying by four approximately (C_s 3E = C_s 2E*4).

From EIS technique;

$$C_s = 1/\omega Z'' m \qquad \textbf{(2.6)}$$

Where ω (2πf, Hz) is the angular frequency and Z'' is the complex component of impedance at low frequency (Ω) and m is the active electrode material mass (g).

Energy density or specific energy (ED, $Whkg^{-1}$) can be determined by;

$$ED = \int_0^t IV(t)dt/m_{tot} \qquad \textbf{(2.7)}$$

where V and I is the voltage and current responses in the constant current charging-discharging or cyclic voltammetry tests, respectively; and m_{tot} is the total mass of the two electrodes.

Lastly, power density can be determined from the following equation;

$$PD = IV(t)/m_{tot} \qquad \textbf{(2.8)}$$

2.1.4 Electrode Materials

Typically, electrode materials used for SCs can be classified into three main groups, (i) double layer materials, (ii) redox pseudo- capacitive materials and (iii) composite materials.

2.1.4.1 Double layer materials

Carbon materials in different forms such as activated carbons, carbon nanotubes, carbon fibres and carbon aerogels, are intensively studied for electrode materials for SCs due to their high specific surface area, high conductivity, high thermal stability, good corrosion resistance, high porosity, easy processability and good compatibility in composite materials and relatively low cost.[27]

Activated Carbons:

Activated carbons (ACs) can be described as an amorphous solid with a large internal surface area and pore volume. Cokes, chars and activated carbon are frequently termed as amorphous carbons. The main characteristic in common for all types of activated carbons is the twisted graphite-like planes, cross-linked by aliphatic bridging groups (Fig.2.6) and the high porosity created as a result of the spacing between these planes.[28]

Figure 2.5 A scheme demonstrating the cross-linked structure of activated carbons.[29]

Commercial activated carbon products are produced from organic materials that are rich in carbon and poor in inorganic impurities such as coal, lignite, wood, nut shells, peat, pitches, and cokes.[28] In addition to that, various agricultural waste and by products have been successfully converted to AC such as macadamia nutshell[30] and peach stones[31]

Among many attractive features, ACs has become the most popular electrode materials used for EDLCs due to their large surface area (1000 ~ 3000 m^2g^{-1}), relatively good electrical properties, and moderate cost. [32,33,34,35]

Most of the commercial activated carbons are produced by steam activation (physical activation). In this process, the carbonized product is reacted with steam over 900^oC. The chemical activation method involves the use of chemical activating agents such as phosphoric acid, zinc chloride and salts of sodium and magnesium.[30]

The production and activation methods highly influence the porous structure of carbon. Because of that, most activated carbons contain pores of different sizes; micropores, mesopores and macropores. According to the IUPAC classification, pores smaller than 2nm are micropores, mesopore size are defined as 2 – 50 nm and pores larger than 50nm are categorized as macropores (> 50 nm). There is a strong relation between the porous structure and the performance of the SC electrodes.[36] Smaller micropores cannot support the diffusion of electrolyte ions into them, hence preventing the contribution of some pores for charge storage.[37] Higher capacitance values were reported for ACs in aqueous than in organic media because of the smaller ion size of aqueous electrolytes. It has previously been reported that a pore size below 0.4 nm does not contribute to double layer capacitance since pores smaller than 0.4nm are not accessible to ions in aqueous electrolyte [38]. Later on, Beguin et al. confirmed that the capacitance reaches a maximum value when the pore size is close to 0.7 nm in aqueous and 0.8 nm in organic media.[39] A further important contribution by Simon and Gogotsi reveals that the capacitance can potentially be improved by matching the pore size of the electrode material to ion size of the electrolyte. This concept maximizes the electrode surface area accessible to electrolyte ions.[40,41]

Surface Functionality of Activated Carbons;

Control of the surface chemistry of carbon materials allows modifying carbon properties and opens ways for many different applications. Several different strategies were reported for surface modifications of carbons up to date. It is possible to introduce oxygen and nitrogen containing functional groups by acid (or ozone) and ammonia treatment respectively. However heat treatment can remove some hydrophilic surface functionality.[42] Upon oxidative treatments, some of the oxygen containing functional groups can be produced on the surface of the carbon such as: quinones, phenols, ethers, lactones, and carboxylic acids (Fig. 2.7).

It is well known that the performance of SCs is influenced by the nature of surface functionality of carbon. It is demonstrated that the presence of oxygenated redox active groups, i.e. quinones, on

the surface of the activated carbon might increase the specific capacity by pseudocapacitive processes and the wettability of the material by adding hydrophilic character.[43]

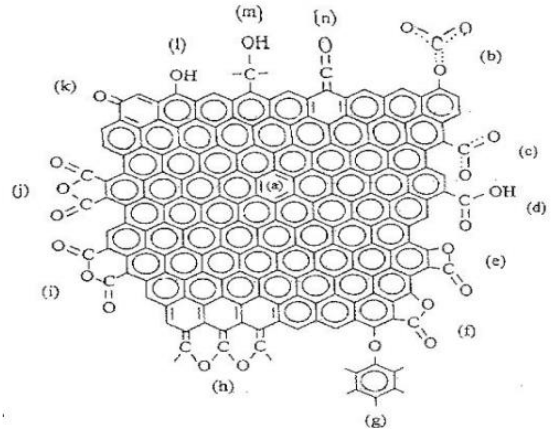

Figure 2.6 A demonstration of surface functionality on a graphitic layer of activated carbon.[44]

2.1.4.2 Pseudocapacitive materials

The most studied pseudocapacitive materials are transition metal oxides and conducting polymers for SCs due to fast and reversible redox processes. Specific capacitance of these materials is significantly larger than that of the double layer materials.

Metal Oxides:

Among several pseudocapacitive materials, metal oxides have been extensively investigated as electrode materials for SCs due to their high conductivity. Metal oxides such as RuO_2[45], Fe_3O_4 [46], NiO [47], Co_3O_4 [48], V_2O_5 [49] and MnO_2 [50] have attracted great attention for supercapacitor electrode materials. The majority of research efforts were focused on ruthenium oxide, especially for hydrous ruthenium oxide ($RuO_2.xH_2O$), specific capacitance values as high as 700 F g^{-1} has been reported [45]. This huge specific capacitance of hydrous ruthenium oxide comes from the insertion and removal, or intercalation, of protons into its amorphous structure. Moreover, the ESR of hydrous ruthenium oxide is lower than that of the other electrode materials. Ruthenium oxide pseudocapacitors have the potential to achieve higher energy and power densities than EDLCs and conducting polymer pseudocapacitors. However, despite several advantages, relatively high cost limits its large scale applications.[51]

Therefore, recent research attempts are focused on exploring cheaper and non-polluting similar electrode materials instead of ruthenium oxide and fabricating alternative composite materials such as crystalline or amorphous MnO_2[52] to reduce the cost without reducing the performance.

Conducting Polymers;

Likewise other pseudocapacitive materials, conducting polymers (CPs) undergo fast redox reactions to promote the capacitive response and they display superior specific energies to double layer type materials**.** The increasing interest in CPs as electrode materials is stimulated by the demand of active materials with high specific capacitance, power performance and low cost. The most important advantageous properties of such materials are : (i) high specific capacitance, due to involvement of the whole polymer mass in the charging process; (ii) high conductivity in the doped state; and (iii) fast charge/discharge electron-transfer kinetics.[53] However, cycle life stability is a major drawback for an industrial application of CPs. Doping of polymers requires the insertion/desertion of counter ions, which cause a volume change during charge-discharge and thereby, swelling and shrinkage processes result in degradation of the electrode during consecutive cycling. Consequently, cycle life is much poorer compared with carbon-based supercapacitors which generally use solely adsorption and desorption of ions.[54]

The polymers that are commonly studied in supercapacitor research are polypyrrole, polyaniline, and derivatives of polythiophene due to their excellent capacity for energy storage, easy synthesis, higher conductivity and lower cost than many other CPs. [55]

Composite Materials:

The main idea when developing hybrid or composite materials is to take advantage of the different desired properties of each component. This concept also allows to compensate the limitations of each component by combining them in a single material with new properties, such as integration of carbon-based materials with either conducting polymer or metal oxide materials.[56] Carbon-based

materials contribute a significant double-layer capacitance by providing a high-surface-area, whereas pseudocapacitive materials are able to further increase the capacitance of the composite electrode through Faradaic reactions**.** This type of combination allows eliminating cycle life limitations of CPs and generating new composites with better specific capacity and cycling stability.

Previous study of Beguin on composite electrodes confirmed that supercapacitors with better performance than either carbon nanotubes or CPs could be achieved by composite materials fabricated from carbon nanotubes and conducting polymers such as polyaniline and polypyrrole.[54]

2.1.5 Quinones as pseudocapacitive source

2.1.5.1 Biological Importance of Quinones

Quinone-hydroquinone couples have been studied over many decades as the prototypical examples of organic redox systems[57]

In this sense, their electrochemical behaviour, including coupled electron and proton transfer reactions, explains how those basic processes are affected by molecular structure and environment.[58] These studies are particularly important in view of the key biological functions of quinone-based couples, since they participate as electron-proton transfer agents in oxidative phosphorylation or photosynthesis.[59] Quinone redox systems play an important role as electron and proton carriers in the photosynthetic electron transport system of photosynthetic bacteria, algae, and higher plants, as well as in mitochondria. Besides mediating electron transfer, many more roles have recently been discovered for quinones in biologic systems. They have been found to protect against lipid peroxidation in the membrane, regenerate vitamin E, prevent DNA damage, control low-density lipoprotein peroxidation and regulate the permeability of transition pores in mitochondria and physicochemical properties of the membrane itself.[60] There is also an increasing use of quinones for treatment of diseases, including myopathies, cardiovascular diseases and age-related degenerative diseases.

The most widely studied class of quinones in the field of biology is ubiquinone, or coenzyme Q, which has a long isoprenoid chain with a benzoquinone ring. Other naturally occurring well-known quinones are menaquinone, plastoquinone and a number of quinone derivatives such as plumbagin, phylloquinone and juglone. An important property of natural quinones is their hydrophobicity which restricts them to within the lipid bilayer of the cell membrane, but also enables them to diffuse freely within it.[61]

2.1.5.2 Quinones as pseudocapacitive materials

In the last years some studies have reported on the incorporation of redox-active molecules into either the electrode [62] or the electrolyte [63] as an alternative route to improve the performance of carbon-based supercapacitors.

Quinone species attached to the surface of carbon electrodes in aqueous electrolytes contribute to the overall cell capacity via highly reversible 2-electron transfer process. This concept is based on the utilization of quinone pseudocapacitance coupled to EDLC of activated carbon in order to boost the performance of the system (Fig. 2.8).

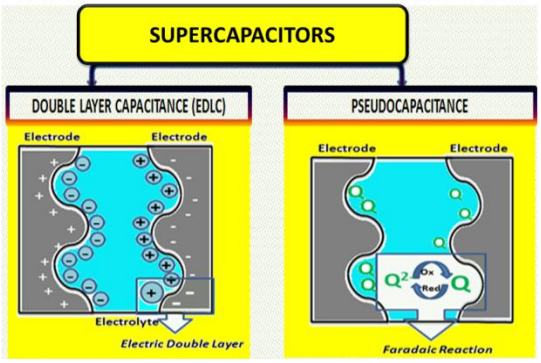

Figure 2.7 A schematic representation of the combination of EDLC and quinone pseudocapacitance.

In a recent work of Roldan et al. quinone-based redox electrolyte was confirmed to be highly effective to enhance energy densities of SCs.[64] They studied the incorporation of the quinone/hydroquinone couple into the acidic electrolyte and the pseudocapacitive nature of this redox electrolyte resulted in a very significant increase in the capacitance of SCs made of different

carbon materials. The cell capacitance was demonstrated reaching to outstanding values as high as 220 F $g^{-1}$and therefore; a very high energy density of 30.6 $Whkg^{-1}$ was reported for a supercapacitor built by an activated carbon as electrode active material.

2.1.6 Different grafting strategies

Recent advances in the development of reliable methods for the chemical and electrochemical functionalization of conductive carbon substrates brings about an additional impulse towards extending the scope of their applications. In particular, covalent modification schemes allow useful alteration of physical and electrochemical properties of carbon, making them suitable for a specific application.

2.1.6.1 Electrochemical grafting

In general, electrografting process can be described as the electrochemical reaction that permits organic layers to be attached to solid conducting substrates. These strategies are promising as they provide a solid covalent bond between the surface and the organic layer. Electrografting can be implemented to a variety of substrates including carbon, metals and their oxides, as well as polymers. [65] Strategies for electrochemical grafting can be considered into two main groups; (i) direct electrochemical oxidation and (ii) formation of covalently bonded species. The direct electrochemical oxidation of the carbon surfaces is achieved by applying an oxidizing potential sufficiently high to produce oxygenated functional groups on carbon. [66] On the other hand, several different covalent modification methods have been developed and herein, important ones will be explained in a more detailed way.

Oxidation in the presence of alcohols:

When a high positive potential is applied to a glassy carbon electrode in an anhydrous solution of primary aliphatic alcohols such as octanol and ethanol, a layer of alkyl group can be covalently attached through an ether linkage. Ohmori and co-workers proposed a reaction mechanism in which

oxidation of the carbon surface produces an aromatic radical which undergoes a nucleophilic attract by the alcohols (Fig.2.9).[67]

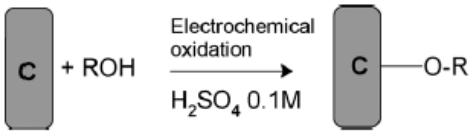

Figure 2.8 Electrochemical grafting of alcohols onto carbon surface[65]

Electro-oxidation of amines:

Primary and secondary amines can be coupled to glassy carbon and carbon fiber surfaces via oxidation of amine in anhydrous ethanol or acetonitrile solution. Barbier, Prinson and coworkers discovered a monolayer coverage of surface with attached groups of aminomethyl-9-antracene and p-aminomethyl-nitrobenzene.[68] Steric effect inhibits the access of highly substituted amines to active sites of the electrode surface and so, there is no evidence of the covalent attachment of tertiary amines to the glassy carbon surface. Also poor surface coverage of secondary amines was previously verified.

Electro-oxidation of carboxylates:

Electrochemical oxidation of carboxylates is also known as Kolbe reaction which proposed in 1848 by Adolph Wilhelm Hermann Kolbe**.** The Kolbe reaction is formally a decarboxylative dimerization and proceeds by a radical reaction mechanism.

Saveant's group demonstrated the oxidation of arylacetates in acetonitrile as a method for modifying glassy carbon (GC) and the basal plane of highly ordered pyrolytic graphite (HOPG). They studied a series of carboxylates in order to attach a monolayer of arylmethyl groups. The extent of surface modification was controlled by cyclic voltammetry as a function of cycle number. They also confirmed the electrical contact between grafted groups and electrode surface by means of electron hopping. In their work, the mechanism of electrode coupling is described based on Kolbe reaction.

Oxidation of carboxylate results in elimination of carbon dioxide yielding an arylmethyl radical. Later, the radical can be oxidized to the corresponding carbocation which reacts with the carbon surfaces to form C-C bond.[69]

Figure 2.10 summarizes the formation of radical based on Kolbe reaction.

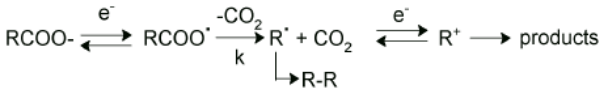

Figure 2.9 A schematic representation of Kolbe reaction.[65]

Electro-oxidation of hydrazides:

Hydrazides are another class of compounds which can be covalently attached to the carbon surfaces. Kuhr's group demonstrated a covalent attachment of biotin hydrizide in phosphate buffer at pH 8.5. Both oxidation and reduction cause surface modification. Although the surface attachment is not characterized, the influence of surface modification was observed from the cyclic voltammetries of NADH. They proposed a covalent bond formation between hydrizide and surface carbon.[70]

Electro-reduction of diazonium salts:

One electron reduction of aryl diazonium salts at carbon electrodes leads to grafting of aryl groups to the surface (Fig. 2.12). Acetonitrile was used mostly as a modification medium. However modification was also demonstrated in acidic aqueous electrolytes. Reduction of diazonium salt was achieved on carbon fibres, carbon powders, graphite electrodes and glassy carbon electrodes. Grafting of different aryl derivatives on the surface of carbon electrodes was first reported by Pinson et al .The aryl groups attached to carbon electrodes and presented in the literature were listed in the figure 2.11.

R-group	*R-group*
4-Nitrophenyl	4-Phenylacetate
4-Carboxyphenyl	4-Cyanophenyl
4-Bromophenyl	4-Benzoylphenyl
4-Nitronaphthalene	4-Acetamidolphenyl
2-Methyl-3-chlorophenyl	4-Diethylaminophenyl
2′, 3-Dimethylazobenzen-4′-yl	Phenyl
1-Naphthyl	9,10-Anthraquinon-1-yl
4-Nitroazobenzen-4′-yl	Azobenzen-4′-yl
3,3′-Dimethoxy-biphenylene-4,4′ bisdiazonium [b]	1,4-Benzenebisdiazonium [b]
4-Methylphenyl	4-Benzoylbiocytin
4-Ethylphenyl	4-Trifluoromethyphenyl
4-Decylphenyl	4-Biphenyl
	4-Methoxyphenyl

Figure 2.10 List of aryl groups attached to the carbon electrodes via diazonium coupling method.[65]

Pinson and Savéant proposed the reaction mechanism of the modification process and they stated that the coupling reaction was both favoured by diazonium adsorption prior to reduction and sufficiently positive potential of diazonium reduction potential which helps the stability of aryl radical by preventing it from any further reduction. [71]

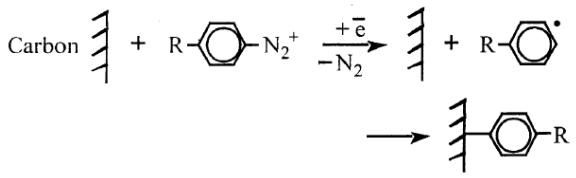

Figure 2.11 The mechanism of electrochemical reduction of an aromatic diazonium salts on carbon electrode.[71]

2.1.6.2 Diazonium coupling method and alternative chemical strategies

Electro-reduction of diazonium salts can be thought as a very significant contribution for the further studies of carbon surface modification. Following the study of Pinson and Savéant, Compton´s group presented a chemical method to carry out homogeneous reduction of diazonium salts by hypophosphorous acid, and that reaction provides an easy methodology for the derivatization of carbon powder. They demonstrated the derivatization of carbon particles with anthraquinone and nitrobenzene diazonium salts throughout a covalent bonding (Fig.2.13).[72] This chemical modification technique which proposes the reduction of diazonium salts by hypophosphorous acid has become a novel method in order to modify different types of carbon carbons for supercapacitor electrodes.

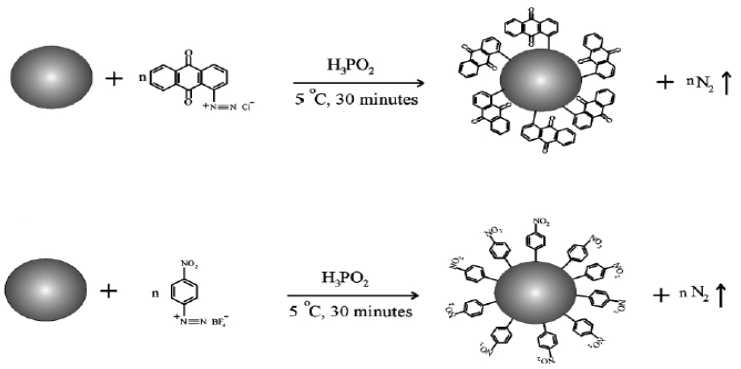

Figure 2.12 Schematic representation of homogeneous derivatization of carbon particles via diazonium coupling strategy.[72]

Up to now, several studies have been presented by applying this method to modify supercapacitor electrodes with anthraquinone molecules. Specifically, Pickup´s group has reported various recent studies on this subject. They discussed improved energy and power density for antraquinone modified carbon fabric as negative supercapacitor electrode and asymmetric unmodified carbon fabric[73], ruthenium oxide[62] and 1-2-dihydroxybenzene[74] as positive electrodes. Lastly, Bélanger et al. studied a series of high surface area activated carbon powders modified with various loadings of electroactive anthraquinone groups. They presented almost double specific capacitance values for the modified electrodes compared with unmodified ones.[75]

Despite being an effective strategy for quinone grafting, diazonium coupling is the unique method applied for quinone grafting for SC applications. Besides, solely anthraquinone derivatives were investigated for these purposes. So, considering the rich variety of quinonoid compounds and different electrochemical properties, there is an absolute need for proposing further alternative strategies to attach different quinones on carbon surface. One of the extensively studied reaction type for grafting of organic moieties onto different carbon surfaces is Friedel-Crafts reactions. Friedel-Crafts alkylation reaction catalysed with strong Lewis acids was implemented for the grafting of polymers onto the ends and side-walls of the carbon nanotubes.[76]

Baek et al. proposed Friedel-Crafts acylation reaction in poly(phosphoric acid) and phosphorus pentoxide medium for the covalent attachment of polyetherketones[77] and 4-subtituted benzoic acids[78] onto the surface of the electron-deficient carbon nanotubes and nanofibres. They further reported a novel approach to chemical exfoliation of graphite by grafting organic molecular wedges to the defect sites located mainly on the edges of natural graphite via the same strategy.[79]

2.2 Redox Flow Batteries

With the rapidly expanding implementation of energy production from renewable sources around the world, research attempts were greatly directed to the solutions strategies of grid instability and poor reliability issues by the implementation of renewable energies. Electrochemical storage technologies is greatly beneficial for integration of the produced energy into the future`s "*smart grids*".

The leading battery technologies that are attracting great attention for medium to large-scale grid-connect energy storage applications are the sodium–sulphur, lithium ion and redox flow batteries.[80]

2.2.1 General Overview

Redox Flow batteries ***(RFB)*** are large energy storage devices that have a wide range of potential applications in a distributed generation network. The energy can be stored in two solutions containing different redox couples with highly separated electrochemical potentials in order to supply an electromotive force to drive the oxidation and reduction reactions for charging and discharging of the cell[81].

Figure 14 illustrates the main parts of a RFB in which the electrolytes in each half-cell store the chemical energy. Electrolytes containing active redox couples are pumped through the cell stack where redox reactions take place at electrode surface. Typically each redox cell employs ion exchange membranes to separate the two half-cell electrolytes. The electrolyte solutions contain electroactive species and a high concentration of a supporting electrolyte to minimize the solution resistance.[81] As displayed in the figure 2.14, each half- cell electrolyte is stored in a separate storage

tank and there are two redox species with different electrochemical potentials involved. An external source of power is applied at the terminals and as the two half-cell solutions are pumped through the cell stack, the discharged form of each redox couple is converted into the corresponding charged form. When a load is connected across the terminals of the charged or partially charged cell or battery, electrons flow between the redox species and chemical energy is converted to electrical energy.[82] Energy is therefore stored in the solutions and the capacity of the system is determined by the concentration of the active redox species.

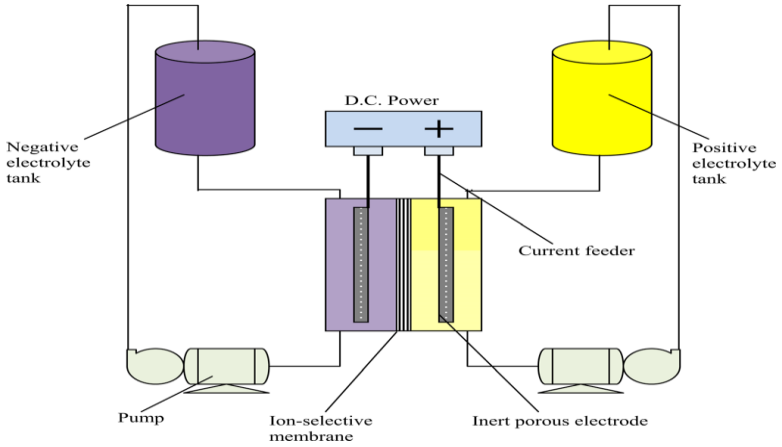

Figure 2.13. Schematic of the RFB structure.[83]

RFB can be distinguished from traditional battery systems in that the energy-bearing chemicals are not stored within the electrode-electrolyte interface, however, redox materials are stored in separate liquid reservoirs and pumped to the power converting device for either charging or discharging.[84]Since RFB employs two soluble redox couples, solid-state reactions with their accompanying morphological changes at the electrodes are absent. Therefore, unlike traditional batteries, there are no fundamental cycle life limitations due to battery type processes such as shedding or shape changes.[85].

Redox flow batteries are also referred to as electrochemically regenerative fuel cells because the electrical charge can be supplied from the soluble redox electrolytes which act as a fuel and an oxidant as they undergo oxidation and reduction reactions at inert electrodes that are separated by

an ion exchange membrane in an electrochemical cell. Redox flow batteries are distinguished from fuel cells in that the electrochemical reactions involved are reversible. The other different feature is that the overall battery efficiency of the redox flow system is close to 75-80%, whereas fuel cells efficiency can reach only up to 40%. [83]

The main characteristics of flow batteries are:

- ***Non-coupling energy and power density:*** Power and energy capacity of the system can be separated. The power of the system is determined by the number of cells in the stack and the size of the electrodes, whereas the energy storage capacity is determined by the concentration and volume of the electrolyte.[84]

- ***High power:*** the cell potential depends on the nature of the electrochemical reactions. The power rating is determined by the design and size of the power stack.

- ***High energy density:*** the energy density of the system depends on the amount and concentration of electrolyte used.

- ***High durability:*** The most distinctive characteristic of the RFB is that the electrodes do not take part in the reactions. Therefore the device performance stays unchanged contrary to most of the traditional rechargeable batteries in which repeated cycling result in deterioration of the electrode materials. Also, the system is re-fillable, and therefore, electrolytes can be replaced easily.

- ***Flexible modular design:*** RFBs can be designed for a wide range of power and energy needs. They are easily scalable.

- ***Short response time:*** Most redox reactions for RFBs are very rapid (fast reaction kinetics), which makes the reaction time very short. Flow batteries have a fast response and can go from charge to discharge modes in about 1/1000 s.

- **Cycle efficiency**: The full-cycle efficiency of the battery is around 75% - 80%. The most significant part of the efficiency loss arises from the energy needed to circulate the electrolyte and electrolyte decomposition reactions.

- Low self-discharge: The system does not have any self-discharge, as the electrolytes are stored in separate tanks. This is an important advantage in situations where electricity is stored for longer durations.

2.2.2 Historical Developments

Modern RFBs were invented in the 1970s by Lawrence Thaller at the National Aeronautics and Space Administration (NASA).[86] Since its invention, RFB technology has gone through a continuous development. The first true RFB was a ferric/ferrous (Fe^{2+}/Fe^{3+}) and a chromic/chromous (Cr^{2+}/Cr^{3+}) halide solutions in the positive and negative half-cell respectively. However, cross contamination problems resulted in a low storage capacity in this system and prevented its widespread use. In the 1980s, further efforts were directed to eliminating the complications due to cross contamination and two important RFB systems were proposed as a result of these attempts including Generation (GEN)-2 Fe/Cr redox flow batteries, which employ a mixed electrolyte as both positive and negative electrolyte. [87] The other one is all-vanadium flow batteries, which are based on the same redox species with different oxidation state as both positive and negative electrolytes.[88] Afterwards, several different types of RFB were proposed depending on different active redox species as the anolyte and catholyte. These RFBs can be classified as follows: polysulphide/bromine flow batteries ,[89] zinc/bromine flow batteries [90], vanadium/cerium flow batteries, soluble lead-acid batteries, etc.

2.2.3 Different types of RFBs

2.2.3.1 Vanadium Redox Flow Battery (VRB)

A vanadium redox battery consists of two half-cells in which separate electrochemical reactions take place. During discharge, electrons are produced in the reaction in the negative half-cell and are consumed in the reaction in the positive half-cell. Figure 2.15 indicates the principle and the basic structure of a VRB, where two electrolyte tanks and a battery stack are involved. VRB is composed of two half-cells, each containing a solid electrode in contact with the liquid electrolyte. Electrolytes are stored in separate electrolyte tanks, and circulated by pumping system into the cell continuously.

The concentration of the vanadium species and also the volume of the electrolyte determine the total amount of energy stored in the system. On the other hand, the system power is determined by the rate of electrochemical reaction of the vanadium species at each electrode. Vanadium ions must be adsorbed onto the surface of the electrodes before they can change their valence states, so reaction rates are limited by the total surface area of the electrodes. Therefore, the larger the electrodes, the more vanadium ions can be absorbed and react at a given moment and the greater the power.

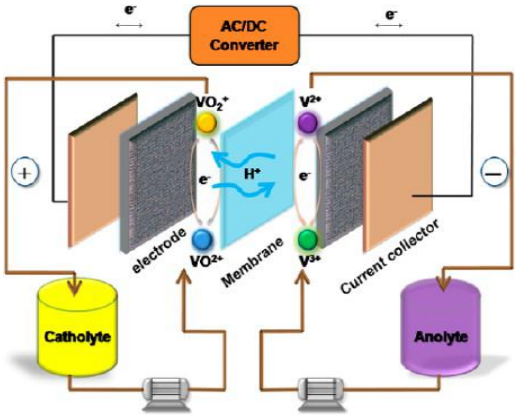

Figure 2.14. Principle components of a VFB.[91]

In the negative half-cell during discharge, vanadium (II) ions in solution are converted to vanadium (III) ions, by losing an electron.

$$V^{2+} \rightleftharpoons V^{3+} + e^- \qquad E^0 = -0.255V$$

In the positive half-cell during discharge, vanadium (V) ions are converted to vanadium (IV) ions, gaining an electron.

$$VO_2^+ + e^- + 2\,H^+ \rightleftharpoons VO^{2+} + H_2O \qquad E^0 = 1.000V$$

The overall equation is:

$$VO_2^+ + 2H^+ + V^{2+} \rightleftharpoons VO^{2+} + H_2O + V^{3+} \qquad E^0 = 1.255V$$

Since protons are consumed in the process, the pH of the positive electrolyte can be expected to change over time. To maintain charge balance within the half cells, a mechanism for the transit of

hydrogen ions from the negative half-cell to the positive half-cell is required, which is fulfilled easily by placing an ion-permeable membrane between the two half cells.

The vanadium redox chemistry described above has two important advantages over other flow battery technologies:

- ***The use of same redox species***: Migration of ions from one electrolyte to the other through the membrane does not cause contamination because the positive and negative electrolytes species are essentially the same compound but in different oxidation state. The ions in the two electrolytes are in different valence states when the electrolytes are charged, and mixing would cause self-discharge; for this reason, an ion exchange membrane is still required between the two cells.
- ***Less hazardous materials:*** Electrolytes based on different halides which are used in some other flow battery technologies are hazardous chemicals. In vanadium redox batteries, sulfuric acid based aqueous electrolyte has relatively low environmental impact.

2.2.3.2 Polysulphide Bromide Batteries (PSB)

Electrolytes for this battery system are the solutions of sodium bromide (NaBr) and sodium polysulphide (Na_2Sn_4). The Na^+ ions travel through the membrane during charging or discharging, while Br and S are the components that give and accept electrons. So, this cell is generally called as a Br/S system.

Reactions during charging:

$$S + 2e^- \rightleftharpoons 2S_2^- \longrightarrow (Na_2S_4 + 2e^- + 2Na^+ \rightarrow 2Na_2S_2)$$

$$Br_2 + 2e^- \rightleftharpoons 2Br^- \longrightarrow (3NaBr^- \rightarrow NaBr_3 + 2Na^+ + 2e^-)$$

During discharge the reverse reactions take place.

2.2.3.3 Zinc Bromine Batteries (ZnBr)

This type of battery combines a zinc-negative electrode and a bromine-positive electrode separated by a micro-porous membrane. Solutions of zinc and a complex bromine compound are circulated

through the two compartments. The distinct part of this battery from both VRB and PSB is the participation of electrode materials in redox reactions. Herein the electrodes (Zn^- and Br^+) serve as substrates for the reaction and their performance capacity can be affected negatively by the degradation of active materials when the battery is not completely and regularly discharged.

During charging, the zinc is electroplated at the anode and bromine is evolved at the cathode, according to the following reactions:

$$Zn^{2+}(aq) + 2e^- \rightleftharpoons Zn(s)$$

$$2Br^-(aq) \rightleftharpoons Br_2(aq) + 2e^-$$

$$Zn^{2+}(aq) + 2Br^-(aq) \rightleftharpoons Zn(s) + Br_2(aq)$$

These reactions are reversed during the discharge process.

Figure 2.16 summarizes some important features of the well-known RFBs.

System	Reactions	E_{cell}^o	Electrolyte
Redox			Anode/Cathode
All Vanadium [3]	Anode: $V^{2+} \overset{charge\ discharge}{\longleftrightarrow} V^{3+} + e^-$ Cathode: $VO_2^+ + e^- \overset{charge\ discharge}{\longleftrightarrow} VO^{2+}$	1.4 V	H_2SO_4/H_2SO_4
Vanadium-Polyhalide [5]	Anode: $V^{2+} \overset{charge\ discharge}{\longleftrightarrow} V^{3+} + e^-$ Cathode: $½\ Br_2 + e^- \overset{charge\ discharge}{\longleftrightarrow} Br^-$	1.3 V	VCl_3-HCl/NaBr-HCl
Bromine-Polysulfide [6]	Anode: $2\ S_2^{2-} \overset{charge\ discharge}{\longleftrightarrow} S_4^{2-} + 2e^-$ Cathode: $Br_2 + 2e^- \overset{charge\ discharge}{\longleftrightarrow} 2\ Br^-$	1.5 V	$NaS_2/NaBr$
Iron-Chromium [7]	Anode: $Fe^{2+} \overset{charge\ discharge}{\longleftrightarrow} Fe^{3+} + e^-$ Cathode: $Cr^{3+} + e^- \overset{charge\ discharge}{\longleftrightarrow} Cr^{2+}$	1.2 V	HCl/HCl
H_2-Br_2 [8]	Anode: $H_2 \overset{charge\ discharge}{\longleftrightarrow} 2H^+ + 2e^-$ Cathode: $Br_2 + 2e^- \overset{charge\ discharge}{\longleftrightarrow} 2Br^-$	1.1 V	PEM*-HBr
Hybrid			
Zinc-Bromine	Anode: $Zn \overset{charge\ discharge}{\longleftrightarrow} Zn^{2+} + 2e^-$ Cathode: $Br_2 + 2e^- \overset{charge\ discharge}{\longleftrightarrow} 2\ Br^-$	1.8 V	$ZnBr_2/ZnBr_2$
Zinc-Cerium [9]	Anode: $Zn \overset{charge\ discharge}{\longleftrightarrow} Zn^{2+} + 2e^-$ Cathode: $2Ce^{4+} + 2e^- \overset{charge\ discharge}{\longleftrightarrow} 2Ce^{3+}$	2.4 V	CH_3SO_3H (both sides)

*Polymer Electrolyte Membrane

Figure 2.15. Characteristics of different RFB systems.[83]

2.2.4 Properties of electrodes and electrolyte materials

2.2.4.1 Electrolyte Materials

The electrolytes of RFBs serve as the medium to store and release energy. The two important features of the electrolyte, volume and concentration of active species, play a critical role to determine the energy density of the system.[92] For the sake of performance and cycling stability of the battery, materials for electrolyte should be highly stable. To improve the energy density and the cycle life of a redox flow system, high solubility and stability of the electrolyte material should be established.[93]

The electrolyte is composed of active species and supporting electrolytes. Active species are referred to redox compounds such as vanadium at difference valence states. The principal criteria for the selection of active species are the fast electrochemical kinetics at the electrode-electrolyte interface and very high solubility with minimum cross contamination. Sulphuric acid, hydrochloric acid, methane sulfonic acid and the mixture of them were employed as supporting electrolyte for VFB systems.[94]

Non-aqueous systems were also studied for redox flow batteries in order to widen the potential window and thereby, the energy storage. However, the low conductivity of the organic electrolyte emerged as a critical issue that needs to be solved for further applications of them in RFBs.[95]

Alternative organic electrolyte materials:

The vanadium itself is an expensive material and therefore, it significantly raises the cost of the entire battery system. It is suggested that the vanadium material contributes between $50/kWh to $110/kWh , at current vanadium prices, to the total cost of the battery.[96] It is also known that an aqueous solution with high concentration of vanadium is toxic. Taking into consideration both issues, identifying low-cost redox couples with high solubility and less negative environmental impact is essential to meet the future demand.

Novel organic RFB was proposed by Cao et al. They demonstrated the use of hydroquinone /quinone and their derivatives as the positive active material of a RFB, due to their electrochemical reversibility with relatively high electrode potentials, controllable water-solubility and stability. Among a series of

quinones, sulfonic benzoquinones was selected due to the highest electrode potentials of benzoquinone species and high solubility coming from the sulfonic functional groups.[97] Here, the main disadvantage is the low solubility of sulfonic benzoquinones (0.05M) in acidic aqueous solution and consequently, low energy density that can be obtained from the system. So, quinones are promising redox active species for redox flow batteries due to highly reversible kinetics, abundance and low cost but water solubility is still a technical issue to overcome to further applications in RFB systems.

2.2.4.2 Electrode Materials

VFB electrodes do not take place in electrochemical reactions; their primary role is to provide proper sites for electrochemical reactions. The most important features of the electrode materials are high electrochemical activity which permits to reduce the electrochemistry polarization, good conductivity to reduce the ohmic polarization, a stable 3D structure with a high active specific area and excellent chemical, mechanical, and electrochemical stability and finally reasonable cost to meet the requirements of a large-scale production. High surface area materials provide smooth channels for the electrolyte, increasing the mass-transfer rate and decreasing the concentration polarization.[93]

Widely applied electrodes materials for RFBs can be considered into two groups: metal and carbon materials. A range of metal electrode materials such as lead, gold, platinum, platinized titanium and iridium oxide have been employed for VFBs.[98]

On the other hand, carbon-based materials are the most suitable materials for RFB technology due to their wide operation range, high chemical stability and reasonable cost. Various carbon materials such as carbon felt, graphite felt, carbon paper, and graphite powder have been investigated as the electrodes for VFBs.[99,100]Among them, graphite and carbon felts were selected as the most proper electrode materials for both positive and negative half-cells in the VRBs, given that the cell can be protected from excessive overcharge and, additionally, sufficient chemical and mechanical stability can be accomplished when combined with a suitable low cost and chemically resistant bipolar

substrate material. On the other hand, gold and other metals are too expensive electrode materials for practical applications in RFB and hence, their widespread applications are limited.

References

1. P. Simon and Y. Gogotsi, *Nature Materials*, 2008, **7**, 845–54.
2. M. Conte, *Fuel Cells*, 2010, **10**, 806–818.
3. D. Cericola and R. Kötz, *Electrochimica Acta*, 2012, 1–17.
4. M. Winter and R. J. Brodd, *Chemical Reviews*, 2004, **104**, 4245–69.
5. Kotz R; Carlen M., *Electrochimica Acta*, 2000, 45, 2483–98.
6. V. S. Arico W, Bruce, P, Scrosati B, Tarascon JM, *Nature Materials*, 2005, 366–77.
7. H. L. F. von Helmholtz, *Ann. Phys.*, 1879, 337, 7.
8. H. E. Becker, *General Electric, US Patent , No. 2 800 616*, 1957.
9. B. E. Conway, *Electrochemical Supercapacitors: Scientific Fundamentals and Technological Applications*, Kluwer Academics/Plenum Publishers, New York, 1997.
10. S. Zurek, *Wikimedia Commons. Maxwell's European PR representative*.
11. J. Chmiola, C. Largeot, P. L. Taberna, P. Simon, and Y. Gogotsi, *Angewandte Chemie*, 2008, **47**, 3392–5.
12. Z. O. Stern, *Electrochem.Angew. Phys. Chem*, 1924, 508.
13. A. J. Bard, L. R. Faulkner, E. Swain, and C. Robey, *Electrocehmical Methods:Fundamentals and Applications*, John Wiley & Sons, United States, 2nd edn.
14. E. Frackowiak, *Phys. Chem. Chem. Phys.*, 2007, 1774.
15. M. Mastragostino and F. Soavi, *Encyclopedia of Electrochemical Power Sources, Vol 1.Electrochemical Capacitors: Ionic Liquid Electrolytes. In: J. Garche, C. Dyer, P. Moseley, Z. Ogumi, D. Rand, B. Scrosati, editors.*, 2009, 649. 1.9.
16. L. L. Zhang and X. Z. Zhao, *Chemical Society Reviews*, 2009, **38**, 2520–2531.
17. K. Naoi and P. I. Simon, *Interface*, 2008, 17, 34.
18. A. Burke, *Electrochimica Acta*, 2007, 53, 1083.
19. B. E. Conway, V. Birss, and J. Wojtowicz, *Journal of Power Sources*, 1997, **66**, 1–14.
20. G. Lota and E. Frackowiak, *Fuel Cells*, 2010, **10**, 848–855.

21. P. Delahay, *Journal of Electroanalytical Chemistry*, 1968, 131.

22. T. Brousse, M. Toupin, and D. Belanger, *Journal of Electrochemical Society*, 2004, A614.

23. M. S. Hong, S. H. Lee, and S. W. Kim, *Electrochemical Solid State Letters*, 2005, A227.

24. V. Khomenko, E. Raymundo-Piñero, and F. Béguin, *Journal of Power Sources*, 2010, **195**, 4234–4241.

25. H.-G. Jung, N. Venugopal, B. Scrosati, and Y.-K. Sun, *Journal of Power Sources*, 2013, **221**, 266–271.

26. B. Z. Jang, C. Liu, D. Neff, Z. Yu, M. C. Wang, W. Xiong, and A. Zhamu, *Nano letters*, 2011, **11**, 3785–91.

27. A. F. Pandolfo, A. G, Hollenkamp, *Journal of Power Sources*, 2006, **157**, 1539.

28. Kirk-Othmer, *Encyclopedia Of Chemical Technology*, John Wiley & Sons, 5th edn., 2004.

29. R. C. Bansal, J. B. Donnet, and F. Stoeckli, *Active Carbon*, New York:Marcel Dekker, 1988.

30. A. Ahmadpour and D. D. Do, *Carbon*, 1997, **35**, 1723–1732.

31. G. Soto-Garrido, C. Aguilar, R. García, and R. Arriagada, *Journal of the Chilean Chemical Society*, 2003, **48**, 65–69.

32. D. Qu and H. Shi, *Journal of Power Sources*, 1998, **74**, 99–107.

33. D. Hulicova-Jurcakova, A. M. Puziy, O. I. Poddubnaya, F. Suárez-García, J. M. D. Tascón, and G. Q. Lu, *Journal of the American Chemical Society*, 2009, **131**, 5026–7.

34. M. P. Bichat, E. Raymundo-Piñero, and F. Béguin, *Carbon*, 2010, **48**, 4351–4361.

35. J. H. Chae, K. C. Ng, and G. Z. Chen, *Journal of Power and Energy, A*, 2009, **224**, 479–503.

36. S. Lowell, J. E. Shields, A. T. Martin, and T. Matthias, *Characterization of Porous Solids and Powders: Surface Area, Pore Size and Density*, Kluwer Academics, 2004.

37. A. G. Hollenkamp and A. F. Pandolfo, *Journal of Power Sources*, 2006, 1539.

38. G. Salitra, A. Soffer, L. Eliad, Y. Cohen, and D. Aurbach, *Journal of The Electrochemical Society*, 2000, **147**, 2486.

39. E. Raymundo-Piñero, K. Kierzek, J. Machnikowski, and F. Béguin, *Carbon*, 2006, **44**, 2498–2507.

40. J. Chmiola, G. Yushin, Y. Gogotsi, C. Portet, P. Simon, and P. L. Taberna, *Science*, 2006, **313**, 1760–3.

41. C. Largeot, C. Portet, J. Chmiola, P. Taberna, Y. Gogotsi, and P. Simon, *Journal of American Chemical Society*, 2008, **130**, 2730–2731.

42. W. Shen, Z. Li, and Y. Liu, *Recent Patents on Chemical Engineering*, 2008, **1**, 27–40.

43. E. Frackowiak and F. Béguin, *Carbon*, 2001, **39**, 937–950.

44. L. Radovic and F. Rodriguez-Reynoso, *Chemistry and Physics of Carbon vol.25*, New York:Marcel Dekker, 1997.

45. J. P. Zheng, P. J. Cygan, and T. R. Jow, *Journal of Electrochemical Society*, 1995, **142**, 2699–703.

46. S. Y. Wang and N. L. Wu, *Journal of Applied Electrochemistry*, 2003, **33**, 345–8.

47. F. B. Zhang, Y. K. Zhou, and H. L. Li, *Materials Chemistry and Physics*, 2004, **83**, 260–4.

48. V. Srinivasan and J. W. Weidner, *Journal of Power Sources*, 2002, **108**, 15–20.

49. H. Y. Lee and J. B. Goodenough, *Journal of Solid State Electrochemistry*, 1999, **148**, 81–4.

50. H. Y. Lee and J. B. Goodenough, *Journal of Solid State Electrochemistry*, 1999, **144**, 220–3.

51. P. Kurzweil, *Journal of Power Sources*, 2009, **190**, 189–200.

52. A. Yuan, X. Wang, Y. Wang, and J. Hu, *Energy Conversion and Management*, 2010, **51**, 2588–2594.

53. F. Marchioni, J. Yang, W. Walker, and F. Wudl, *The Journal of Physical Chemistry B*, 2006, **110**, 22202–6.

54. V. Khomenko and E. Frackowiak, *Electrochimica Acta*, 2005, **50**, 2499–2506.

55. S. A. Hashmi, R. J. Latham, R. G. Linford, and W. S. Schlindwein, *Polymer International*, 1998, **47**, 28–33.

56. A. K. Cuentas-Gallegos, R. Martínez-Rosales, M. Baibarac, P. Gómez-Romero, and M. E. Rincón, *Electrochemistry Communications*, 2007, **9**, 2088–2092.

57. J. Q. Chambers, *In The Chemistry of the Quinonoid Compounds; Patai, S., Rappoport, Z.*, John Wiley & Sons, 1988.

58. C. Russel and W. Jaenicke, *Journal of Electroanalytical Chemistry*, 1986, **199**, 139–151.

59. P. R. Rich, *Biochemistry Biophysics Acta*, 1984, **768**, 53.

60. M. Turunen, J. Olsson, and G. Dallner, *Biochemistry Biophysics Acta*, 2004, **171**, 1160.

61. S. Weiss and J. Jouken, *Biochemistry Society Transactions*, 2009, **37**, 707.

62. Z. Algharaibeh, X. Liu, and P. G. Pickup, *Journal of Power Sources*, 2009, **187**, 640–643.

63. S. Rold, M. Granda, R. Men, R. Santamaría, and C. Blanco, *Jounal of Physical Chemistry C*, 2011, **115**, 17606–17611.

64. S. Roldán, C. Blanco, M. Granda, R. Menéndez, and R. Santamaría, *Angewandte Chemie*, 2011, **50**, 1699–701.

65. D. Bélanger and J. Pinson, *Chemical Society Reviews*, 2011, **40**, 3995–4048.

66. S. Suematsu and K. Naoi, *Journal of Power Sources*, 2001, **98**, 2000–2002.

67. H. Maeda, Y. Yamauchi, M. Hosoe, T. X. Li, E. Yamaguchi, M. Kasamatsu, and H. Ohmori, *Pharmaceutical Bulletin*, 1996, **44**, 860.

68. B. Barbier, J. Pinson, G. Desarmot, and M. Sanchez, *Journal of The Electrochemical Society*, 1990, **137**, 1757–1764.

69. C. P. Andrieux, F. Gonzalez, and J. M. Saveant, *Journal of American Chemical Society*, 2004, **7863**, 4292–4300.

70. M. A. Hayes and W. G. Kuhr, *Analytical Chemistry*, 1999, **71**, 1720–7.

71. P. Allongue, M. Delamar, B. Desbat, O. Fagebaume, R. Hitmi, J. Pinson, and J. M. Saveant, *Journal of American Chemical Society*, 1997, **7863**, 201–207.

72. M. Pandurangappa, N. S. Lawrence, and R. G. Compton, *The Analyst*, 2002, **127**, 1568–1571.

73. K. Kalinathan, D. P. DesRoches, X. Liu, and P. G. Pickup, *Journal of Power Sources*, 2008, **181**, 182–185.

74. Z. Algharaibeh and P. G. Pickup, *Electrochemistry Communications*, 2011, **13**, 147–149.

75. G. Pognon, T. Brousse, L. Demarconnay, and D. Bélanger, *Journal of Power Sources*, 2011, **196**, 4117–4122.

76. X. L. Wu, *eXPRESS Polymer Letters*, 2010, **4**, 723–728.

77. J.-B. Baek, *Chemistry of Materials*, 2005, **46**.

78. H.-J. Lee, S.-W. Han, Y.-D. Kwon, L.-S. Tan, and J.-B. Baek, *Carbon*, 2008, **46**, 1850–1859.

79. E. Choi, I. Jeon, S. Bae, H. Lee, and S. Shin, *Chemical Communications*, 2010, 6320–6322.

80. A. Parasuraman, T. M. Lim, C. Menictas, and M. Skyllas-Kazacos, *Electrochimica Acta*, 2013, **101**, 27–40.

81. M. Bartolozzi, *Journal of Power Sources*, 1989, **27**, 219–234.

82. J. Garche, P. Moseley, Z. Ogumi, D. Rand, and B. Scrosati, *Chapter on "Secondary Batteries: Redox Flow Battery—Vanadium Redox" by Maria Skyllas-Kazacos Encyclopedia of Electrochemical Power*, Elsevier, New York, USA, 2009.

83. M. Skyllas-Kazacos, M. H. Chakrabarti, S. A. Hajimolana, F. S. Mjalli, and M. Saleemd, *Journal of Electrochemical Society*, 2011, **158**, 7–10.

84. C. Ponce de León, A. Frías-Ferrer, J. González-García, D. A. Szánto, and F. C. Walsh, *Journal of Power Sources*, 2006, **160**, 716–732.

85. M. H. Chakrabarti, R. A. W. Dryfe, and E. P. L. Roberts, *Electrochimica Acta*, 2007, **52**, 2189–2195.

86. L. H. Thaller, 1976, US Patent 3996064.

87. J. S. Gahn, G F Hagedorn , N H Ling, NASA, Lewis Research Center , Cleveland, OH,1983, .

88. M. Rychcik and M. Skyllas-Kazacos, *Journal of Power Sources*, 1988, **22**, 59–61.

89. C. Ponce de Leon, A. Frías-Ferrer, J. González-García, D. A. Szánto, and F. C. Walsh, *Journal of Power Sources*, 2006, **160**, 716.

90. D. J. Eustace, *Journal of Power Sources*, 1980, **127**, 528.

91. C. Ding, H. Zhang, X. Li, T. Liu, and F. Xing, *The Journal of Physical Chemistry Letters*, 2013, **3**, 1281.

92. F. Rahman and M. Skyllas-Kazacos, *Journal of Power Sources*, 2009, **189**, 1212–1219.

93. C. Ding, H. Zhang, X. Li, T. Liu, and F. Xing, *Physical Chemistry Letters*, 2013, 1282–1294.

94. A. Parasuraman, T. Mariana, C. Menictas, and M. Skyllas-Kazacos, *Electrochimica Acta*, 2013, **101**, 27–40.

95. Q. H. Liu, A. E. S. Sleightholme, A. A. Shinkle, Y. D. Li, and L. T. Thompson, *Electrochemistry Communications*, 2009, 2312−2315.

96. T. Nguyen and R. F. Savinell, *The Electrochemical Society Interface*, **Fall 2010**, 54–56.

97. Y. Xu, Y. Wen, J. Cheng, Y. Yanga, Z. Xie, and G. Cao, in *IEEE 2009*, 2009, pp. 2–5.

98. M. Rychcik and M. Skyllas-Kazacos, *Journal of Power Sources*, 1987, 45–54.

99. S. Zhong, C. Padeste, M. Kazacos, and M. Skyllas-Kazacos, *Jounal of Power Sources*, 1993, **45**, 29–41.

100. H. S. Kim, *Bull. Korean Chem. Soc.*, 2011, 571–575.

Chapter 3: Experimental

3.1 Materials

Table 3.1 summarizes the materials and chemicals used with details of suppliers for experimental work of this thesis.

Materials/Chemicals	Formula	Abbrevi-ation	Purity	Supplier
Activated CarbonPicactif	C	Pica	>95%	Usine
Acetylene Black	C	CB	>99.9%	Sigma Aldrich
Vulcan XC 72R	C	Vulcan	>99%	Cabot Corp.
Glassy Carbon	C	GC D:6mm	>99%	Basi Corp.
Mili-Q Water	H_2O	Milli-Q	> 99.9%	Milipore,USA
2-propanol	$(CH_3)_2CHOH$	iPrOH	99.5%	Scharlau
Methanol	CH_3OH	MeOH	> 99.9%	Sigma-Aldrich
Acetone	C_3H_6O	ACE	> 99.5%	Sigma-Aldrich
Sulphuric Acid	H_2SO_4	-	%95-97	Scharlau
Acetonitrile	CH_3CN	AN	%99.8	Sigma-Aldrich
Dimethlysufoxide	$(CH_3)_2SO$	DMSO	> 99%	Sigma-Aldrich
Dimethyl formamide	$HCON(CH_3)_2$	DMF	> 99%	Sigma-Aldrich
1-methyl-2-pyrrodilinone	C_5H_9NO	NMP	> 99,9%	Acros organics
Dichloromethane	CH2Cl2	DCM	98.9%	Sigma-Aldrich
Polyvinylideneflouride	$-(C_2H_2F_2)n-$	PVDF	> 99%	Sigma-Aldrich
Tetrabuthlyamoniumhex aflourophosphate	$(CH_3CH_2CH_2CH_2)_4N(PF_6)$	$TBAPF_6$	99.0%	Sigma-Aldrich
1,4-Benzoquinone	$C_6H_4O_2$	pBQ	> 99,5%	Sigma-Aldrich

Naphthoquinone	$C_{10}H_6O_2$	NQ	97%	Sigma-Aldrich
2-hydroxy-1,4-naphthoquinone	$C_{10}H_6O_3$	2OHNQ	97%	Sigma-Aldrich
5-hydroxy-1,4-naphthoquinone	$C_{10}H_6O_3$	5OHNQ	97%	Sigma-Aldrich
Tetrahydroxy-1,4-benzoquinone	$C_6H_4O_6$	THBQ	99%	Sigma-Aldrich
Chloroanilic Acid	$C_6H_2O_4Cl_2$	CAA	>99%	Acros Organics
Anthraquinone	$C_{14}H_8O_2$	AQ	>99%	Sigma-Aldrich
2,3-dichloro-5,6-dicyano-1,4-benzoquinone	$C_8N_2Cl_2$	DDQ	98%	Sigma-Aldrich
Anthracenetetraone	$C_{14}H_6O_4$	AT	99%	Sigma-Aldrich
Iron(III) Chloride	$FeCl_3$	$FeCl_3$	≥99.99%	Sigma-Aldrich
Potassium Bromide	KBr	KBr	99.5%	Scharlau
Potassium Chloride	KCl	KCl	99.0%	Scharlau
Stainless steel mesh (0.09mm)			97%	Goodfellow
Platinum wire/mesh	Pt	Pt	99.9%	Sigma-Aldrich
Silver/Silver chloride (NaCl-sat)reference electrode	Ag/AgCl	Ag/AgCl	-	Basi Corp.
Carbon Fiber	C	CF	-	Textron Mat.
Gold wire	Au	Au	>99.99%	Goodfellow
Silver wire	Ag	Ag	99.9%	Sigma-Aldrich

Table 3.1 Details of all chemicals used for the experimental work.

3.2 Experimental Procedure

The overall experimental procedures of this thesis work are summarized in Figure 3.1. This research work mainly consists of two parts: the first part is the fabrication and characterization of the composite carbon-quinone materials for supercapacitors electrode fabrication; while the second part involves the application of these quinone materials as electrolyte active species in redox flow battery systems. Furthermore, standard rate constant of quinone species was studied for further

understanding of the electron transfer phenomenon of different quinone derivatives which substantially influence the performance of electrochemical storage devices.

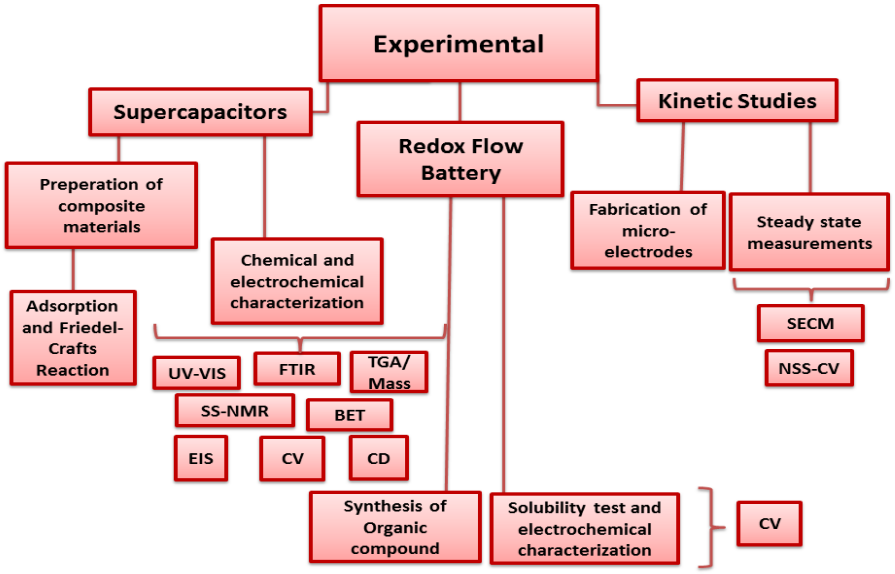

Figure 3.16 The overall procedure of the experimental part.

3.3 Supercapacitors

3.3.1 Preparation of composite materials

In the experimental part of this thesis, two different methods were used for fabrication of carbon-quinone composite electrodes. The first one is the solution impregnation of electroactive species directly into the pores of pre-prepared carbon electrode and the second method is an organic chemistry route for grafting of quinone moieties on the surface of several type of carbons.

For the adsorption of AT, carbon electrodes were prepared previously. This was done by mixing and grinding carbon material (70 wt.%), CB (20 wt.%) and PTFE (10 wt.%) by using 2-propanol until reduced to a pasty mass. The paste was coated on a coin shape stainless steel mesh current collector (1 cm in diameter). The electrodes were then pressed with a uniaxial press (CARVER model 3853-0) applying a pressure of 450 kg cm^{-2} and dried at room temperature overnight. Average mass of dry electrodes was 15–20 mg cm^{-2}. Afterwards, pristine carbon electrodes were soaked in 5 × 10^{-3}M AT in acetonitrile at different immersion times and dried overnight at room temperature.

However for the rest of the work, electrodes were made by the following method: Carbon slurry was prepared by mixing Pica and acetylene black (carbon black, acetylene, 100% compressed, >99.9%, Alfa Aesar) in a mortar by grinding with polyvinylidene fluoride (PVdF, MW≈540,000) at a 8:1:1 weight ratio and using *N*-methylpyrrolidinone (NMP) as dispersive medium. The resulting slurry was spread on a stainless steel mesh (AISI 3024, 97% open, Goodfellow) on 1 cm diameter disk-shaped pieces, pressed at 450 $kgcm^{-2}$, and dried at 120^{o}C for 4-5 hours under vacuum. Prior to experiments vacuum impregnation of sulfuric acid (H_2SO_4, 95-97%, p.a., Scharlau) electrolyte into carbon electrode was performed to ensure good penetration into carbon pores.

In a different study, electrode modification was done by the same technique explained above except that the soaking solution was prepared in DMSO with a concentration of 1.5 M and dried under vacuum at 40 ^{o}C for 3-4 hours.

Another approach that has been used in this thesis is a covalent modification technique. Friedel-Crafts reaction of p-BQ with Pica activated carbon was studied. In this modification method, composite material was prepared in a one-pot two-steps process initiated by a typical Friedel-Crafts reaction: 250 mg Pica, 108 mg of p-BQ, 40 mg of anhydrous $FeCl_3$ and 4 ml of dichloromethane were mixed into a round bottom flask. The mixture was stirred vigorously at room temperature under nitrogen atmosphere overnight and finally DDQ was added and the reaction was stirred 3 hours more for the complete oxidation of the hydroquinone intermediate. The final product was collected by vacuum filtration on a nylon filtration membrane and thoroughly washed with MeOH, CH_3CN, DMF, water and acetone several times until getting a very clear aliquot.

This reaction on Pica carbon allowed the direct introduction of hydroquinone fragments through a 1,4-addition of the aromatic Pica carbon rings to the p-benzoquinone followed by a spontaneous enolization process. We treated these initially formed hydroquinones with a more powerful oxidant such as DDQ to oxidize the hydroquinone moieties incorporated to the Pica carbon into quinones. The solvent of choice for the Friedel-Crafts reaction of Pica carbon was CH_2Cl_2 due to the poor

solubility of the starting materials and reagents used in other solvents compatible with these conditions.

3.3.2 Chemical characterization techniques

3.3.2.1 UV-Vis Spectroscopy

UV-Vis characterization was recorded in order to determine the amount of p-BQ adsorbed during each immersion time. Measurements were acquired in a Perkin Elmer Lambda 1050 spectrometer, since the absorbance of initial solutions is decreased due to the decreased concentration of soaking solutions. The amount adsorbed is calculated by applying the Beer –Lambert law according to the decrease of absorbance peak of π-π* transition of p-BQ soaking solutions at 245nm after each immersion time. The Beer-Lambert law states that the absorbance of a solution is directly proportional to the concentration of the absorbing species in the solution and the path length.

3.3.2.2 FT-IR Spectroscopy

Fourier transform infrared (FTIR) spectra were measured in a Thermo NICOLET 6700 spectrometer. A few milligrams of carbon were homogeneously mixed with dried KBr in a mortar, and pellets were pressed using a compressed hydraulic press. KBr was dried under vacuum at 100^{o}C prior to measurements and solid carbon samples were embedded in KBr disks. All spectra were measured between the range of 4000 to 500 cm^{-1} at 4 cm^{-1} resolution, and the number of scans was typically 32, in order to reduce signal to noise ratio. Measurements were performed at Transmission E.S.R. mode with DTGS-TEC type detector, XT-KBr beam splitter, IR-Turbo source and at 1.2659 optical velocity.

3.3.2.3 Thermogravimetric Analysis (TGA) and Mass Spectroscopy

Thermogravimetric analysis (TGA) is a type of measurement that is performed on samples to determine changes in weight in relation to change in temperature. In this doctoral work, thermogravimetric measurements (TGA) were carried out with a TGA apparatus (T.A. Instruments, model SDTQ 600) coupled to a mass spectrometer (OmniStar Spectrometer, Pfeiffer Vacuum) in

order to identify the surface functionalities of non-modified carbon and detect possible modifications of surface functionalities after grafting. The analysis was carried out under argon flow rate of 50 ml min^{-1} and heating from 25 to 1000 °C at a rate of 10 °C min^{-1}. The container for the sample is made of alumina. The loading mass of a sample is generally 5-15 mg, depending on the sample type.

3.3.2.4 Brunauer Emmett Teller (BET)

The BET method is a very crucial analysis technique for the measurement of the specific surface area of many different materials. Especially for carbon materials, it provides very important information regarding pore size modification in carbon composite materials. The BET theory was suggested by Stephen Brunauer, Paul Hugh Emmett, and Edward Teller in 1938.[3] This theory is actually based on Langmuir theory (for monolayer molecular adsorption) and later on, described for multilayer adsorption including the following concepts: (i) gas molecules are physically adsorbed on a solid in layers; (ii) there is no interaction among the various adsorption layers (iii) the Langmuir theory can be implemented to each layer. The BET equation can be expressed in the following equation:

$$\frac{1}{v\left[\left(\frac{P_0}{P}\right)-1\right]} = \frac{c-1}{v_m c}\left(\frac{P}{P_0}\right) + \frac{1}{(v_m - c)} \qquad \textbf{(3.1)}$$

where P and P_0 are the equilibrium and the saturation pressures of adsorbates (N_2 for the experiment of this thesis) at the temperature of adsorption, v is the adsorbed gas (N_2) quantity, v_m is the monolayer adsorbed gas quantity, and c is the BET constant, which is stated as follow:

$$c = \exp(E_1 - E_L)\,/RT \qquad \textbf{(3.2)}$$

where E_1 and E_L is the heat of adsorption for the first layer, and the second and higher layers, respectively. The linear relationship between $1/v[(P_0/P)-1]$ on the y-axis and P/P_0 on the x-axis of equation (3.1) is maintained only in the range of $0.05 < P/P0 < 0.35$. This plot is called a BET plot.

Porous texture and pore size distribution properties were analysed by N_2 adsorption isotherms obtained at 77 K with a Autosorb-1, Quantachrome Instruments apparatus. Prior to measurements, the samples were outgassed under vacuum at 120 ^{o}C overnight. The specific surface area was calculated from the isotherm by applying both BET (S_{BET}) and DFT (S_{DFT}) models. The micro- and meso- pore volume and the pore size distribution were obtained from N_2 adsorption isotherm by applying the QSDFT model.

3.3.2.5 Solid State Nuclear Magnetic Resonance Spectroscopy

Solid-State Nuclear Magnetic Resonance Spectroscopy (SS-NMR) technique is an attractive tool for compound analysis since it does not require derivatization or dissolution in a solvent medium. Furthermore, this technique can provide a wealth of information on chemical structure and dynamics on the samples.

In this thesis work, this technique was implemented for the confirmation of a covalent bond between quinones and carbon structure. SS-NMR measurements were carried out on a Bruker AV-400-WB spectrometer, at ^{13}C NMR frequency of 100.61 MHz, using a 2.5 mm double-resonance MAS probe, spinning speed of 10 kHz, a $\pi/2$ pulse of 4.4 μs, a spectral width of 35 kHz and a relaxation time of 40 s. All measurements were taken at room temperature, using adamantine as secondary external reference at 29.5 ppm (CH_2) relative to TMS as primary external reference.

3.3.3 Electrochemical characterization techniques

Electrochemical measurements including cyclic voltammetry, galvanostatic charge-discharge and electrochemical impedance spectroscopy were used to characterize the performance of the electrodes in supercapacitor systems. Electrochemical measurements were performed using a Biologic VMP3 multichannel potentiostat-galvanostat (Biologic, France) (Fig.3.2a) coupled with EC-Lab v10.18 software using 0.5 M H_2SO_4 aqueous electrolytes.

For studying a single carbon or carbon composite electrode, a three-electrode system was used with a Ag/AgCl reference electrode and Pt mesh or activated carbon with double mass as counter

electrode in a 3-electrode configuration Swagelok® cell(Fig.3b). In performance evaluation of symmetric/asymmetrics systems, supercapacitors were built by assembling a cellulosic paper between two carbon electrodes of similar weight in a two electrode Swagelok® cell (Fig.3c). During 3-electrode charge-discharge test, potential of each electrode were recorded with respect to an external Ag/AgCl reference electrode.

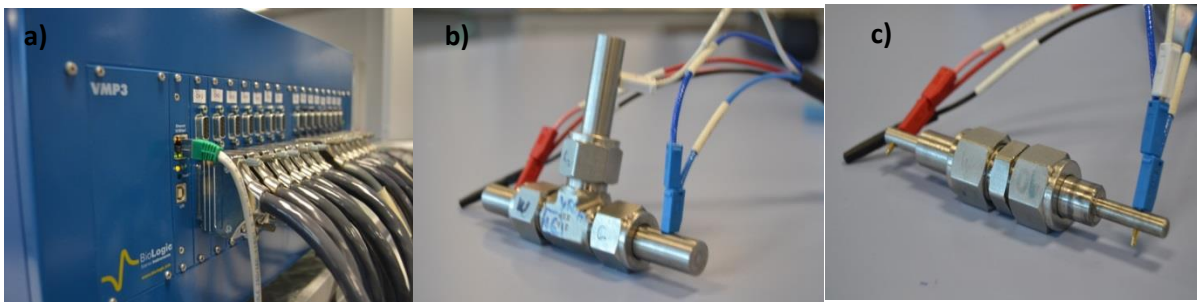

Figure 3.2. Biologic VMP3 multichannel potentiostat-galvanostat (a), 3-electrode (b) and 2-electrode (c) Swagelok® cells.

3.3.3.1 Cyclic Voltammetries (CV)

CV is a widely used technique for characterizing electrochemical performance for both supercapacitors and batteries. In CV experiments the potential of the working electrode was cycled within a pre-determined potential window at a constant scan rate. Scan rate can be defined as the potential change as a function of time (dE/dt). Observation of peak current provides information about the thermodynamic and kinetics of a redox process occurring at the electrode-electrolyte interface.

In the research of supercapacitors, CV curves are widely used for the calculation of charge accumulated and specific capacitance. Capacitance of a single electrode can be obtained directly by integrating the area of the CV curve (Fig.3.3).

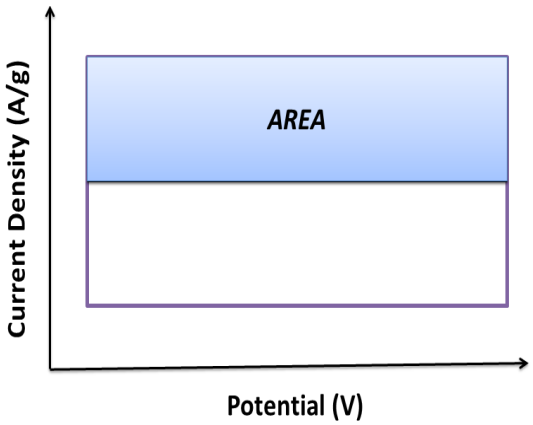

Figure 3.3. Area of CV curve for calculation of charge and specific capacitance.

Charge accumulated can be calculated by using the equation *Q=Area/v* where Q is the charge accumulated (C), v is the scan rate (mV/s);

So, specific capacitance can be obtained from the equation 3.3;

$$C = Q/Vm_{active} \quad \textbf{(3.3)}$$

where:

Q: charge accumulated (C)

V: Voltage window (V)

m_{active}= Active mass (equals to mass of only Pica or total mass of Pica and redox active compound).

3.3.3.2 Galvanostatic charge-discharge (CD)

The charge-discharge tests were conducted under a constant current density. The energy stored in the system (E) can be calculated based on the charge or discharge time using the formula E = Area × I, where I is current density and Area is the region under the discharge curve (Fig.3.4)

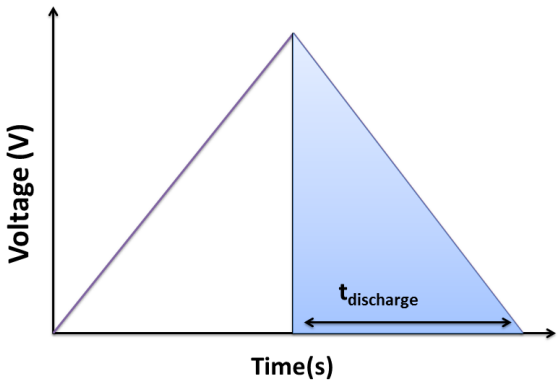

Figure 3.4. Area of CD curve for calculation of energy and power densities.

Specific energy of the system can be calculated from the equation 3.4:

$$E_S = \frac{E}{3{,}6 m_{total}} \qquad \textbf{(3.4)}$$

where;

E_S: specific energy of the system (Wh/kg)

E: energy calculated from the discharge curve (J)

m_{total}: total mass of both electrodes (g)

Power density corresponds to the rate at which stored energy delivered. The maximum power density of a supercapacitor is given V_i^2 /4R (where V_i is the initial voltage and R is the equivalent series resistance (ESR)). [4] In this thesis, specific power of the system (also mentioned as real power, P_{real}) was determined from the equation 3.5;

$$P_S = \frac{E}{t_D m_{total}} \qquad \textbf{(3.5)}$$

where;

P_s: specific power of the system (kW/kg)

E: Energy accumulated in the system (J)

t_D: discharge time that can be obtained from CD curve (s).

m_{total}: total mass of both electrodes (g)

3.3.3.3 Electrochemical Impedance Spectroscopy (EIS)

EIS is an important electrochemical technique used to obtain information about the characteristic frequency responses of supercapacitors and the capacitive phenomena occurring in the composite electrodes. EIS technique consists of the application of a small potential perturbation between a frequencies range at a given DC potential. A common impedance plot, also known as Nyquist plot, displays real and imaginary components of impedance on x and y axis respectively. It depicts a low-frequency semi-circle and a high-frequency straight line combined with a 45^{o} line between these two regions (Fig.3.5).

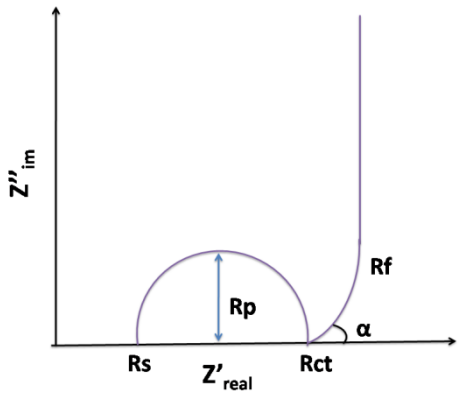

Figure 3.5. Components of a Nyquist plot for a supercapacitor.

At the high frequency region, this semi-circle type behaviour is likely to appear because of the charge-transfer process and/or the different contact resistances and double layer capacitance. At lower frequencies, the straight line shows the diffusive processes, and is at 90^{o} for an ideal supercapacitor. These two regions are generally combined with a 45^{o} inclined mid-frequency line which is consistent with the porous nature of the electrode when saturated with the electrolyte. At high frequencies, the resistance characteristics of the different supercapacitors are expressed by the so-called electric series resistance (Rs or ESR), which includes electrolyte resistance, collector/electrode contact resistance, and the resistance of the electrode/electrolyte interface.[5] The radius of the semi-circle expresses the polarization resistance (Rp) which gives information about the

electrolyte access into the pores. Rct is the charge transfer or electrolyte resistance and lastly, Rf is the contact resistance between thin electrode and current collector.

Impedance spectra were recorded with 5 mV AC perturbation in the frequency range of 100 kHz to 10 mHz at 0V OCV for the supercapacitor test (two electrodes test).

3.4 Redox Flow Battery

3.4.1 Synthesis of Organic Compounds

All compounds used in the "Redox Flow Battery" part of this thesis were synthesized by the organic synthesis group of Carmen Carreño in the Autonomous University of Madrid.

3.4.2 Solubility test and CV experiments

Solubility test was performed for synthesized quinone compounds in aqueous solution at different conditions. The change in solubility for all compounds was studied at different pH values and temperatures.

All electrochemical measurements were performed in a traditional three electrode setup glass cell with a 5mL electroanalyte solution with drying and maintenance of inert atmosphere by purging high quality Ar gas. Electrochemical measurements were performed with a Biologic VMP3 multichannel potentiostat-galvanostat (Biologic, France) using 6mm diameter glassy carbon (GC) as a working, Pt mesh as a counter and Ag/AgCl as a reference electrode respectively.

The glassy carbon electrode was cleaned immediately before each experiment by polishing with 1 and 0.05 μm alumina slurries respectively and rinsed with Mili-Q water.

3.5 Kinetic studies

3.5.1 Fabrication of micro-electrodes

For fabrication of UME tips, an established procedure was employed [6], involving heat sealing of a 25 μm Au microwire, or a 7 μm CF in a glass capillary under vacuum. The microwire/CF was connected

with silver epoxy to a larger copper wire on the back side (Fig.3.6a). UMEs were fabricated by different materials such as Pt (Fig. 3.6b), Au(Fig.3.6c) and CF(Fig.3.6d).

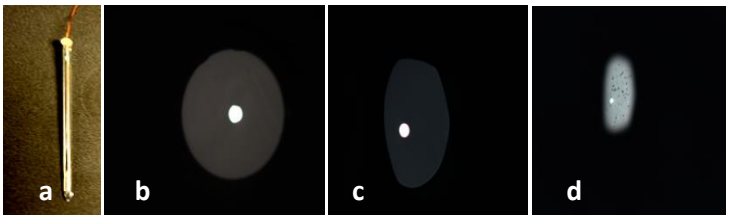

Figure 3.6. Au UME(a) Optical images of Pt-25µm (b) ,Au-25µm (c) and Cf-7µm (d) UMEs.

Tips were cleaned and polished using a 50nm alumina particles suspension. The important parameters of the tip geometry are the radius of the conductive core, *a*; and the total tip radius, r_g. The dimensionless parameter RG is the ratio of the tip radius to the conductive wire radius (r_g / *a*) which is generally ≤ 10. The substrate used was an evaporated gold film (thickness ~125 nm, measured by atomic force microscopy).

3.5.2 Scanning Electrochemical Microscopy (SECM) and Non-Steady-State Voltammetry (NSS-CV)

The home-built SECM instrument (Fig.3.7) was mounted on a vibration-free optical table inside a Faraday cage. An UME tip was mounted in a tip holder on a piezo-bender actuator, which in turn was mounted to a 3D piezoelectric positioner controlled by a computer running custom LabVIEW code (LabVIEW 9.0, National instruments), which was also used for data acquisition. The potentials of the tip and/or the substrate versus the silver-silver chloride (Ag/AgCl) reference electrode were applied through a home-built bipotentiostat and the tip current was measured. Experiments were performed by positive feedback mode.

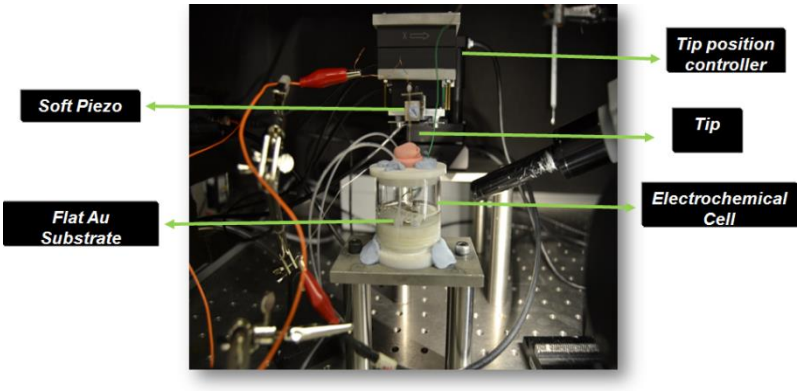

Figure 3.7. Basic components of a home-built SECM.

Tip-substrate separation was controlled by monitoring changes in the oscillation amplitude which results from the IC of the tip with the substrate surface. As the tip encounters the surface, damping of oscillation amplitude occurs and tip approach toward the substrate stops.

NSS-CV measurements were carried out in a two-electrode configuration using a potentiostat (CH Instruments model 760C, Austin,TX) at a scan rate of 1 V s^{-1}.

References

1. J. B. Affiliation and C. Engineering, *Chemistry of Materials*, 2005, **46**.

2. J.-B. B. Sang-Wook Han, Se-Jin Oh, Loon-Seng Tan, *Carbon*, 2008, **46**, 1841–1849.

3. E. T. S. Brunauer, P. H. Emmett, *Journal of American Chemical Society*, 1938, **60**, 309.

4. C. Du and N. Pan, *Nanotechnology*, 2006, **17**, 5314–5318.

5. F. Lufrano and P. Staiti, *Energy & Fuels*, 2010, **24**, 3313–3320.

6. R. M. Wightman and D. O. Wipf, *In Electroanalytical Chemistry; Bard, A. J., Ed.; Marcel Dekker: New York, 1989; vol. 15, p. 267*.

Chapter 4: Modification of Carbon Electrodes via Non-covalent Strategies

4.1 Introduction

The study of modified carbon electrodes for supercapacitors (SCs) in order to enhance their energy density has currently become the focus of many research efforts. One of the most active areas to achieve this goal proposes the combination of high surface area carbons with materials having faradaic-type charge transfer [1].

One strategy based on the concept of combining high surface area carbons with materials having faradaic type charge transfer is to add quinones on high surface area carbons. As it has long been known that at certain carbons pseudocapacitance by redox contribution of naturally occurring surface functionalities such as phenols, carboxylic acids, lactones and quinonoid structures [2] is added to the carbon electrical double layer capacitance. Particularly, diazonium coupling method is the most well—known strategy for grafting of aromatic diazonium salts on carbon electrodes. This method was demonstrated by Savéant et al. for the first time on glassy carbon and highly oriented pyrolytic graphite via an electrochemical route, leading to the covalent attachment of the corresponding aromatic radicals[3].

Compton's group presented a chemical method to carry out the homogeneous reduction of diazonium salts by hypophosphorous acid, providing an easy methodology for the derivatization of carbon powder. They demonstrated the derivatization of carbon particles with anthraquinone and nitrobenzene diazonium salts throughout a covalent bonding [4].

When using diazonium chemistry, in addition to the covalently bound species, it has already been pointed out the presence of loosely bound species which, in some cases, diminish the carbon surface

coverage by covalently bound species [5]. As these physisorbed species were also likely to be electrochemically active, and as physisorption using impregnation was likely to be a promising alternative method for the addition of pseudocapacitive species to the surface of carbons, non-covalent physical adsorption strategy was explored in this doctoral study.

Although many studies have been based on covalent modification of electrode surfaces by redox active species in order to attain higher energy densities, there are few studies discussing surface adsorption of redox species and its capacitive contribution as redox active additives. Recently a study of Gaubicher et al proved a non- covalent concept based on redox functionalization of composite electrodes with a multi-redox pyrene derivative. They reported that carbon fibre electrodes loaded with a pyrene derivative can deliver up to 130 kW/kg without significant capacitance loss over 60 000 charge-discharge cycles [6].

The key features of our non-covalent impregnation method are the simplicity, low energy consumption, low cost, non-toxic source materials and easily scalability for the addition of different compounds on the surface of suitable substrates. For supercapacitors, it provides an alternative strategy for attaining higher energy densities by combining high surface area carbon electrodes with surface species adding a pseudocapacitive contribution. In this first part of this chapter, the effect of adsorption by using electroactive 1,4,9,10-anthracenetetraone (AT) (see Fig. 4.1a) was demonstrated on different carbons [7]. For that, two different carbons were impregnated with AT. Porous structure, pore size distribution and surface area alterations of the electrodes before and after modification will be discussed. This, together with electrochemical measurements, will show a substrate-dependent AT redox activity which establishes significant differences on the amount and stability of AT present, and more importantly on the performance of the resulting supercapacitor device. In the second part of this chapter, a study of the impregnation with a smaller size molecule; 1,4-benzoquinone (p-BQ) (See Fig.4.1b) will be detailed. This

method contains the quantification of the amount of quinone added, the modification of the carbon porous structure, and the study of the electrochemical performance. This study clearly shows the dependence of the impregnation method on the particular quinone used.[8]

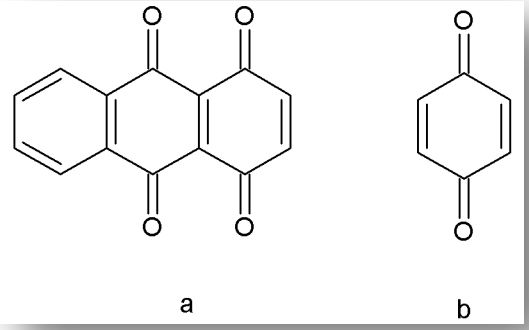

Figure 4.1 Molecular structure of AT (a) and p-BQ (b)

4.2 Characterization and performance evaluation of supercapacitor electrodes modified with AT

In this part of this chapter, the impregnation method with AT molecules on different carbon substrates will be described. This part involves the quantification of AT adsorbed, the study of the electrochemistry of AT in 0.5M H_2SO_4 media, the modification of the carbon porous structure, and the study of the electrochemical performance of symmetric SC device. This study confirms a substrate-dependent performance of SCs with AT modified carbon electrodes.

The electrochemical characterization of supercapacitor devices based on pristine and modified electrodes was performed by using cycling voltammetry (CV), galvanostatic charge-discharge (CD) and electrochemical impedance technique (EIS).

4.2.1 Electrode fabrication and modification method

Picactif BP 10 (hereby referred as Pica) and Vulcan XC-72R (CABOT Corporation, hereby referred as Vulcan) are commercially available activated carbons which we used as received for disk-shaped electrode fabrication. Pica or Vulcan Carbon (70 wt.%), acetylene black (100% compressed, >99.9%, Alfa Aesar, 20 wt.%) and Polytetrafluoroethylene (PTFE 60 wt.% dispersion in water, Sigma–Aldrich, 10 wt.%) were mixed and grinded using 2-propanol (>99.5%, Scharlau) until reduced to pasty mass. PTFE was used as a binder and acetylene black carbon was added as a conductive agent for carbon paste preparation.

The paste was coated on a coin shape stainless steel mesh current collector (AISI 3024, 97% open, Good-fellow) (1 cm in diameter). The electrodes were then pressed with a uniaxial press (CARVER model 3853-0) applying a pressure of 450 kg cm^{-2} and dried at room temperature overnight. Average mass of dry electrodes was 15–20 mg cm^{-2}. Pristine carbon electrodes were soaked in 5×10^{-3}M AT (Sigma-Aldrich) in acetonitrile (>99.5%, Sigma–Aldrich) with different immersion periods and dried at room temperature around 3 hours.

4.2.2 Optimization of AT loading on different carbon substrates

The electrodes can be loaded up to a maximum of 0.75 and 0.55 wt% of AT for Pica and Vulcan respectively, where they reach an equilibrium in which adsorption–desorption rate between substrates and soaking solutions becomes equal. Pica electrodes reach constant weight after 180 min immersion time (Fig. 4.2a), while Vulcan electrodes reach equilibrium after only 5 min (Fig. 4.2b).

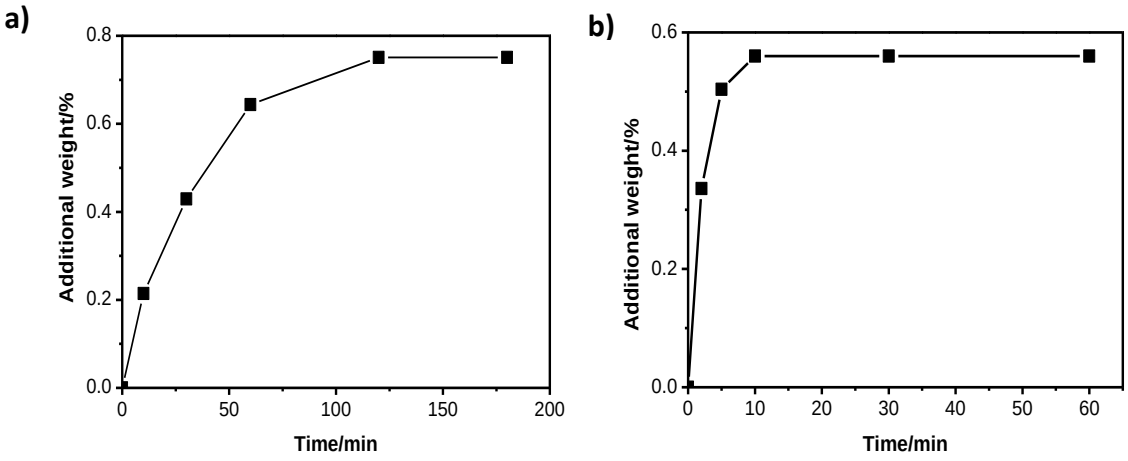

Figure 4.2 Amount of AT grafted vs. time on (a) Pica electrodes and (b) Vulcan electrodes.

The fast AT adsorption kinetics showed by Vulcan may be attributed to both a different affinity, possibly through a different adsorption mechanism than that taking place at Pica, and also the lack of diffusion limitations through micropores, as further discussed below.

After each immersion time, the specific capacitances of modified electrodes were measured for both carbons and the results show that with the amount of AT adsorbed (Fig.3)

Taking into account these results, all the experiments below were performed with either pristine electrodes or electrodes modified with the maximum possible amounts of AT (0.75 wt.% for Pica and 0.55 wt.% for Vulcan).

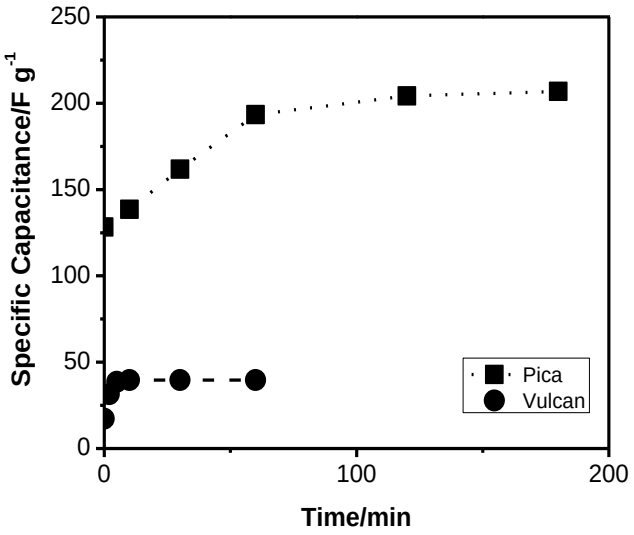

Figure 4.3 Specific capacitances of Pica and Vulcan electrodes upon modification with various amounts of AT calculated from cyclic voltammetry at 10 mV s^{-1} in aqueous H_2SO_4 (0.5 M) electrolyte.

4.2.3 Physical and structural characterization

Porous texture of the modified and unmodified electrodes was analysed by N_2 adsorption at 77 K (Autosorb-1, Quantachrome Instruments). The analyses were performed using whole electrode paste material including binder and acetylene black. Before the measurements, the sample was outgassed under vacuum at 120^{o}C overnight. The specific surface area was calculated from the isotherm by applying the BET equation (S_{BET}). The micro and meso pore volume and the pore size distribution were obtained from N_2 adsorption isotherm by applying the QSDFT model.

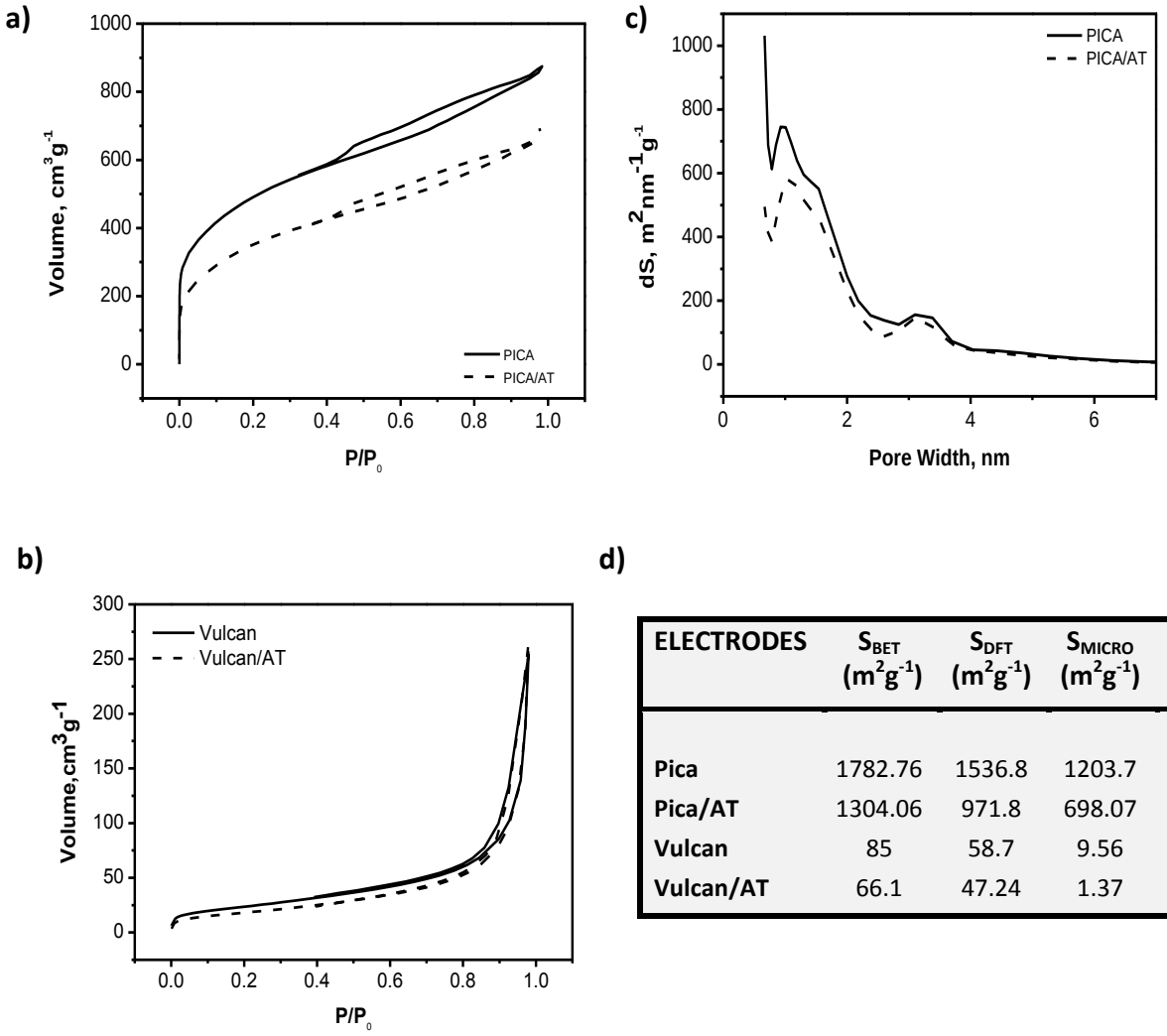

ELECTRODES	S_{BET} (m^2g^{-1})	S_{DFT} (m^2g^{-1})	S_{MICRO} (m^2g^{-1})	S_{MICRO} (%)
Pica	1782.76	1536.8	1203.7	78
Pica/AT	1304.06	971.8	698.07	71.9
Vulcan	85	58.7	9.56	16.2
Vulcan/AT	66.1	47.24	1.37	2.9

Figure 4.4 N_2 adsorption isotherms of unmodified and AT-modified (a) Pica electrodes for loading of 0.75 wt.% and (b) Vulcan electrodes for loading of 0.55 wt.%; (c) pore size distribution of unmodified and AT-modified Pica electrodes for loading of 0.75 wt.% and (d) textural properties for all electrodes.

Figure 4.4a demonstrates the nitrogen adsorption isotherms of pristine and AT grafted Pica carbon, and both curves are well correlated with both type I and type IV isotherms within the IUPAC classification of adsorption isotherms [9]. Substantial volume adsorbed at low P/P_0 is a characteristic of extended microporous structure [10]. After modification, significant volume decrease was detected at low P/P_0. The pore size distribution graph (Fig. 4.4c) confirms the presence of micropores (<2 nm) and the contribution of a significant amount of mesopores (2–4 nm) to the total surface area as well. Additionally, both BET

and DFT surface area decrease from 1782.76 to 1304.06 $m^2 g^{-1}$ and 1536.8 to 971.8 $m^2 g^{-1}$ respectively upon grafting. The total and micropore area loss were calculated according to DFT model. A substantial amount of the total DFT area lost (36.8%) comes from micropores (Fig. 4.4d) which may be blocked by AT molecules. Nitrogen adsorption isotherm of Vulcan electrodes is presented in Fig. 4.4b. The shape of isotherm shows a type III curve, which describes the adsorption on mesopores and macropores. Vulcan carbon is not a microporous carbon and it has very small BET and DFT surface area (Fig. 4.4d). The loss of 20% DFT surface area can be attributed to AT adsorption.

4.2.4 Electrochemical Characterization

4.2.4.1 Cyclic voltammetry analysis of AT and modified carbons

In order to have a better understanding of the electrochemical behavior of impregnated AT on the two different carbons, cyclic voltammetry (CV) experiments were performed at both modified carbon electrodes in aqueous sulphuric acid solution. Electrochemistry of AT in solution was studied by using three-electrode cell with glassy carbon (BASI Corp. 3 mm in diameter) as a working electrode in 0.5M H_2SO_4 solution. Before experiments, this electrode was polished with 0.1 and 0.05 µm alumina slurry polishing solution and then rinsed with copious amounts of purified water (Milli-Q system, Milli-pore).

The redox chemistry of quinones in aqueous solution has been well described as a one-step $2e^-$, $2H^+$ reaction giving the hydroquinone as the final product [11]. Figure 4.5 shows the cyclic voltammetry of AT in 0.5 M H_2SO_4 solution with sweep rate of 50 mV s^{-1}. Highly reversible and quasi-reversible redox waves were observed around −0.253 V and 0.844 V (vs. Ag/AgCl) with peak separations of 44 mV and 147 mV respectively (Fig. 4.5d). These results suggest that AT redox mechanism follows the characteristic aqueous redox mechanism of typical para-benzoquinone (p-BQ) type but since it has two quinonoid units, every single molecule allows 4-electron transfer.

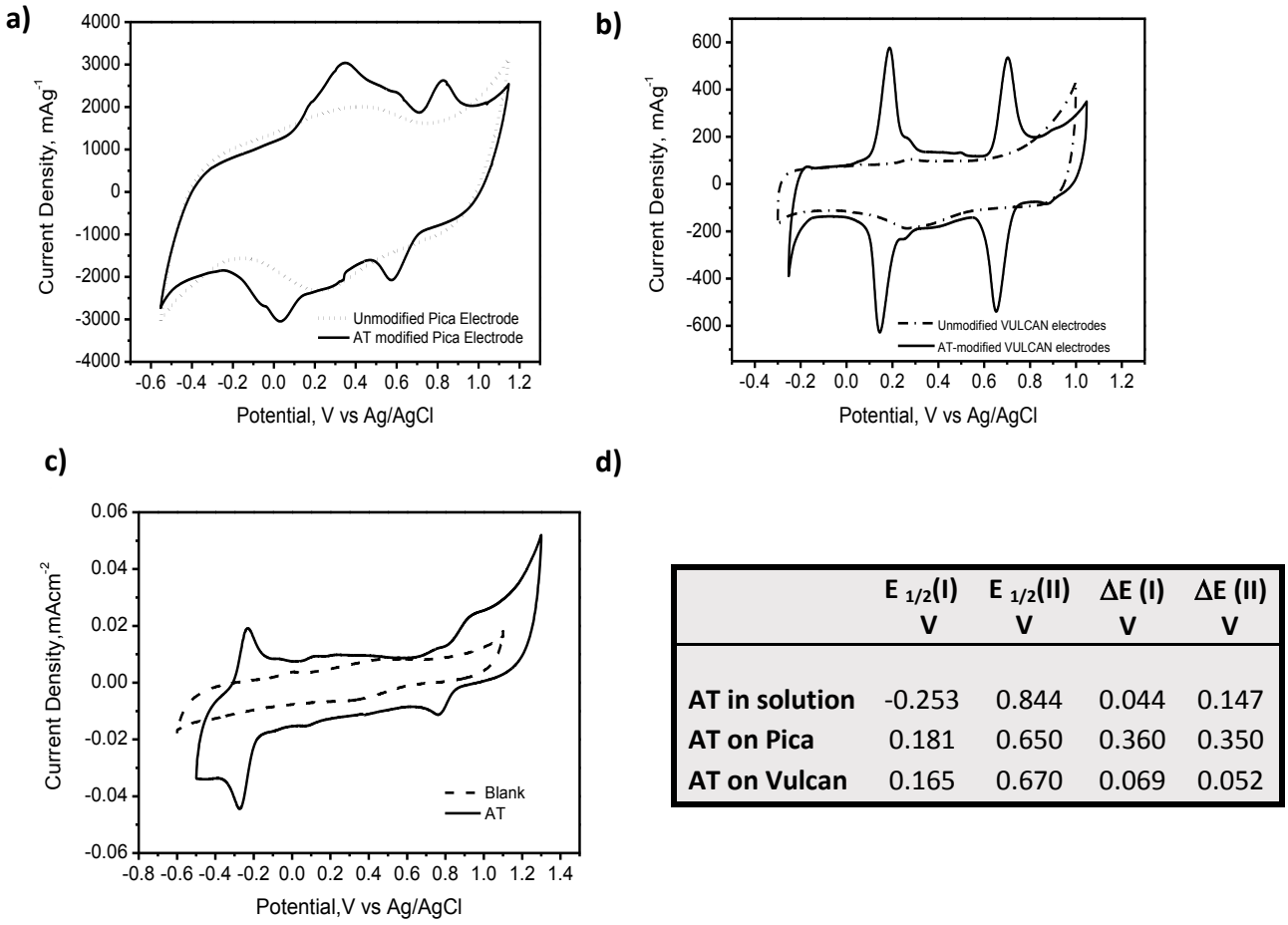

	$E_{1/2}$(I) V	$E_{1/2}$(II) V	ΔE (I) V	ΔE (II) V
AT in solution	-0.253	0.844	0.044	0.147
AT on Pica	0.181	0.650	0.360	0.350
AT on Vulcan	0.165	0.670	0.069	0.052

Figure 4.5 Cyclic voltammetries in aqueous H_2SO_4 (0.5 M) electrolyte: unmodified and modified Pica (a) and Vulcan (b) electrodes at optimum grafting time. Scan rate: 10 mV s^{-1}; (c) 1.67 × 10^{-4}M AT using glassy carbon working electrodes at 50 mV s^{-1}; (d) half wave potentials and peak separations extracted from CV experiments**.**

Compared to the voltammetries of AT-grafted carbons also shown in Figure 4.5, half wave potentials ($E_{1/2}$) of first and second redox couple at modified electrodes are shifted towards less negative and less positive values in comparison with aqueous electrolyte results respectively. Thus, AT grafting on both carbons complicates the oxidation of AT, while later the first radical anion is slightly destabilized. This kind of behaviour can be attributed to a partial charge transfer from AT to the carbon support. Moreover, the remarkable positive potential value for the second redox unit (0.844 V), can be attributed

to a better stabilization of the anion radical in AT due to the more extended π-conjugation of this molecule. It is also noteworthy the wider anodic/cathodic peak separation and the broad redox peaks for redox reaction on Pica, which may respectively be attributed to an additional kinetic barrier and slow electron transfer on this particular substrate.

4.2.4.2 Cycling rate performance

Cyclic voltammetries were performed at different scan rates by using 0.5 M H_2SO_4 electrolytes for all electrodes.

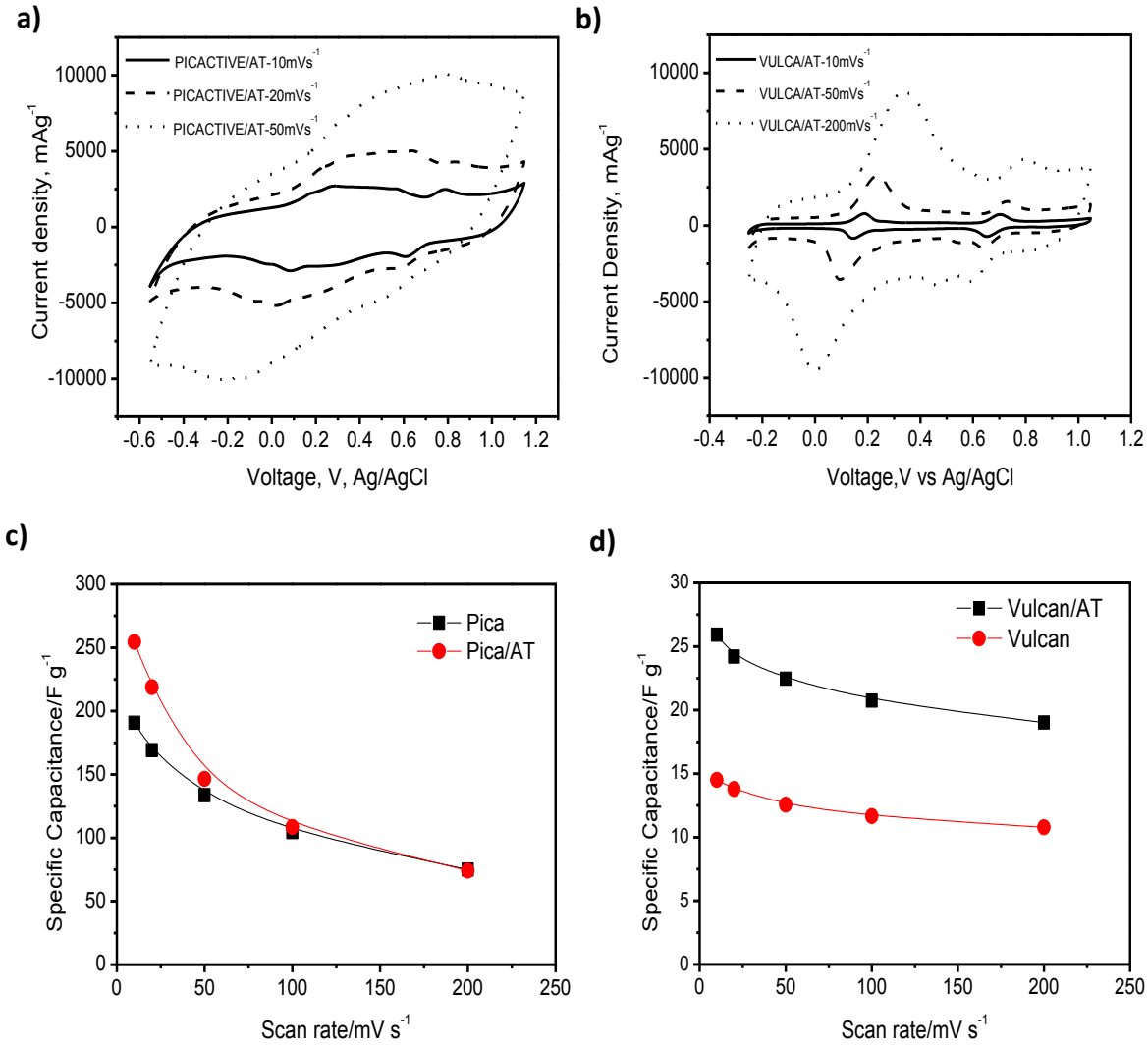

Figure 4.6 Cyclic voltammetries of AT modified (a) Pica and (b) Vulcan electrodes in aqueous H_2SO_4 (0.5 M) electrolyte; capacitance values extracted from CVs at different scan rates of unmodified and AT modified (c) Pica and (d) Vulcan electrodes.

Figure 4.6a and 4.6b illustrates the scan rate dependence of the capacitance of AT grafted Pica and Vulcan carbon electrodes. As can be clearly observed, in the case of Pica electrodes the CV shapes are distorted even at 50 mV s^{-1}. Compared with pristine Pica electrodes, the decrease of the total capacitance is much more important for the modified carbon at higher scan rates (Fig. 4.6c), indicating poorer kinetics for the AT redox processes on Pica carbon substrate. Vulcan electrodes exhibit excellent cycling rate stability up to very high scan rates such as 200 mV s^{-1}, even after AT modification (Fig. 4.6b). Nevertheless, AT redox peak separation increases with the scan rate, thus showing kinetic limitations which are confirmed when extracting capacitance values at different rates (Fig. 4.6d), but which are much less important than those present on Pica electrodes. Previously, Bélanger at al. reported that for covalently bound species the decrease of the total capacitance becomes much more important for the highest anthraquinone loaded electrodes and at high scan rates [12].

4.2.4.3 Galvanostatic charge-discharge and cycle life stability

Electrodes were further investigated by galvanostatic charge/discharge experiments at 200 mA g^{-1} Figure 4.7a presents potential–time plots recorded for a Pica and AT-modified Pica carbon electrode with a 0.75 wt.% AT loading, while Figure 4.7b presents potential–time plots recorded for a Vulcan and AT-modified Vulcan carbon electrode with a 0.55 wt.% AT loading. In both cases, the influence of additional charge storage due to AT electrochemistry is seen as a gentler slope in the curves.

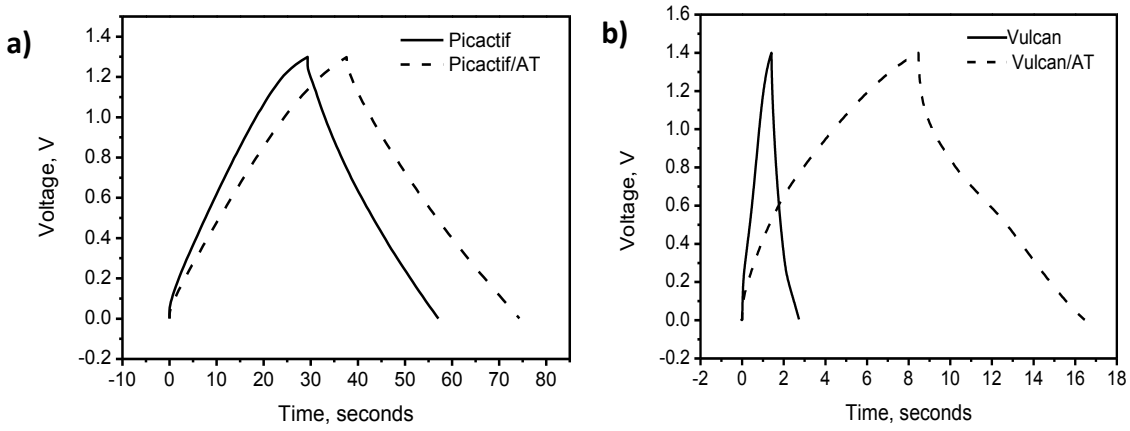

Figure 4.7 Potential vs. time charge/discharge curves during galvanostatic cycles of the symmetric cells at 200 mA g^{-1} with (a) unmodified and AT modified Pica electrodes; and (b) unmodified and AT modified Vulcan electrodes.

The variation of the capacitance of pristine electrodes and AT loaded Pica and Vulcan electrodes during 1000 charge/discharge cycles is shown in Figure 4.8.

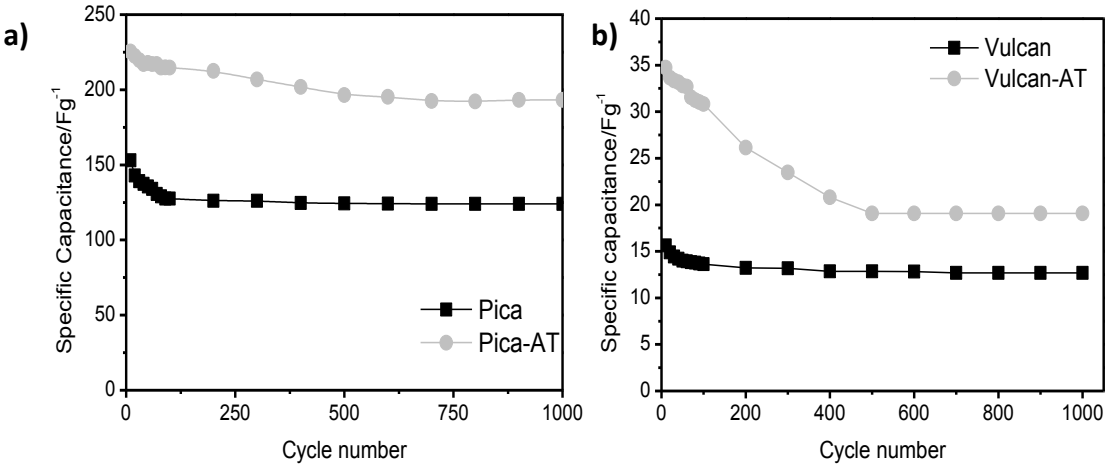

Figure 4.8 Discharge capacitance as a function of cycle number for the symmetric cell in H_2SO_4 (0.5 M) aqueous electrolyte at 200 mA g^{-1} with unmodified and AT modified (a) Pica and (b) Vulcan electrodes.

Modified Pica electrodes lose 10% of the initial specific capacitance during the first 700 cycles (Fig. 8a), and afterwards capacitance is quite stable up to 1000 cycles, while pristine Pica loses 3% of its capacitance after 1000 cycles under the same conditions. The small amount of additional capacitance

loss in modified Pica indicates very effective immobilization and excellent chemical stability of the redox system on this substrate. The capacitance fades out quite rapidly for modified Vulcan electrodes, and after 500 cycles it loses approximately 40% of its initial capacitance, afterwards stabilizing up to 1000 cycles, whereas the capacitance of unmodified Vulcan decreases by 7% upon 1000 cycles (Fig. 4.8b). This reveals the fact that Vulcan carbon is less able than Pica to adsorb this redox species effectively. One possible reason may be a process resembling an electrochemical grafting taking place on the physical mixture of Pica (a highly functionalized carbon) and AT [13], different from the case of the non-functionalized Vulcan carbon, which would have more weakly adsorbed AT species that would desorb after the initial charge/discharge cycles. Nevertheless, even after 1000 cycles the specific capacitance of both AT modified Pica and AT modified Vulcan are around 50% higher than those of pristine carbons, thus showing the good stability and capacitance improvement present in both modified electrodes.

4.3 Characterization and performance evaluation of supercapacitor electrodes modified with p-BQ

In this part of this chapter, impregnation of activated carbon electrode with p-BQ was studied. The method includes the quantification of the amount of quinone added, the modification of the carbon porous structure, and the study of the electrochemical performance. This study clearly shows the dependence of the impregnation method on the particular quinone used.

4.3.1 Electrode fabrication and modification technique

Disk-shaped carbon electrodes were prepared prior to modification (Fig.4.9a). All details about electrode fabrication procedure were explained in experimental part of this thesis (See Chapter 3). The method for the modification of the electrodes was the same as in the first part of this chapter for impregnation with 1,4,9,10-anthracenetetraone (AT), except that in this study, the soaking p-BQ

solution was prepared in dimethylsulfoxide (DMSO) (>99.9%, Sigma-Aldrich) with a concentration of 1.5 M(Fig.4.9b) and dried under vacuum at 40 ^{o}C for 3-4 hours.

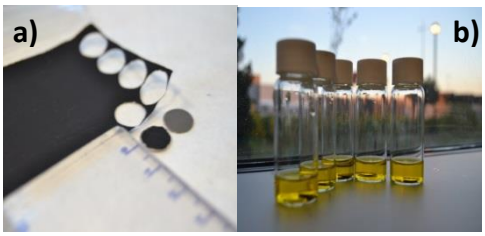

Figure 4.9 Disk-shaped carbon electrodes (a) and solution modification technique (b)

4.3.2 Optimization of p-BQ loading

UV-Vis characterization was performed in order to determine the amount of p-BQ adsorbed during each immersion time. Measurements were acquired in a Perkin Elmer Lambda 1050 spectrometer and the absorbance of initial solutions was found to decrease due to the decreased concentration of p-BQ after adsorption on electrodes (Fig. 4.10a). The amount of p-BQ adsorbed is calculated by applying the Beer – Lambert law to the decrease of p-BQ observed in soaking solutions after each immersion time (Fig.4.10b)

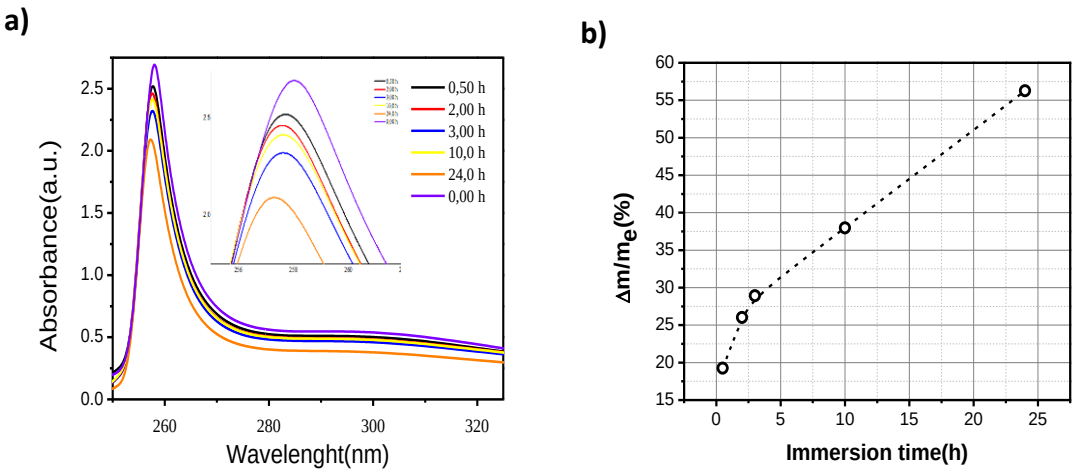

Figure 4.10 UV-VIS Spectra obtained upon immersion of electrodes into soaking solutions (a) and amount of p-BQ adsorbed during different immersion times, (b).

Thus, the amount of p-BQ which can be adsorbed is much higher than in the case of 1,4,9,10-anthracenetetraone (AT). The electrodes can be loaded with p-BQ up to at least 55 wt.% after 24 h, with an initial fast adsorption rate up to 3 hours of soaking and a nearly linear adsorption behavior afterwards (Fig. 4.10b).

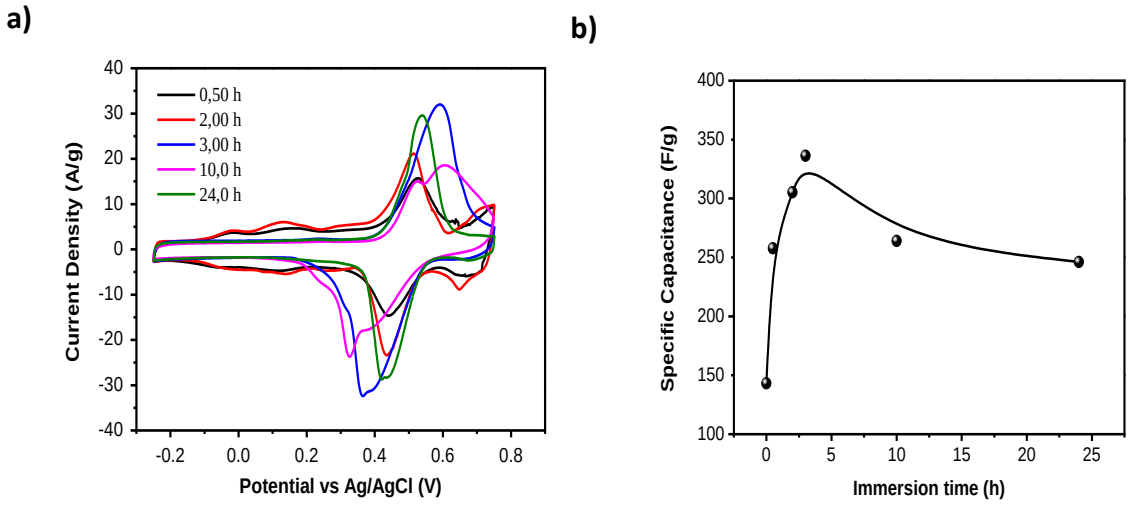

Figure 4.11 Specific capacitance values measured from cyclic voltammetries in aqueous 0.5 M H_2SO_4 at 20 mVs^{-1}.

After each immersion time, the specific capacitances of modified electrodes were measured by performing CV experiments at 20 mVs^{-1} in 0.5 M H_2SO_4 solution (Fig. 4.11a). The optimal soaking time is determined to be 3 h (Fig.4.11b), where a loading of 30 wt.% of p-BQ is achieved with maximum specific capacity value.

Table 4.1 demonstrates the relationship among specific capacity, surface area and adsorbed amount of p-BQ with respect to different immersion times. Equation 1.1 was employed to calculate the amount of electrochemically active p-BQ adsorbed into the pores of activated carbon electrode.

$$Q_{faradaic} = ne^- F \quad \Gamma\ (molcm^{-2})\ S\ (m^2g^{-1}) \qquad \textbf{(1.1)}$$

Here, n is the number of moles of electrons transferred, F is the Faraday constant, S refers to the electroactive surface for ion double layer adsorption, Γ is the surface density of grafted molecules.

Charge accumulated was determined by integrating the area under the curve of CV experiments at 20mV/s (Fig 4.11a).

Immersion Time (hours)	Specific Capacity (F/g)	Surface Area (m^2/g)	Amount p-BQ (mg)
0.50	266.598	1318.106	0.311
1.00	305.025	1289.231	0.324
3.00	329.173	1153.743	0..365
10.00	252.895	1022.220	0.309
24.00	163.345	940.740	0.130

Table 4.1. Specific capacitance, BET surface area and the amount impregnated p-BQ relation with different immersion times

Table 4.1 values show that the surface area of carbon electrodes decreases with increasing immersion time. However there is an obvious correlation between the specific capacitance and the electrochemically active amount of p-BQ moieties. It is clear that the specific capacitance reaches its maximum after 3 hours of immersion, precisely when a maximum amount of active p-BQ units are identified. This table verifies the fact that not all impregnated species are electroactive and thus, not all the amount of material adsorbed contributes to the specific capacitance.

This is a much higher amount of adsorbed quinone than the one previously reached with AT, possibly due to the lower size of p-BQ, which facilitates its penetration into micropores. Taking into account these results, all the experiments below were performed with either pristine electrodes or electrodes modified after soaking with p-BQ for 3 hours.

4.3.3 Porous texture and pore size distribution of modified and unmodified electrodes

The porous texture of the modified and unmodified electrodes was analysed by N_2 adsorption at 77 K (Autosorb IQ2, Quantachrome Instruments). The analyses were performed using whole electrode paste material including binder and acetylene black likewise AT case. Before the measurements the sample was outgassed under vacuum at 120^{o}C overnight. The specific surface area was calculated from the isotherm by applying the BET equation (S_{BET}). The micro- and meso-pore volume and the pore size distribution were obtained from N_2 adsorption isotherm by applying the QSDFT model.

Figure 4.12a demonstrates the nitrogen adsorption isotherms of pristine and p-BQ grafted Pica carbon. Both curves are well correlated with both type I and type IV isotherms within the IUPAC classification of adsorption isotherms[9]. Volume adsorbed at low pressures demonstrates a extended microporous structure [10]. After modification, significant volume decrease was detected at low pressures. The pore size distribution graph (Fig. 4.12b) confirms the presence of micropores (< 2 nm) and the contribution of a significant amount of mesopores (2-4 nm) to the total surface area as well. Additionally, both BET and DFT surface area decrease by 18.6% and by 23.6% respectively upon grafting, which are lower diminutions than in the case of AT, due to the smaller molecular size of p-BQ compared to AT. The total and micropore area loss were calculated according to the DFT model. Most of the total DFT area lost comes from micropores (Fig. 4.12c) which, as is usually reported, are blocked by the added quinones, in this case p-BQ molecules

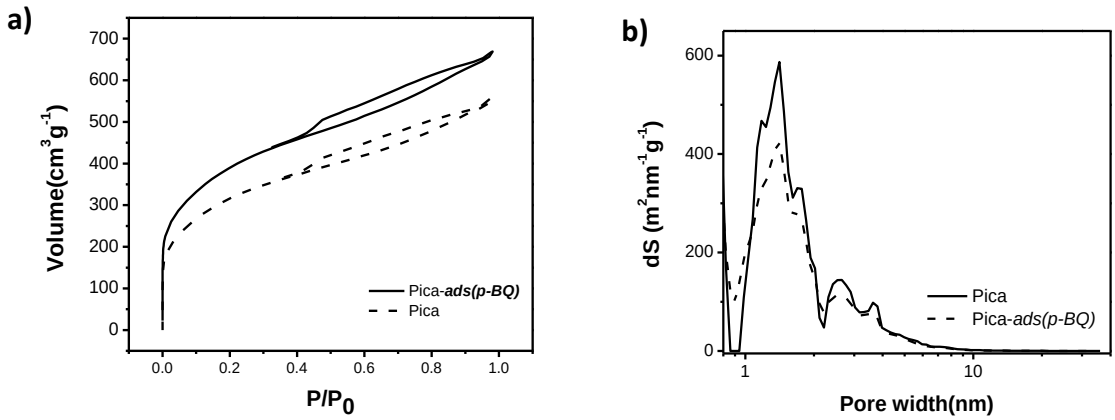

c)

ELECTRODES	S_{BET} (m^2g^{-1})	S_{DFT} (m^2g^{-1})	S_{MICRO} (m^2g^{-1})	$\%S_{MICRO}$
Pica	1416.62	1060.25	774.65	73.06
Pica-*ads(pBQ)*	1153.74	809.81	560.75	69.24

Figure 4.12 N_2 adsorption isotherms of unmodified and p-BQ-modified Pica electrodes, (b) pore size distribution of unmodified and p-BQ-modified Pica electrodes, and (c) textural properties of electrodes.

4.3.4 Electrochemical characterization of supercapacitor electrodes

4.3.4.1 Impedance Spectroscopy

Nyquist plots of symmetric cells are illustrated in Figure 4.13. The Nyquist plot (Fig. 3a) consists mainly of three parts: The first one is the noticeably depressed semicircle. The shape of the semicircle depends on the adsorption kinetics of ions at the micro/mesoporous carbon electrode and resistance properties such as resistance of material, mass transfer resistance inside the macro/mesoporous carbon structure, as well as on the mass transfer resistance in the micropores at higher frequency. The second one is the double-layer capacitance region (“knee” at low frequencies f<1Hz), obtained by the finite length effect, and the last one is the so-called “porous” region.

In symmetric cells constructed using pristine and modified electrodes, semicircles of very small radius are obtained at the high frequency region, and a straight line is obtained in the low frequency region. At

very high frequencies, the intercept at the real axis is described as equivalent series resistance (ESR). ESR values for the cell constructed with pristine and p-BQ modified carbon are 0.743 and 0.813Ωcm^2 respectively. ESR for the modified electrode system is slightly bigger than the unmodified one, which can be associated with the p-BQ loading. The impedance spectra at low frequencies represent the capacitive behaviour of the electrode and approach a 90° vertical line likewise in an ideal capacitor in both cases.

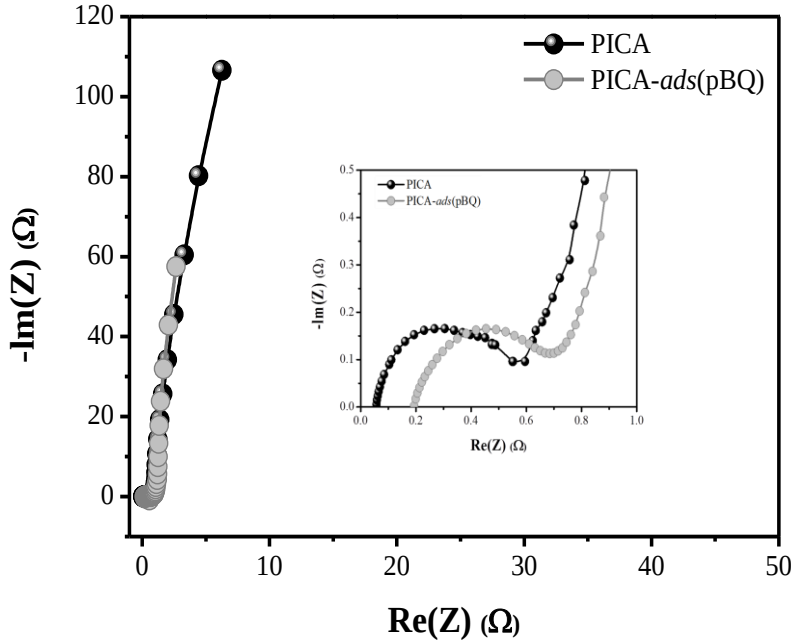

Figure 4.13 Nyquist plots for Pica and p-BQ modified Pica electrodes. The inset shows the high frequency region of impedance

4.3.4.2 Capacitance-scan rate relation

Cyclic voltammetries (CVs) were performed at different scan rates in 0.5 M H_2SO_4 electrolytes. Figure 4.14a displays the CVs of pristine Pica electrodes performed at different potential scans.

As can be observed the CV shapes of pristine electrodes are not distorted and have rectangular shapes with variation of intensities versus scan rate typical of electrical double layer capacitors. The shape of CVs of modified electrodes has clear peaks due to the added redox reactions of p-BQ, and these peaks

are clearly distorted at 50 mV s^{-1}. In this case, CVs are less distorted than those of Pica carbon modified with AT in the same scan rate range (Fig.4.14b). Lastly, Figure 4.14c shows the CV curves of unmodified and p-BQ modified Pica upon 3 hours modification. The important difference between the area encircled by CV stems from the additional pseudocapacitance of p-BQ.

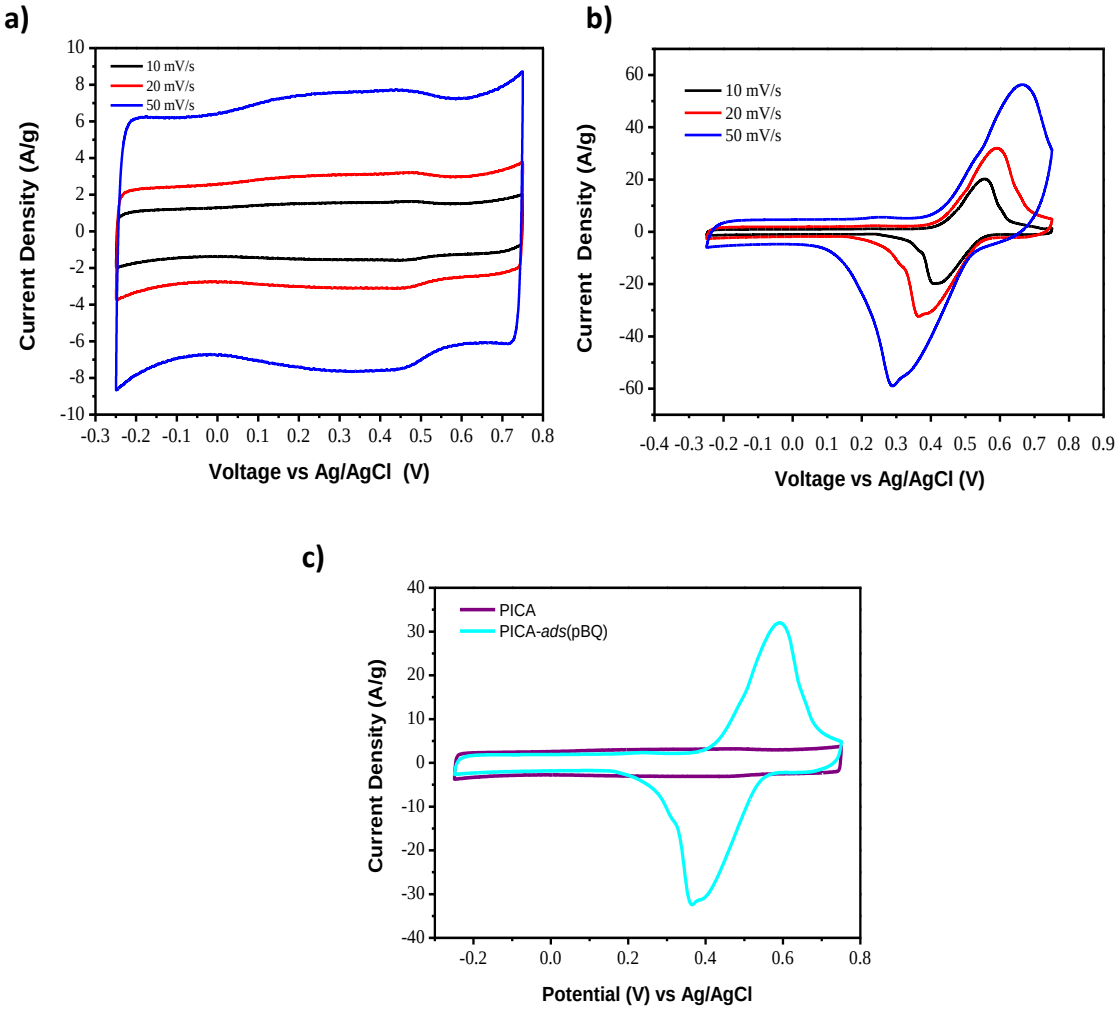

Figure 4.14 Cyclic voltammetries at different scan rates of: (a) Pica, and (b) p-BQ modified Pica electrodes in aqueous H_2SO_4 (0.5 M) electrolyte.

Figure 4.15 illustrates the scan rate dependence of the capacitance of pristine and p-BQ modified Pica electrodes. Even though the decrease in the total capacitance of p-BQ modified electrodes is more

important than the pristine carbon at high scan rates (Fig. 4.15a), the overall capacitance loss with respect to pristine electrode is only 15%.

Figure 4.15b shows the capacitance values obtained from CVs at the same scan rate for p-BQ modified Pica electrodes at different loading ratios. This study reveals that the loss in specific capacitance at higher scan rates is getting bigger as the p-BQ loading increases (Fig 14.15b).

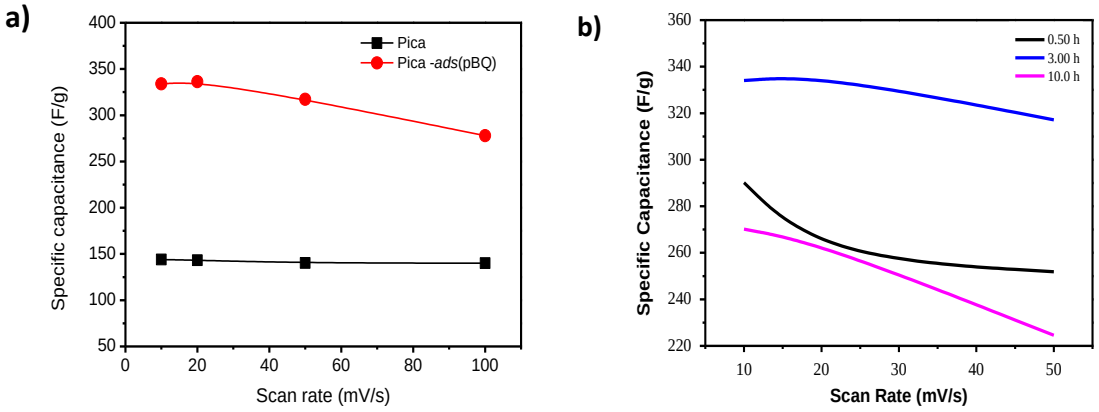

Figure 4.15. Specific capacitance values extracted from cyclic voltammetries at different scan rates of unmodified and Pica electrodes soaked in p-BQ for 3h (a), variation in specific capacitance of the electrodes prepared at different immersion times at 50 mVs^{-1} scan rates (b)

4.3.4.3 Galvanostatic discharge capacity of symmetric and asymmetric cells

Symmetric and asymmetric cells were prepared for measuring galvanostatic discharge capacity. Since p-BQ reduction occurs approximately around 0.5 V, an asymmetric type capacitor with proper mass balance has been prepared to acquire additional energy from the system and compare with the symmetric type device. The following formula was implemented in order to calculate the mass ratio between positive and negative electrodes.

$$m^{-}C_S{}^{-}\Delta E^{-} = m^{+}C_S{}^{+}\Delta E^{+} \qquad \textbf{(4.2)}$$

where:

m: mass of the electrodes (g)

C_S: Specific capacitance(F/g)

ΔE: working potential of each electrode (V)

Herein, negative(-) and positive (+) signs refer to the electrode polarization.

Equation 1 was transformed in the following form (eq.2) and electrode mass balance was calculated by numerical determination of specific capacitance and voltage window for each electrode. These values were obtained from CV experiments performed in 3-electrode system. For asymmetric supercapacitors, the mass ratio of positive and negative electrode was determined as 1 at which maximum capacitance within the stability window of each electrode has been achieved.

$$\frac{m_{pica}^{-}}{m_{pica-ads(pBQ)}^{+}} = \frac{(329.173F/g)((+0.7)-(+0.4))V}{(141.683F/g)((+0.4)-(-0.3))V} \qquad \textbf{(4.3)}$$

$$\frac{m_{pica}^{-}}{m_{pica-ads(pBQ)}^{+}} = 1.00$$

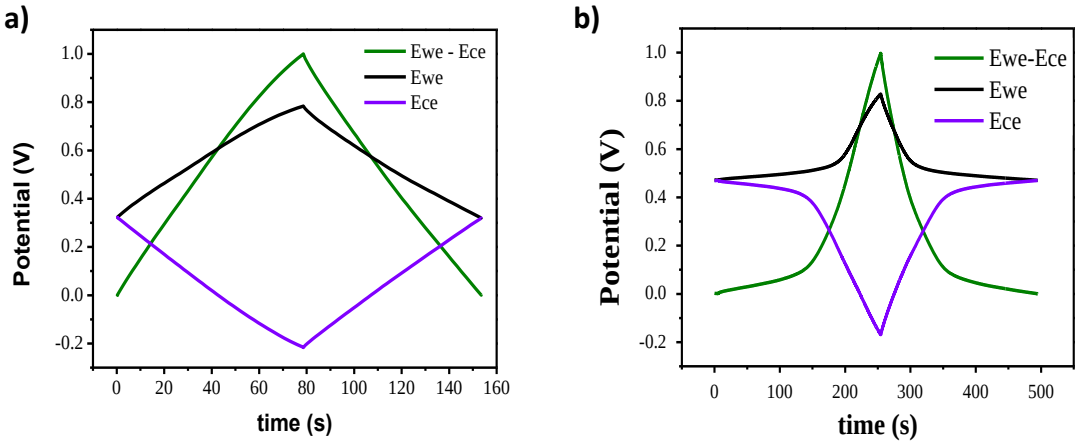

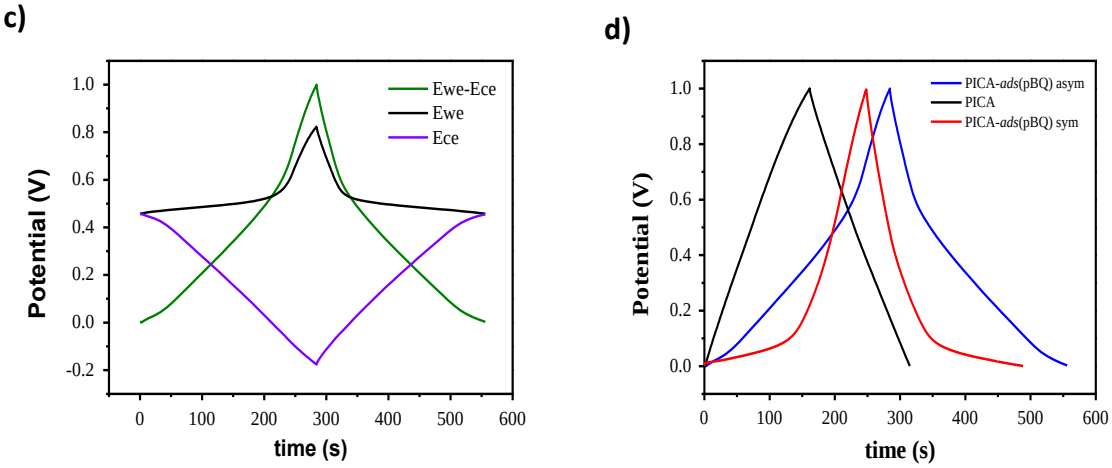

Figure 4.16 Galvanostatic charge-discharge curves of symmetric cell constructed by Pica (a) and p-BQ modified Pica (b) and asymmetric cell fabricated by Pica-pBQ modified positive electrode and Pica pristine negative electrodes. Comparison of symmetric and asymmetric cells (d).Current load: 200 mA/g for each experiment.

Figure 4.16 displays CD profiles of symmetric Pica (Fig.4.16a) and p-BQ modified Pica electrodes (Fig.4.16b). The cell potential and the potential of each side were observed using a Ag/AgCl reference electrode. In the case of the modified symmetric capacitor, a plateau was observed around 0.5 V where p-BQ redox activity is taken place. However in the case of asymmetric capacitor, the negative electrode swings in a wider potential window since it does not contain any redox active species. The discharge time for the asymmetric configuration is clearly longer than in the symmetric type, which is the indication of the additional energy that is accumulated due to the higher voltage difference acquired in this type of combination (Fig.4.16d). This additional charge can further be associated with the conserved double layer capacitance of the negative electrode because no blockage of surface with p-BQ species occurs and the surface area remains accessible to the ions in the electrolyte.

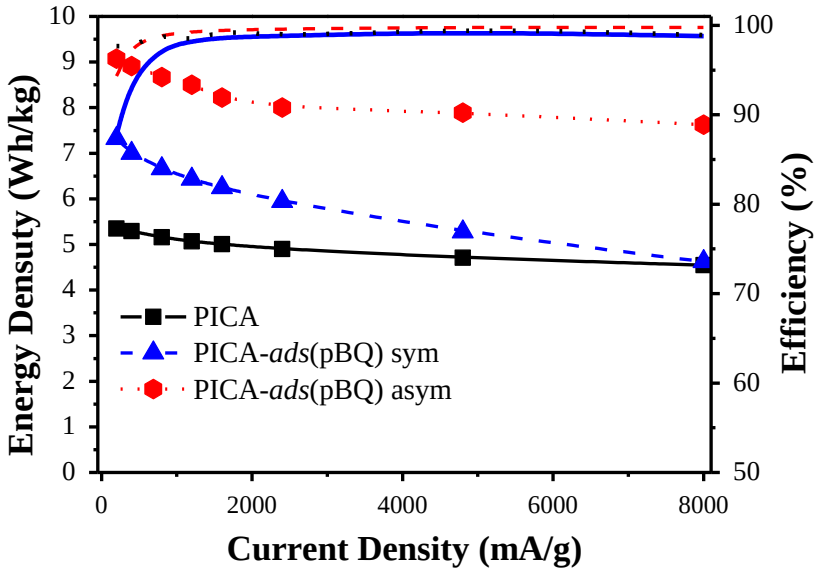

Figure 4.17 Effect of different current loadings on energy density and efficiency for Pica and p-BQ modified Pica symmetric cell and asymmetric cell.

Galvanostatic CD behavior at different current loads was also studied and the capacitance relation to different current densities was displayed in figure 4.17 with corresponding coulombic efficiencies of each system. The capacity gained due to p-BQ redox activity was suppressed at high current loads for the symmetric cell constructed with modified electrodes on both side of the cell. On the other hand, asymmetric cells fabricated by using Pica on the negative side and p-BQ modified Pica on the positive side show highly stable current rate stability. This behaviour can be correlated with the redox potential of p-BQ, which lies in the range of the positive electrode working potential. Since the negative electrode does not contain electro-active p-BQ species, the rate capability of the system is independent of the kinetics of this redox activity. It is well-known that the ion adsorption-desorption process is always faster than any faradaic type electron transfer. Overall coulombic efficiencies of the systems are close to 100 % at different ranges of current densities.

4.3.4.3 Performance comparison of symmetric and asymmetric cells

Power and energy performance of both symmetric and asymmetric type device was compared to pristine Pica electrode symmetric device in Ragone plots.

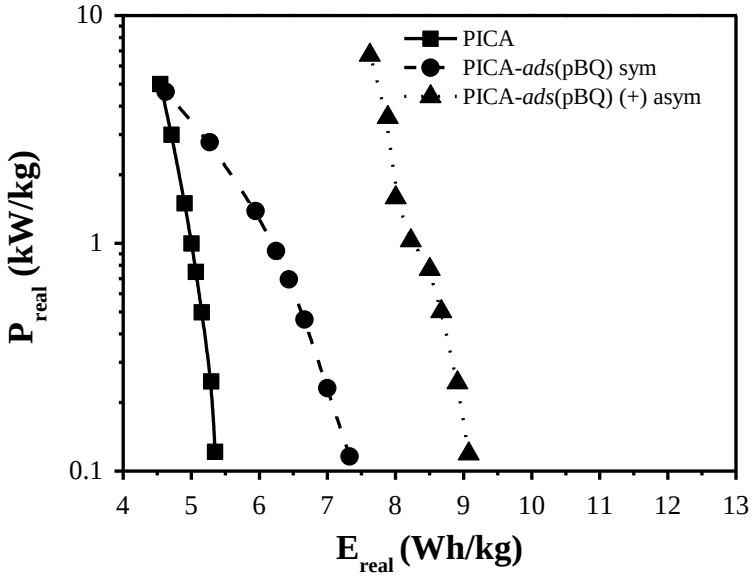

Figure 4.18 Performance plot of symmetric cells made of Pica and Pica-p-BQ modified electrodes and asymmetric cell of modified Pica electrodes.

The energy performance of the symmetric device decreases in a similar fashion as in Figure 4.17, which shows the poor performance of the symmetric device at high current loads (Fig.4.18). Thus, the negative electrode can be considered as a limiting factor in terms of energy density of the system.

The comparable power characteristics of symmetric Pica and asymmetric cell can also be seen in the Ragone plot. Curves from both symmetric and asymmetric capacitors showed a similar trend in power density except that the energy density of asymmetric device is almost double for the asymmetric device compared to the Pica symmetric cell.

4.4 Summary

In this chapter, a simple adsorption technique was demonstrated by impregnation of AT and p-BQ on the surface of different carbon substrates. Performance of supercapacitor devices made by modified

carbons and pristine carbon was evaluated and compared. In the first part of this chapter high surface area functionalized Pica carbon and low surface area Vulcan carbon electrodes were modified with different loadings of AT (maximum of 0.75 wt.% for Pica and 0.55 wt.% for Vulcan electrodes). Variations of redox peak potentials and reversibility were observed on carbon-supported AT in comparison with AT in solution. Those differences were attributed to different properties of each carbon. Extended charge/discharge cycling behavior shows a loss of 10% of total capacity for modified Pica carbon and 40% for modified Vulcan carbon after 1000 cycles at 200 mAg^{-1} compared to a 3% and 7% loss of unmodified carbons in the same conditions.

Thus, the mesoporous structure and the non-functionalized surface of Vulcan carbon give rise to a more unstable grafting, while Pica carbon shows a fairly stable grafting. For both, the total capacitance is nearly doubled after modification with AT even after 1000 cycles at 200 mA g^{-1}.

In the second part of this chapter, Pica activated carbon electrodes were modified with p-BQ by adsorption. The loading achieved up to 55 wt.% or higher, but at those loadings the layer of p-BQ adsorbed results in a lower specific capacitance. The maximum capacitance, 350 Fg^{-1} at 10 mVs^{-1}, was achieved for a load of 30 wt.%, which is a significant increase of capacitance compared to the unmodified carbon, especially taking into account that the loss of performance at high rates is low.

Extended charge/discharge cycling behaviour shows a loss of 6.5% of total capacity for modified Pica after 5000 cycles at 2 Ag^{-1}, which is similar to the one of unmodified carbon electrodes.

Results presented in this chapter points out the importance of carbon properties such as surface area, porous structure and conductivity on the stability of the modification method and SC performance. As explained in the first part of the present chapter, AT modified Pica carbon showed more effective modification and stable electrochemical performance due to its micro-porous structure. Besides, high surface area carbon substrates enable to reach significantly high specific capacitance values for SC. On

the other hand AT impregnated on Vulcan carbon demonstrated better kinetics according to its higher electronic conductivity, but specific capacitance is not good enough, even after modification, to be used as SC electrodes.

The nature of the adsorbed quinone molecule has also a great influence on the performance of the SC device. Low molecular weight quinones such as p-BQ result in a high degree of surface coverage with respect to high molecular weight compounds (AT), and such compounds potentially offer very high specific capacitance especially when the loading level is adjusted to an optimum value. In addition to that, high packing of p-BQ loading on Pica carbon also represented better stability as electrode materials for SCs.

Thus, the results presented in this chapter show the possibility to greatly increase energy densities using simple and cost effective methods such as impregnation, thus call for new strategies to promote full coverage by non-covalently bound species to take full advantage of this approach.

REFERENCES

1. P. Gomez-Romero, *Advanced Materials*, 2001, **13**, 163–174.
2. B. E. Conway, *Electrochemical Supercapacitors: Scientific Fundamentals and Technological Applications*, Kluwer Academics/Plenum Publishers, New York, 1997.
3. P. Allongue, M. Delamar, B. Desbat, O. Fagebaume, R. Hitmi, J. Pinson, and J. M. Saveant, *Journal of American Chemical Society*, 1997, **7863**, 201–207.
4. M. Pandurangappa, N. S. Lawrence, and R. G. Compton, *The Analyst*, 2002, **127**, 1568–1571.
5. R. D. L. Smith and P. G. Pickup, *Electrochimica Acta*, 2009, **54**, 2305–2311.
6. L. Madec, A. Bouvrée, P. Blanchard, C. Cougnon, T. Brousse, B. Lestriez, D. Guyomard, and J. Gaubicher, *Energy & Environmental Science*, 2012, **5**, 5379.
7. S. Isikli and R. Díaz, *Journal of Power Sources*, 2012, **206**, 53–58.

8. A. Mendez, S. Isikli, and R. Diaz, *Electrochemistry Accepted Manuscript*, 2013.

9. S. Lowell, J. E. Shields, A. T. Martin, and T. Matthias, *Characterization of Porous Solids and Powders: Surface Area, Pore Size and Density*, Kluwer Academics, 2004.

10. G. Pognon, T. Brousse, and D. Bélanger, *Carbon*, 2011, **49**, 1340–1348.

11. I. M. Ritchie and S. I. Bailey, *Electrochimica Acta*, 1985, **30**, 3–12.

12. G. Pognon, T. Brousse, L. Demarconnay, and D. Bélanger, *Journal of Power Sources*, 2011, **196**, 4117–4122.

13. K. Pirnat, R. Dominko, R. Cerc-Korosec, G. Mali, B. Genorio, and M. Gaberscek, *Journal of Power Sources*, 2012, **199**, 308–314.

Chapter 5: Modification of Carbon Electrodes via Covalent Strategies

5.1 Introduction

Although non-covalent strategies provide an easy route to modify carbon electrodes, drawbacks such as low power capability and the limited suitable electrolyte media for quinone species (quinones are highly soluble in organic media and ionic liquids) prevents their widespread applications. Consequently, there has been increased research activity in the modification of carbon surfaces by different electrochemical and chemical grafting methods. Electrochemical grafting is best described as an electrochemical process that permits the formation of an organic layer covalently attached to the surface of a conducting substrate such as carbon or metals. [1] The most well-known electrochemical procedures for derivatizing carbon surfaces consist of the electrochemical oxidation of amines [2], carboxylates [3], hydrizides [4] and electrochemical reduction of aryldiazonium salts. [5] Especially, reduction of diazonium salts is a quite straightforward and widely employed method. The aryl radicals generated upon reduction of the aryldiazonium salts attack the surface and form covalent C-C or C-O bonds. This process leads to produce highly stable modified electrodes, and a wide range of applications has already been reported in many fields such as chemistry, electrocatalysis, combinatorial chemistry and analytical sensors. [6]

Electro-reduction of diazonium salts can be thought as a very significant contribution for the further studies of carbon surface modification. Following the study of Pinson and Savéant [5] Compton´s group presented a chemical method to carry out the homogeneous reduction of diazonium salts by hypophosphorous acid, and that reaction provides an easy methodology for the derivatization of carbon powder. They demonstrated the derivatization of carbon particles with antraquinone and nitrobenzene diazonium salts throughout a covalent bonding. This chemical modification technique which proposes the reduction of diazonium salts by hypophosphorous acid has become a novel method in order to

modify different types of carbons for supercapacitor electrodes. Up to now, several studies have been presented by applying this method to supercapacitor electrodes. [7] However, derivatization of carbon particles by diazonium coupling reaction was only established for anthraquinone species according to easy accessibility of the anthraquinone precursor for this particular reaction. Thus, there is a need to find alternative processes able to establish covalent bonds between carbons and organic redox compounds such as quinones which may further increase the energy density of current supercapacitors and even may reduce the cost. These alternative techniques may also open ways to use more environmentally friendly materials.

In this chapter the use of a Friedel-Crafts reaction/oxidation was demonstrated as a suitable alternative method to diazonium salts chemistry for grafting quinones on carbons. In this study, para-benzoquinone (p-BQ, Fig.5.1) was grafted to activated carbon particles via Friedel-Crafts reaction. The main objective of this chapter is to explore how novel covalent addition strategies may result in a substantial increase of the specific gravimetric capacitance which can be maintained at high rates and for long cycling periods.

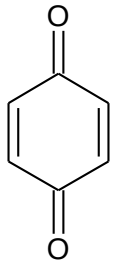

Figure 5.1 Molecular structure of p-benzouinone

5.2 Functionalization of carbons via Friedel-Crafts reaction with p-BQ

One of the main strategies to achieve higher energy densities is the combination of high surface area carbons with redox active species as a pseudocapacitive source. Such systems are associated with redox processes that are highly reversible and which can increase the capacitance up to 10 to 100 times with

respect to double layer capacitance of the same electrode due to Faradaic type reactions.[8] In this chapter, p-BQ is attached covalently to high surface area activated carbon via Friedel-Crafts reaction catalysed by Iron (III) chloride followed by oxidation, in order to explore alternative strategies for obtaining high energy density novel materials for energy storage applications. Furthermore, this strategy allows us to compare results attained via this covalent method with the results presented for the adsorption of p-BQ onto Pica activated carbon electrodes.

5.2.1 Synthesis of composite material

The Lewis acid catalysed Friedel-Crafts reaction of aromatic systems with α,β-unsaturated carbonyl compounds is one of the most powerful C-C bond-forming processes in organic synthesis, giving rise to the alkylation products resulting from the 1,4-conjugate addition.[9,10,11] When p-benzoquinones are used as electrophiles, the reaction is a formal aromatic alkenylation since the initial 1,4-addition product spontaneously enolizes to an aryl substituted hydroquinone.[12,13,14]

Friedel-Crafts alkylation reactions have already been used for covalent grafting of carbons[15] and, in connection with a project directed to extend the applications of quinones both in synthesis[16,17]and in the field of new materials,[18,19] this strategy is employed in order to introduce the quinone moiety into the Pica carbon.The electrophilic aromatic substitution occurring at the aromatic rings of the Pica carbon was effected using benzoquinone as the electrophile, in the presence of catalytic amounts of Iron(III) chloride.[20,21,22] This reaction allows the direct introduction of hydroquinone fragments into the Pica carbon through a 1,4-addition/enolization process occurring at the conjugated benzoquinone system. Treatment of these initially formed hydroquinones with an oxidant such as DDQ[23] leads to the formation of the Pica carbon incorporating p-benzoquinone moieties (Fig.5.2). It is evident that this electrophilic substitution reaction occurs through the defects sides of the carbon which is also

confirmed by using more ordered carbon materials such as carbon black. As carbon black was replaced with activated carbon, reaction simply didn't take place.

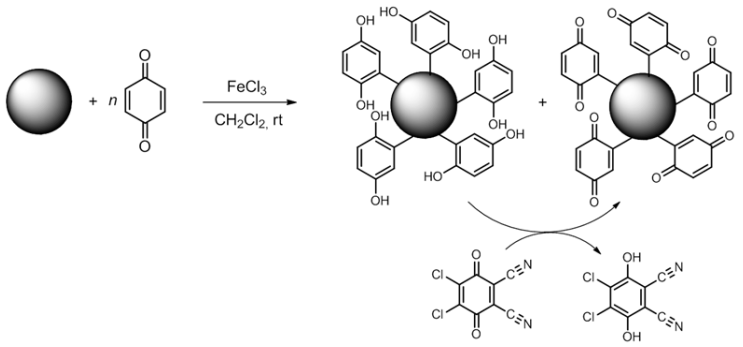

Figure 5.2 A schematic diagram of the p-benzoquinone derivatized activated carbon powder via Friedel-Crafts alkylation.

5.2.2 Characterization of composite electrode material

Covalent bonding between activated carbon particles and p-BQ species was confirmed by FT-IR and solid-state NMR spectroscopies. TGA technique is further used to quantify the grafted amount of p-BQ units, and porous texture was analysed by N_2 adsorption isotherms by applying both BET and DFT methods.

5.2.2.1 FT-IR spectroscopy

To verify the presence of p-BQ on the surface of the final activated carbon, samples were analysed with FTIR spectroscopy. The spectra of unmodified Pica and Pica after modification with p-BQ (named as Pica/p-BQ in the following) are shown in Figure 5.3

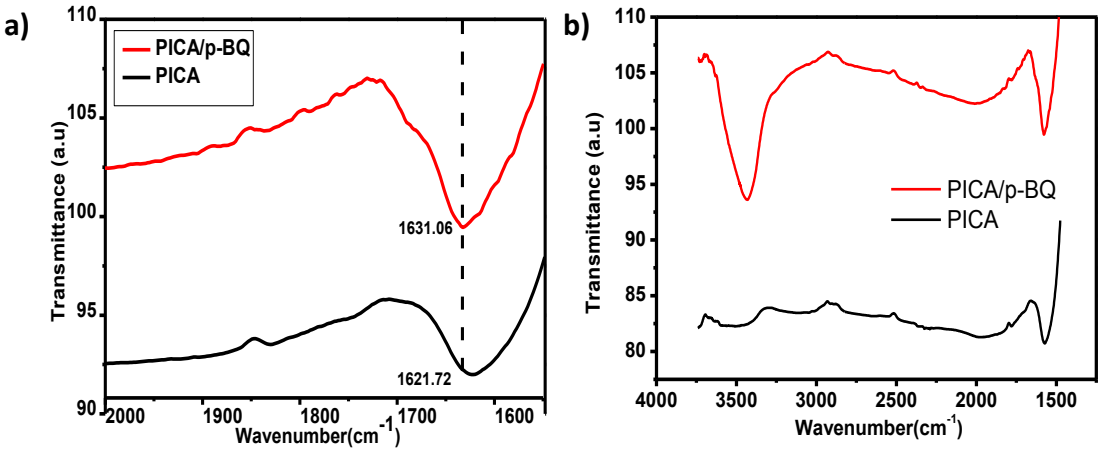

Figure 5.3 FT-IR spectra of initial and modified carbon samples used in this study: full range (a) and detailed comparison of carbonyl bands (b).

FTIR spectra also allows to determine the effectiveness of the washing procedure used after the grafting procedure, since the IR spectrum of functionalized p-BQ Pica carbon in figure 5.3a did not show additional absorption at ca. 2200 cm^{-1} compared to pure Pica carbon. Bands at this position could be attributed to the stretching band of the nitrile group (CN) present in DDQ or its reduced form.

In addition, possible parallel reactions such as chloromethylation could be disregarded since the IR of the functionalized Pica carbon did not show the characteristic stretching band of aliphatic CH_2 groups appearing at ca. 2900 cm^{-1} (Fig. 5.3a). The ^{13}C NMR spectrum neither showed peaks in the region 40-50 ppm, which could be due to CH_2 groups surrounded by aryl and Cl substituents (Fig.5.4).

The spectra shown in figure 5.3b evidenced sharp signals at 1621.72 and 1631.06 cm^{-1} which can be attributed to carbonyl groups of carboxylic acids, thus showing the presence of these functional groups even on Pica carbon prior to treatment. After the synthetic modification leading to the covalently linked p-benzoquinone derivatives, the adsorption band of C=O becomes more intense and slightly shifted because the conjugated C=O stretching vibration of quinone appears at 1637 cm^{-1}, thus allowing us to verify the presence of p-BQ on the surface of the final activated carbon. Nevertheless, the band

appearing at 3450 cm^{-1} in the modified sample (Fig. 5.3a) indicates the presence of phenolic OH groups of hydroquinone which remained unoxidized.

5.2.2.2 Solid state NMR spectroscopy

NMR was used for the determination of the covalent bond between Pica and the quinone moieties. The solid state ^{13}C NMR of unmodified Pica presents a peak at 119.1 ppm which could be assigned to the aromatic carbons. After functionalization, the corresponding ^{13}C NMR signal showed a small but significant downfield shift as presented in Figure 5.4.

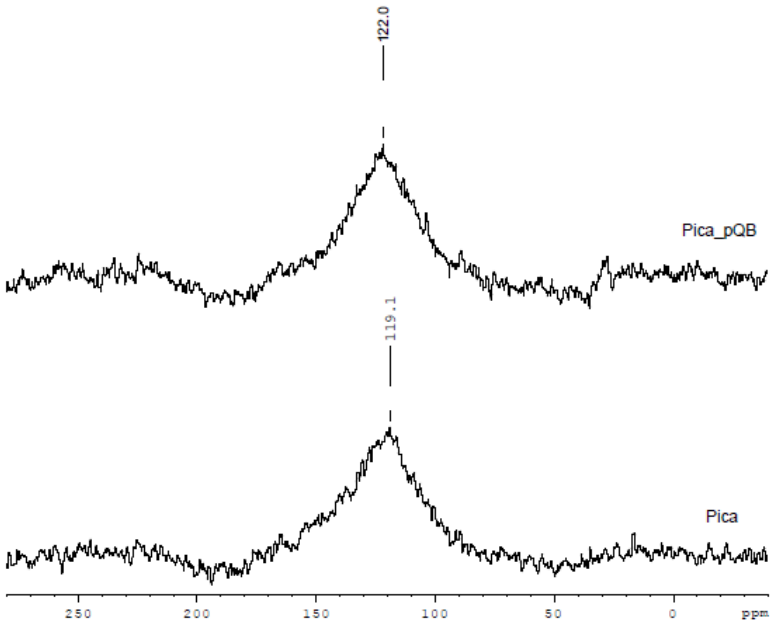

Figure 5.4 Solid ^{13}C NMR spectra of starting material (Pica) and modified samples (Pica-p-BQ).

The signal initially appearing at δ: 119.1 in the spectrum of Pica shifted to 122.0 ppm in the functionalized Pica-p-BQ. This deshielding of the aromatic carbons can be attributed to the incorporation of the quinone moieties on the surface of the carbon grafted molecules, acting as electron withdrawing substituents.

5.2.2.3 Thermogravimetric analysis

Thermogravimetric analysis (TGA) coupled to a mass spectroscopy was performed in order to further identify and quantify the surface grafted p-BQ molecules. Figure 5.5a and 5.5b show both the TGA curves and mass fractions of the associate gases from the decomposition of Pica and Pica/p-BQ samples respectively.

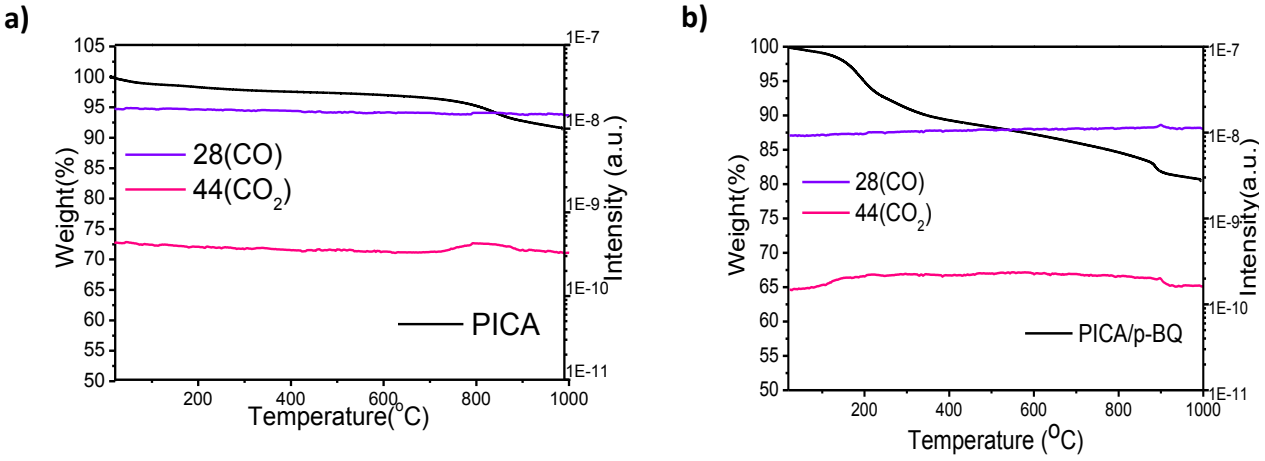

Figure 5.5 Thermogravimetric curves (straight lines) and significant mass fractions of Pica (a) and Pica/p-BQ (b) in argon atmosphere.

Both samples illustrate a first mass loss in TGA curves below 100–150 °C due to dehydration of materials. Further gradual decrease in weight of the unmodified carbon can be interpreted in terms of the removal of the oxygenated surface groups which naturally exist on the activated carbon surface[24]. On the other hand, Pica/p-BQ loses significant additional weight after 150°C probably due to the decomposition of the attached p-BQ molecules at this high temperature. After the first decomposition, Pica-pBQ gradually decomposes in a wider range up to 500°C. Typically, quinone moieties are detected in thermogravimetric analysis by the weight loss around 100°C but thermal decomposition of quinone-activated carbon composites with covalent grafting was confirmed at higher temperatures (at around 150°C).[24] Thus, the sharp mass loss of the modified sample in the temperature range from 100 to 500°C, approximately 7.72 wt%, can be attributed mainly to grafted molecules. Mass spectroscopy analysis

reveals a significant increase in the mass fraction of CO_2 detected at this temperature range in the modified sample which is not present in the pristine Pica carbon, since p-BQ decomposes by forming CO_2. The total mass loss detected in this temperature range corresponding to CO_2 mass fractions is found as 6.57 % (85% of the total weight loss).

5.2.2.4 Structural properties of composite

Nitrogen adsorption isotherms of Pica and Pica/p-BQ samples are illustrated in Figure 5.6a. Both curves show significant volume adsorbed at low P/P_0, which is a characteristic of samples with microporous structure [25]. In medium pressure, a sloped plateau with a small hysteresis loop which is associated with adsorption into mesopores is observed also for both samples, although the area comprised in it is smaller for the covalently modified carbon.[26]

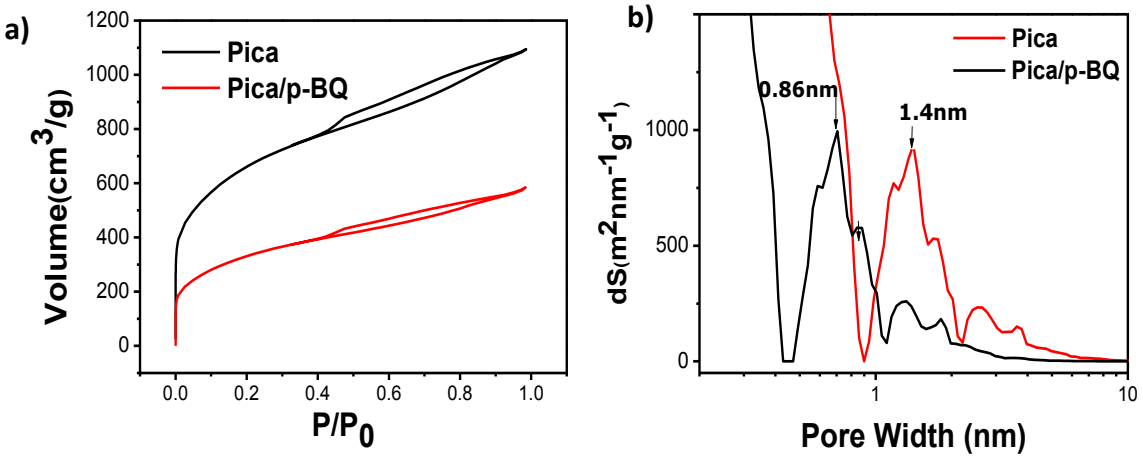

Figure 5.6 Nitrogen adsorption isotherms (a) and pore size distribution (b) for both samples.

The specific surface areas and micropore volumes are represented in table 5.1, where it can be observed that p-BQ grafting brings about important changes in specific surface areas, micropore volume and pore size distribution of carbon samples. In particular, molecular grafting leads to 49.4 % drop in BET surface area (52.8% in DFT area), 60 and 38.7 % loss in micropore area and volume respectively upon compared with Pica unmodified sample, in accordance with previous reports using diazonium chemistry addition.[26]

Porous structure							
SAMPLES	S_{BET} (m^2g^{-1})	S_{DFT} (m^2g^{-1})	S_{MICRO} (m^2g^{-1})	V_{TOTAL} (cm^3g^{-1})	V_{MICRO} (cm^3g^{-1})	S_{MICRO} (%)	V_{MICRO} (%)
Pica	2386.27	1884.70	1429.90	1.55	0.66	75.87	42.58
Pica/p-BQ	1206.90	888.82	813.27	0.82	0.57	91.50	69.51

Table 5.2. Porous structure values of pristine and p-BQ grafted carbon samples.

The main difference of the current method to grafting using diazonium chemistry or other previously reported addition methods is that, after p-BQ addition, even when the surface area and volume decrease, the percentage of micropore volume and surface compared to total pore volume and surface in the samples greatly increases. There is an apparent homogeneous decrease of the micro-pore size from 1.4 to 0.86 nm (Fig.5.6b). Our finding is quite well-correlated with the size of two flat-lying p-BQ molecules, which is approximately 0.75 nm in length[27], within micropores. So, pore size distribution data points to a very homogeneous grafting of p-BQ on this activated carbon substrate via Friedel-Crafts reaction. This can be further observed in Figure 5.6b, which shows a very homogenous shift of pore size distribution towards smaller pore size resulting in new pores with less pore diameter after grafting. Thus, p-BQ Pica modified samples mainly have micropores with sizes of 0.86 nm.

5.2.3 Electrochemical characterization of supercapacitor electrodes

In this part, several electrochemical characterization techniques were used for the determination of specific capacitance, power and energy performance of supercapacitor electrodes made by using both pristine and covalently modified activated carbon.

5.2.3.1 Cyclic voltammetries

Cyclic voltammetry experiments were performed in a three-electrode Swagelok ® cells in 0.5 M H_2SO_4 electrolyte. Unmodified Pica presents the typical rectangular shape of double layer capacitors (Fig.5.7a),

while additional peaks are present in Pica/p-BQ due to the addition of redox functionalities on p-BQ grafting. The reversible redox waves centred at about 0.3 V can be attributed to the grafted p-BQ groups, while the additional redox waves centred at about 0.1 V can be attributed to hydroquinones grafted to the carbon which have not been oxidized by DDQ.

Quinone functionalities have been reported as a source of pseudocapacitance due to highly reversible and relatively fast quinone/hydroquinone redox reactions,[28] and in our case the capacitance of unmodified electrodes can be increased up to 40% by p-BQ.

As the scan rates are increased from 10 to 100 mVs^{-1}, the shapes of the CV curves of the p-BQ grafted electrodes still remain nearly square, indicating the relatively good high-rate capability (Fig. 5.7b).

The Faradaic charge associated with covalently grafted p-BQ molecules ($Q_{faradaic}$) was determined by integration of redox peak area of cyclic voltammetry experiments. Equation 5.1 was employed in order to calculate the number of moles of grafted p-BQ. Here, n is the number of moles of electrons transferred, F is the Faraday constant, S represents the electroactive surface for ion double layer adsorption, and *Γ* is the surface density of grafted molecules.

$$Q_{faradaic} = n(e)\, F \quad \Gamma\ (molcm^{-2})\ S\ (m^2g^{-1}) \qquad \textbf{(5.2)}$$

m = 0.062 mg (grafted amount for 1.5 mg electrode material)

%m= 4.16 % (amount calculated from total area of redox peaks)

m=0.049 mg (grafted amount for 1.5 mg electrode material)

%m= 3.24 % (amount calculated from the area of p-BQ redox peaks)

From these calculations, a total mass of 4.16% is associated with redox active units, coming from both the added p-BQ and unoxidized hydroquinone. Added p-BQ represents 78% of total redox active

quinones. The fact that the mass of redox active quinones (4.16% of total electrode mass) is much lower than the mass of quinones obtained from thermogravimmetric experiments (7.72 wt%) can be attributed to the mass limitations for the access of electrolyte inside micropores and to an incomplete oxidation of the grafted hydroquinone.

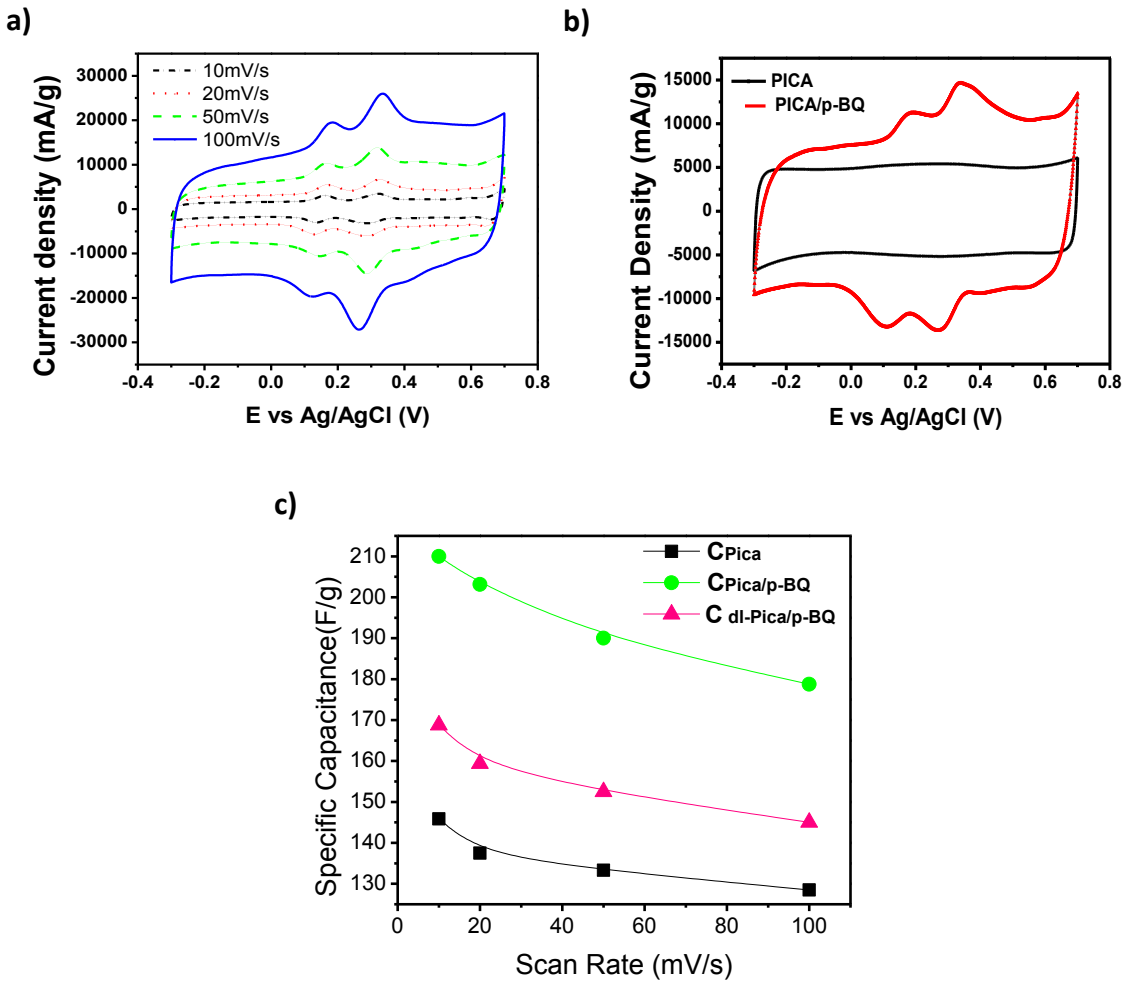

Figure 5.7 Cyclic voltammetries of electrodes prepared from different carbon materials at 50 mVs^{-1} (a) cycling rate behaviour of modified electrodes (b), specific capacitance of all carbon samples(Cpica and Cpica/p-BQ) and double layer capacitance of modified carbon (Cdl-Pica/p-BQ) calculated from cyclic voltammetry experiments with scan rates at 10, 20, 50, and 100 mVs^{-1}(c) in 0.5 M H_2SO_4.

Nevertheless, as shown in Figure 5.7a, the increased capacitance after p-BQ addition is not only due to quinone redox reactions but also due to an increased double layer capacitance. This feature has, to the

best of our knowledge, not been reported previously, as usually after quinone addition surface areas decrease and double layer capacitances accordingly diminish [26]. In our case this same trend should be expected, as surface areas decrease after p-BQ addition. Nevertheless, as previously discussed, the pores remaining on the samples after p-BQ addition are mainly micropores with a size of 0.86 nm. It has recently been reported that the double layer capacitance can increase, even if the surface area decreases, if the pores of electrode active materials match the size of the ions adsorbed.[29,30,31] In our case, the size of hydrated sulphate ions is 0.76 nm [32] which is quite close to the size of the pores remaining on carbons after p-BQ grafting (0.86 nm Fig.5.6b). Thus, we attribute the increased double layer capacitance after p-BQ grafting to this effect.

As the amount of quinone added in this work is similar to the one of previous works using other addition strategies[1] and other possible explanations such as an increased water wetting are thus not likely to be the main reason for the increased double layer capacity also taking into account that the unmodified Pica carbon is already somewhat functionalized with oxygen containing moieties, as clearly shown by the FTIR results, we attribute the increased double layer capacitance after p-BQ grafting to the matching of the pore size after grafting with the size of electrolyte ions.

Moreover, the rate behaviour of both carbons is outstanding, as shown in Figure 5.7b and 5.7c, as Pica electrodes retain at 100 mVs^{-1} more than 85% of their capacity at 10 mVs^{-1}, demonstrating very good rate stability, while the capacitance of the p-BQ modified carbons drops just 4 % more than the unmodified ones in the same interval, showing that power performances are not greatly affected by p-BQ addition.

5.2.3.2 Galvanostatic discharge capacity

Figure 5.8 represents the potential-time plots for Pica and p-BQ modified Pica carbon electrode at 400mAg^{-1}.

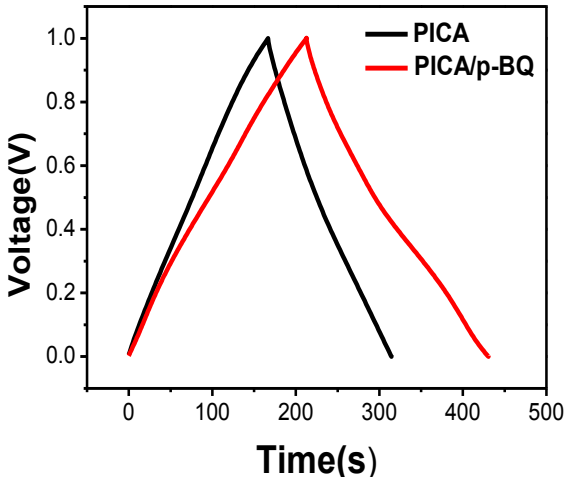

Figure 5.8 Charge/discharge profiles of carbon samples recorded at 400 mAg^{-1} current load in 0.5 M H_2SO_4 electrolyte.

The triangular CD curve for Pica electrodes is typical of double layer capacitors and, after grafting p-BQ, a gentler slope and a wave-like shape of discharge curves typical of pseudocapacitive behaviour can be observed. The area under the curve increases after grafting p-BQ, further confirms that the capacitance of the modified carbon supercapacitor electrodes is higher than that of the unmodified ones.

5.2.3.4 Cycling rate and performance evaluation of symmetric supercapacitors

Extended cycle life stability is a very important factor for testing the electrochemical supercapacitor performance. As shown in Figure 5.9a, specific capacitances of Pica and Pica/p-BQ are given as a function of cycle number at a current density of 800 mAg^{-1}.

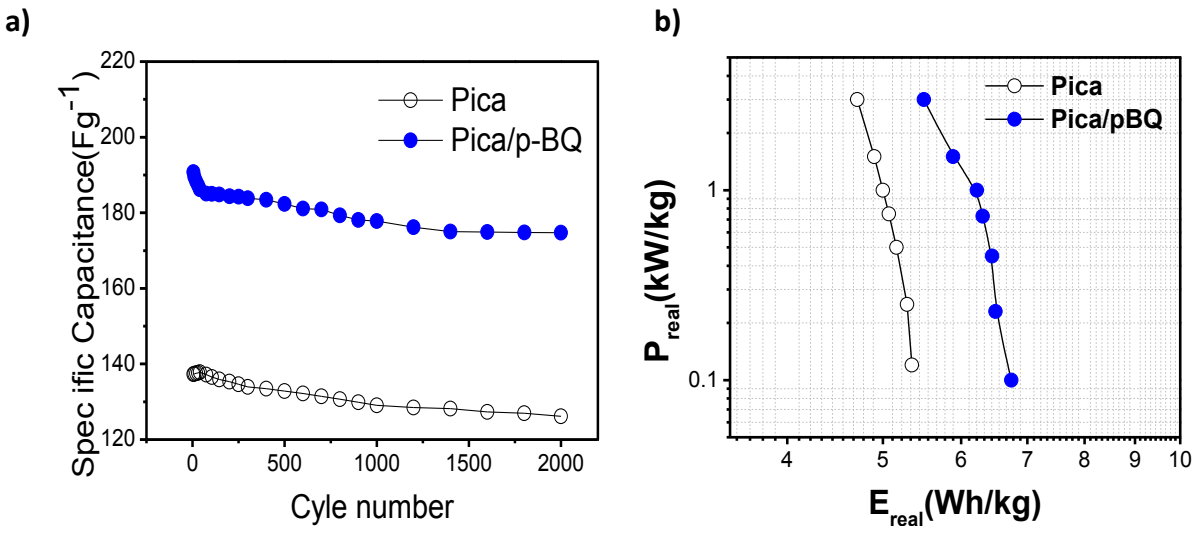

Figure 5.9 Extended cycle life stability of unmodified and grafted Pica electrodes in two-electrode capacitors in 0.5 M H_2SO_4 electrolyte expressed as the capacitances of single electrode obtained at 800 mAg^{-1} current density (a), Ragone plot obtained for Pica and Pica/p-BQ samples (b).

Both materials demonstrate a very good cycling stability, with small capacity loss over 2000 consecutive cycles. The capacity decay for Pica and Pica/p-BQ are 5.8 and 6.3 % after 1000 cycles respectively, and both electrodes show a more stable response afterwards. Electrodes made with grafted carbon display very similar cycling stability behaviour to unmodified carbon electrodes, and loss in gravimetric capacitance values upon long cycling for modified electrodes is only 0.5% more than the capacitance of the electrodes without modification, thus showing a highly stable grafting.

Energy and power density have been evaluated by increasing the current load from 0.2 to 4 Ag^{-1}. In Figure 5.9b the corresponding Ragone plot represents the relation between power and energy density of both unmodified Pica and Pica/p-BQ. Both materials have excellent power density values, and p-BQ modified Pica achieves an energy density 25% higher than unmodified Pica without significant loss in power density.

5.4 Summary

In this chapter, a simple grafting method that enhances the energy density of supercapacitors without significant power loose has been demonstrated. This method is based on the modification of carbons with quinones via Friedel-Crafts alkylation/oxidation reactions. In case of p-BQ grafting, a correlation between the pore size and the electrolyte ion size was achieved. Apart from the increased specific capacity of the carbon material, the novel finding of this study is simultaneously enhanced double layer capacitance due to the better matching of carbon pore size with the size of electrolyte ions.

This new addition strategy demonstrates an alternative strategy for the development of carbon-based materials for supercapacitors with higher energy densities coming from both increased pseudocapacitive reactions and increased double layer capacitance.

Consequently, alternative addition methods may open ways for grafting many different redox moieties and the development of new, environmentally friendly and cheap routes to produce high energy carbon-based materials for supercapacitor applications.

References

1. D. Bélanger and J. Pinson, *Chemical Society Reviews*, 2011, **40**, 3995–4048.
2. M. Barbier, B.; Pinson, J.; Desarmot, G.; Sanchez, *Journal of The Electrochemical Society*, 1990, **137**, 1757–1764.
3. C. P. Andrieux, F. Gonzalez, and J. M. Saveant, *Journal of American Chemical Society*, 2004, **7863**, 4292–4300.
4. M. A. Hayes and W. G. Kuhr, *Analytical Chemistry*, 1999, **71**, 1720–7.
5. P. Allongue, M. Delamar, B. Desbat, O. Fagebaume, R. Hitmi, J. Pinson, and J. M. Saveant, *Journal of American Chemical Society*, 1997, **7863**, 201–207.
6. M. Kullapere, G. Jürmann, T. T. Tenno, J. J. Paprotny, F. Mirkhalaf, and K. Tammeveski, *Journal of Electroanalytical Chemistry*, 2007, **599**, 183–193.

7. R. D. L. Smith and P. G. Pickup, *Electrochimica Acta*, 2009, **54**, 2305–2311.

8. B. E. Conway, *Electrochemical Supercapacitors: Scientific Fundamentals and Technological Applications*, Kluwer Academics/Plenum Publishers, New York, 1997.

9. G. A. Olah, R. Krishnamurti, and G. K. S. Prakash, *Friedel-Crafts Alkylations. In: Trost BM, Fleming I, editors.*, Pengamon, Oxford, 1991.

10. H. Heaney, *The Bimolecular Aromatic Friedel-Crafts Reaction. In: Trost BM, Fleming I, editors. Comprehensive Organic Synthesis*, Pergamon Press, Oxford, 1991.

11. R. M. Roberts and A. A. Khalaf, *Friedel-Crafts Alkylation Chemistry: A Century of Discovery.*, Marcel Dekker, New York, 1984.

12. H. B. Zhan, L. Liu, J. Y. Chen, D. Wang, and C. J. Li, *Advance Synthetic Catalysis*, 2006, **348**, 229–35.

13. J. S. Yadav, B. S. V Reddy, and T. Swamy, *Synthesis*, 2004, **2004**, 106–10.

14. J. S. Yadav, B. S. V. Reddy, and T. Swamy, *Tetrahedron Letters*, 2003, **44**, 9121–4.

15. X. L. Wu, *eXPRESS Polymer Letters*, 2010, **4**, 723–728.

16. M. C. Carreño, M. Ribagorda, A. Somoza, and A. Urbano, *Angewandte Chemie International Edition*, 2002, **41**, 2755–7.

17. M. C. Redondo, M. Veguillas, M. Ribagorda, and M. C. Carreño, *Angewandte Chemie International Edition*, 2009, **48**, 370–4.

18. I. Nuñez, E. Merino, M. Lecea, S. Pieraccini, G. P. Spada, C. Rosini, G. Mazzeo, M. Ribagorda, and M. C. Carreño, *Chemistry -European Journal*, 2013, **19**, 3397–406.

19. M. C. Carreño, I. Garcia, E. Merino, I. Nunez, M. Ribagorda, S. Pieraccini, and G. Spada, *Journal of American Chemical Society*, 2007, **129**.

20. M. B. Smith, *Organic Synthesis*, New York:McGraw-Hill, 1994.

21. B. M. Trost and I. E. Fleming, *Friedel-Crafts Alkylation in Comprehensive Organic Synthesis*, Pergamon, 1991.

22. A. Roberts, R.M., Khalaf, *Friedel-Crafts Alkylation Chemistry: A Century of Discovery*, New York:Marcel Dekker, 1984.

23. J. S. Yadav, B. V. S. Reddy, and T. Swamy, *Tetrahedron Letters*, 2003, **44**, 9121–4.

24. K. Pirnat, R. Dominko, R. Cerc-Korosec, G. Mali, B. Genorio, and M. Gaberscek, *Journal of Power Sources*, 2012, **199**, 308–314.

25. S. Lowell, J. E. Shields, A. T. Martin, and T. Matthias, *Characterization of Porous Solids and Powders: Surface Area, Pore Size and Density*, Kluwer Academics, 2004.

26. G. Pognon, T. Brousse, and D. Bélanger, *Carbon*, 2011, **49**, 1340–1348.

27. J. M. Lu, S. V Rosokha, I. S. Neretin, and J. K. Kochi, *Journal of American Chemical Society*, 2006, **128**, 16708–19.

28. M. P. Bichat, E. Raymundo-Piñero, and F. Béguin, *Carbon*, 2010, **48**, 4351–4361.

29. J. Chmiola, G. Yushin, Y. Gogotsi, C. Portet, P. Simon, and P. L. Taberna, *Science*, 2006, **313**, 1760–3.

30. J. Chmiola, C. Largeot, P. L. Taberna, P. Simon, and Y. Gogotsi, *Angewandte Chemie International Edition*, 2008, **47**, 3392–5.

31. C. Largeot, C. Portet, J. Chmiola, P. Taberna, Y. Gogotsi, and P. Simon, *Journal of American Chemical Society*, 2008, **130**, 2730–2731.

32. N. ER., *The Journal of Physical Chemistry 1959;*, 1959, **63**, 1381–7.

Chapter 6: Organic Redox Flow Batteries Based On Water Soluble Quinones

6.1 Introduction

Since the discovery of the redox flow battery concept by Thaller [1] in 1974, a number of Redox Flow Battery (RFB) systems, such as chromium/iron, zinc/bromine, polysulphide/bromine, all-vanadium, and others have been fabricated and developed. Among these different types, Vanadium Redox Flow Batteries (VRB) are the most well-known and widely investigated. [2] This storage technology has enormous impact on the stabilization and smooth output of renewable energy. Even though VRB technology has obtained substantial progress recently, there still exist some difficult problems to overcome. The rise of mineral resources price and the negative environmental effect of the active materials bring about the demand for novel alternative materials to replace these hazardous chemicals. Moreover, the use of high cost membrane materials such as Nafion® further increases the cost of these systems.

In the present chapter, a novel redox flow battery based on water-soluble organic active materials is proposed. Regarding flow batteries based on vanadium, the principal advantage of developing aqueous organic redox systems is the use of environmentally friendly, abundant and relatively cheap materials as redox active species in combination with the benefits of aqueous electrolytes.

Here, the following characteristics of the redox couples were studied in detail:

- Solubility: Energy density of the device is directly proportional to the solubility.
- Electrochemical reversibility: Kinetic parameters of each redox couple can be measured by the difference/ratio between the anodic and cathodic peak potentials/intensities, and its evolution to different scan rates.
- Electrochemical potential: Any battery system requires two redox couples at each side of the battery and so, the greater the difference between the electrochemical potential of both sides , the higher the energy density that can be obtained

6.2 Aqueous electrochemistry of water soluble quinones

Aqueous media has been by far the most studied electrolyte in view of the biological importance of quinones.[3] The typical model system for a quinone is p-benzoquinone (p-BQ), which undergoes eletrochemical reduction to hydroquinone (BQH_2) in aqueous media according to the following reaction:

$$BQ + 2H^+ + 2e^- \rightleftharpoons BQH_2$$

Simple manipulation of the Nernst equation illustrates that the obtained redox potential for a redox couple giving rise to a transfer of mH^+, ne^- will change -m/n(59 mV)/pH unit at 25 °C. Therefore, under conditions where quinones undergo $2e^-$, $2H^+$ reduction, such as aqueous medium, a plot of potential vs pH should give a slope of -59 mV per pH unit.[4] Based on the above equation, reduction of quinones in aqueous solution consumes protons. Therefore, in the absence of buffer, reduction of the quinone will cause the pH near the electrode to increase, creating an "effective pH" which is greater than in the bulk.[5]

Although most quinone type redox species demonstrate highly reversible $2e^-$ and $2H^+$ transfer in aqueous media, poor water solubility restricts their widespread applications in RFB systems. In this respect, solubility and electrochemistry of water soluble commercial p-BQ derivatives were studied. In the following part of this chapter, tetrahydroxy-1,4-benzoquinone (THBQ. Fig.6.1a) and 2,5-dichloro-3,6-dihydroxy-1,4-benzoquinone, also called as chloroanilic acid (CAA, Fig.6.1b), will be studied as organic redox compounds due to their relatively high water solubility.

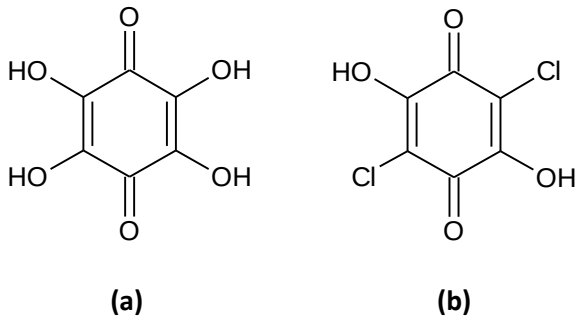

(a) **(b)**

Figure 6.1 Molecular structures of THBQ (a) and CAA (b).

6.2.1 Electrochemical studies of tetrahydroxy benzoquinone and chloroanilic acid

Hydroxyl and sulfonic groups are known to increase the aqueous solubility of quinones.[6] Hence THBQ, a fully hydroxyl substituted p-BQ derivative (Fig 6.1a), was studied due to its significant water solubility. Aqueous solubility as high as 1 M in strongly alkaline medium (pH 13) was obtained for this compound, but solubility significantly decreased in acidic (pH 2) or neutral (pH 7) media. CV analysis was performed at moderate concentrations in acidic medium. Figure 6.2a indicates irreversible redox characteristic of THBQ (ΔE=410 mV) under these conditions. Irreversible behaviour of this compound can be attributed to the stabilization of the hydroquinone ring by the presence of four electron-donating hydroxyl substituents. Therefore, CAA was further tested since this compound has two chlorine substituents instead of two hydroxyl groups, differently from THBQ. As shown in Figure 6.2b, despite better reversibility (ΔE=160 mV), significant loss in water solubility was observed. The maximum soluble concentration at different conditions was determined as 0.05M. Enhanced reversibility of this compound can be related to the chlorine substituents which stabilize the ring by its electron withdrawing nature.

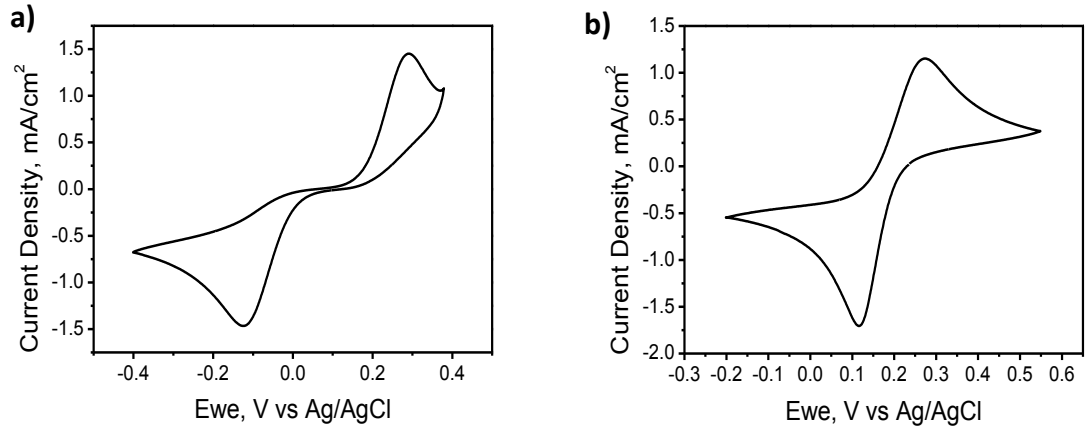

Figure 6.2 Cyclic voltammeties of 10^{-2}M THBQ (a) and 10^{-3}M CAA (b) in pH 0.9 HCl solution with 0.1M KCl as supporting electrolyte at 50mV/s scan rate.

Thus, hydroxyl substituents can maximize the aqueous solubility of the quinone compounds. However, too many hydroxyl units directly attached to the quinone ring stabilize the structure and give rise to irreversible electrochemical response. This is the reason why the covalent bonding of a polyhydroxylated compound was tested as a plausible strategy. This strategy allows maximizing aqueous solubility of the quinone-based compounds whilst preserving good electrochemical properties. To demonstrate this, different methods were used to incorporate polyhydroxy substituted moieties into quinone structures. The different approaches proposed for covalent modification of a quinone with a polyhydroxy substituted compound are: bond formation through an oxygen (O-attachement) directly linked to the quinone skeleton or through a covalent bond with carbon (C- attachement, Fig. 6.3) atoms of the quinone unit. The O-polyhdroxylates derived from sugars are acetals since they result from reaction of the aldehyde or ketone carbon of the carbohydrate and alcohols. These molecules can be hydrolyzed under acidic conditions to recover the polyhydroxylated molecule and the corresponding alcohol. In our case, this reaction would destroy the target molecule. On the other hand, a C-polyhydroxy derivative is a more stable molecule in aqueous media and cannot be easily hydrolysed. Hence, covalent attachment through a carbon atom of a polyhydroxy derivative to the quinone moiety was chosen instead of attaching the polyhydroxilated skeleton through the oxygen atom.

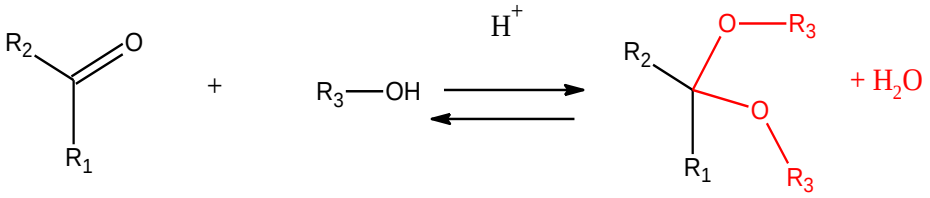

Figure 6.3 Reaction of a hydroxy substituted compound with a carbonyl group.

6.3 Method for introducing a polyhydroxylated structure into the quinone.

6.3.1 Selection of the starting compound

The type of substituent groups of quinones and their binding side have a great influence on quinone redox potentials and thus, they have been widely explored. For example, a series of reports showed that the presence of electron donating substituents on p-BQ decreases the redox potential while electron withdrawing groups increase the redox potential relative to the unsubstituted compound.[7,8]

Intermolecular and intramolecular hydrogen bonds are two different interaction modes which have been detected in molecules with biological activity such as quinones.[9] These bonds constitute the link which determines the chemical properties and functions of both the quinone structure and the protein reaction center.[10] In this framework, electrochemistry appears as an important tool to understand the reduction mechanisms in this kind of systems. In the specific case of hydroxyquinones, intramolecular hydrogen bonding brings about the stabilization of electrochemically generated quinone radical anions, provoking a decrease in reduction potentials.[11,12]

Here, a detailed explanation was given for the selection of the starting quinone compound to develop covalent modification with a polyhydroxy substituted unit. This was achieved by studying aqueous electrochemistry of three different naphthoquinone derivatives which are; 1,4-naphthoquinone (NQ), 2-hydroxy-1,4-naphthoquinone (2OHNQ,Lawsone) and 5-hydroxy-1,4-naphthalenedione (5OHNQ,Juglone) Their molecular structures are presented in figure 6.3.

Juglone (Fig.6.3b)and Lawsone (Fig. 6.3a) are naturally occurring quinones, both are released by plants as allelochemicals.[13]

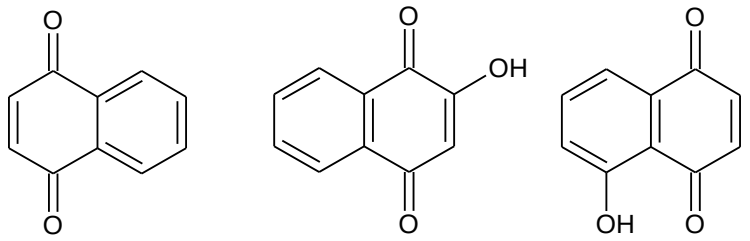

(a) **(b)** **(c)**

Figure 6.4 Molecular structures of NQ (a), 2OHNQ (b) and 5OHNQ (c).

CV analysis of the unsubstituted and hydroxyl substituted napthoquinones are represented in figure 6.4. The apparent half wave potentials, $E_{1/2}$, calculated from the mid-point of the cathodic and anodic peak potentials and listed in table 6.1 together with potential peak separation, ΔE . As can be observed from the table analysis, the redox potentials of 2OHNQ and 5OHNQ shifted to less positive potentials upon comparing to non-substituted compound. Additionally, a clear decrease in peak to peak separation was observed for both OH substituted NQs, confirming a more reversible behaviour. However the substituent site highly influences both the replacement of redox potentials and reversibility of the processes. Measurement of the corresponding 2OHNQ compound indicates that the internal hydrogen bonding in the 2-hydroxy quinone contributes to the stabilization of semiquinone, probably as a result of increased delocalization due to exchange of the hydroxyl hydrogen between the two neighbouring oxygen atoms. Hydroxy group attached from α position shifts the potentials through less positive values and it enhances the reversibility slightly as compared with unsubstituted NQ. On the other hand, attachment of hydroxy group from the *"position 5"* does not have a significant effect on half wave potential values, but reversibility improves drastically with respect to NQ. Differences in reversibility of the OH substituted quinones, i.e. Lawsone and Juglone in this case, were previously discussed. In these kinds of molecules, the OH groups at the quinone rings are reported to be more acidic than those of the analogue phenolic

group lacking the carbonyl linked by hydrogen bonding. Consequently, electron transfer of the hydroxy quinones is a more irreversible process than that of the analogues lacking the OH due to the transfer of the hydrogen bonding proton during the electron addition in the former.[14,15]

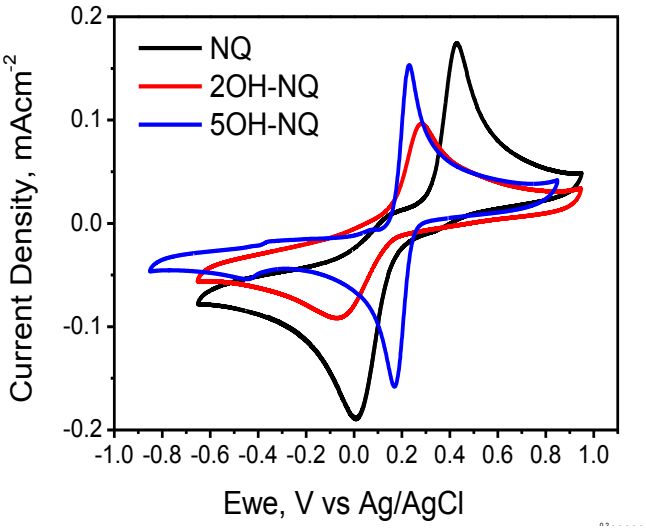

Figure 6.5 CVs of NQ, 2OHNQ and 5OHNQ at 10^{-3} M concentration of pH 0.6 KCl/HCl(0.1M) solution at 50 mV/s scan rate.

Compound	Electrolyte	pH	Substituent	Epc(V)	Epa(V)	ΔE	$E_{1/2}$
NQ	KCl/HCl	0.6	None	0.02	0.43	0.41	0.22
2OHNQ	KCl/HCl	0.6	2-OH	-0.05	0.28	0.33	0.11
5OHNQ	KCl/HCl	0.6	5-OH	0.17	0.23	0.06	0.19

Table 6.1 Redox potentials extracted from CV experiments of 10^{-3}M of NQ, 2OHNQ and 5OHNQ in aqueous media at different pHs. Potentials are referred to Ag/AgCl reference electrode at 50 mV/s.

6.3.2 Synthesis of 5-hydroxy naphthoquinone incorporating a sugar moiety

According to these promising electrochemical features, 5OHNQ, also known as *Juglone*, was chosen as the starting quinone compound for the covalent attachment to a sugar molecule. The molecular structure of the target molecule is illustrated in figure 6.5.

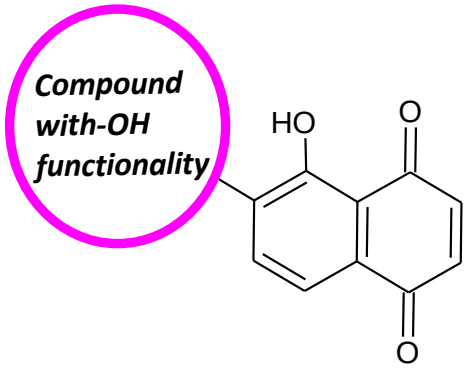

Figure 6.6 Molecular structure of polyhydroxy functionalized juglone.

6.3.3 Electrochemical characterization of polyhydroxyl functionalized juglone

In this part of the present chapter, solubility and electrochemical properties of both functionalized and non-functionilized Juglone compounds will be compared and discussed. Solubility is a very critical factor which determines the charge accumulated per unit volume of the electrolyte. Accordingly, energy density of a RFB system relies prominently on this property of the active material.

The cyclic voltammetry of both compounds was studied in aqueous acidic solution. The CVs show a single reduction peak and a corresponding oxidation peak, the potentials of which exhibit a strong pH dependence in accordance to a Nerstian manner. Figure 6.6 compares the CV curves of both juglone and polyhydroxyled juglone at their maximum solubility in acidic conditions. The difference between the areas encompassed by these two curves can be attributed to the significantly higher aqueous solubility of polyhydroxyl functionalized compound, which is nearly 200 fold better than non-functionalized quinone. It is noteworthy to point out that functionalization of quinones permits modifying many key features of the compound such as: solubility, electrochemical potentials, reversibility and reaction kinetics.

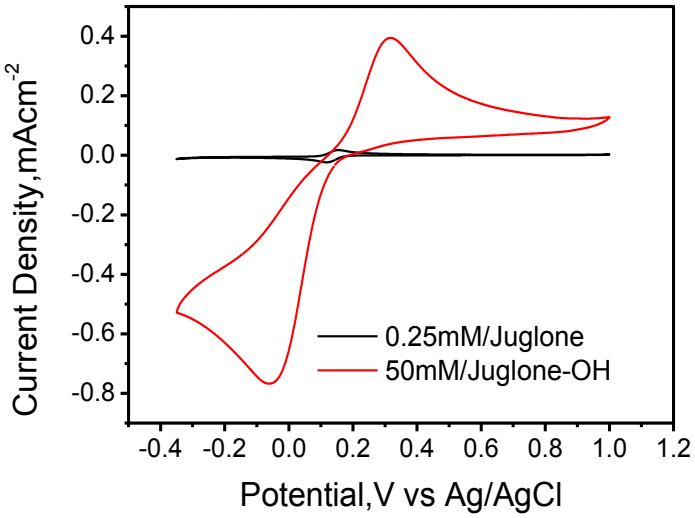

Figure 6.7 Cyclic voltammeties of juglone and polyhydroxy substituted juglone at their maximum solubility in pH 0.9 HCl solution with 0.1 M KCl as supporting electrolyte at 50 mV/s scan rate.

Table 6.2 shows the dependence of peak to peak separation (ΔE) and the ratios of peak intensities of cathodic and anodic peaks (I_{pc}/I_{pa}) with respect to different scan rate values for a 0.25 mM acidic aqueous solution of both juglone and polyhydroxylated juglone in a pH = 0.9 HCl / KCl solution.

Compound	**Scan Rate mVs^{-1}**	ΔE **V**	**I_{pc}/I_{pa}**
Juglone	5	0.038	0.895
	10	0.038	0.890
	20	0.039	0.863
	50	0.049	0.829
	100	0.060	0.813
	200	0.072	0.783
	400	0.083	0.765
Modified Juglone	5	0.052	0.879
	10	0.056	0.866
	20	0.065	0.857
	50	0.079	0.838
	100	0.093	0.811
	200	0.112	0.782
	400	0.129	0.765

Table 6.2 Scan rate dependency of peak to peak separation and ratios of current intensities calculated from CV analysis performed at pH 0.9 HCl/KCl medium for juglone and modified juglone compounds.

At lower scan rates, the CVs of Juglone show a peak separation, ΔE, of 38 mV, over a range of potential sweep rates. This is a very close value to the expected limit (30mV) for a thermodynamically reversible two electron transfer reaction. At higher scan rates, the limit of 30 mV may not be reached, but ΔE remains still within an acceptable range even upon application of high scan rates. Juglone reversibility was further confirmed by measuring peak intensity ratios which is close to unity (1 for a fully reversible system) at lower scan rates and slightly deviates from this value at higher scan rate values. On the other hand, reversibility for polyhydroxy substituted compound was found worse than the unsubtituted juglone regarding ΔE values exceeding 60mV even at slower scans. However, it is also relevant to point out that reported ΔE values for modified Juglone are still better than those of Vanadium redox pairs.

As previously discussed, the electrochemical properties of quinones are highly influenced by factors including: substituents, their binding sites, concentration of active species and electrolyte nature (pH, ionic strength, temperature, etc.). The main difference in reversibility for Juglone and functionalized Juglone arises from the high soluble concentration of the latter (50 mM). As the concentration of polyhydroxylated compound decreases to 0.25 mM level, complete reversibility of juglone is greatly recovered. Upon comparing the results presented in this study to well-studied VRB couples, ΔE for the V(IV)/V(V) couple is much higher (above 100mV) than values reported here even at low scan rates.[16] Furthermore, it should be noted that quinone redox reaction includes two-electron transfer for each molecule giving rise to double the charge storage comparing to one-electron transfer redox couples such as Vanadium.

As a further development of this strategy, we found a commercial natural product composed of a polyhydroxylated quinonic compound which has a solubility limit of 0.2 M in aqueous HCl/KCl electrolyte at pH=0.9 and a $E_{1/2}$≈-0.4 V vs Ag/AgCl in this electrolyte. Since this redox potential is

similar to the one of the V(II)/V(III) redox pair, and the cost of this natural product is similar to the one of VCl_3, polyhydroxylated quinonic compounds can reach commercial competitiveness, since solubility can be further increased for example by a suitable choice of the electrolyte, which may also improve other electrochemical features important for the performance such as redox potential position, reversibility, rate behaviour, etc. Thus, we filed a patent with this development.

6.4 Summary

The present chapter describes the development of organic redox couples for RFB applications. The most attractive features which make organic redox compounds more advantageous over other materials are their low price, easy accessibility and non-toxic nature.

Herein, we demonstrated that very important features of these compounds, such as solubility and electrochemical properties, might be tuned by simple modification techniques. Quinone derivatives were tested for this purpose due to their high reversibility, variety and ease of structural modification. However, the major problem coming with the use of quinones is that they are not offering the high solubility required for a high energy RFB for a practical use.

Therefore, the first strategy developed in this present work is the selection of quinones with proper functionality fostering aqueous solubility (-OH groups). Among them, THBQ and CAA were studied and it is concluded that the fully hydroxylated compounds (THBA) are not satisfying the required electrochemical properties due to strong electron donating nature of the OH substituents. However replacing some of the OH groups with electron withdrawing units, like Cl, seems a plausible approach for the stabilization of the quinone ring and thereby, leading a better electrochemical response.

The other strategy proposed for the enhancement of water solubility is the covalent attachment of polyhydroxylated compounds to the quinonoid structures. In this study juglone was used as the starting material due to its high electrochemical reversibility and C- polyhydroxylation was

performed. After this functionalization, aqueous solubility increased up to 200 fold with respect unmodified juglone compound. Water solubility of functionalized quinones is highly affected by both quinonoid base and attached polyhydroxy molecule. So, the type of the compound used for the functionalization of the quinonoid compound drastically influences the solubility of the resulting compound. Besides, final product conserves the desired kinetic features of Juglone. This can be related to the fact that attachment side of the polyhydroxy-type molecules to the quinone should be determined correctly in order not to alter promising kinetic behaviour of the base compound.

This strategy can be considered as a method for designing "*the model organic redox couples*" to further extend to employ in the selection of natural compounds as redox active species for RFBs.

References

1. L. H. Thaller, 1976, US Patent 3996064.
2. M. Skyllas-Kazacos, G. Kazacos, G. Poon, and H. Verseema, *International Journal of Energy Research*, 2010, 182.
3. S. Hay, K. Westerlund, and C. Tommos, *Journal of Physical Chemistry. B*, 2007, **111**, 3488–95.
4. M. Quan, D. Sanchez, M. F. Wasylkiw, and D. K. Smith, *Journal of the American Chemical Society*, 2007, **129**, 12847–56.
5. O. H. Muller, *Journal of American Chemical Society*, 1940, **62**, 2434.
6. I. M. Ritchie and S. I. Bailey, *Electrochimica Acta*, 1985, **30**, 3–12.
7. C. Frontana, A. Vázquez-Mayagoitia, J. Garza, R. Vargas, and I. González, *The Journal of Physical Chemistry A*, 2006, **110**, 9411–9.
8. I. Novak and B. Kovac, *The Journal of Physical Chemistry A*, 2008, **112**, 3061–5.
9. C. J. H. Schutte, S. O. Paul, and R. Smith, *Journal of Molecular Structure*, 1993, **29**, 235.
10. W. A. Cramer and D. B. Knaff, *Energy Transduction in Biological Membranes*, Springer-Verlag, New York, 1990.
11. G. M. Rao, J. W. Lown, and J. A. Plambeck, *Journal of Electrochemical Society*, 1978, **125**, 534.
12. G. M. Rao, J. W. Lown, and J. A. Plambeck, *Journal of Electrochemical Society Society*, 1978, **125**, 540.

13. J. R. Vyvyan, *Tetrahedron*, 2002, **58**, 1631–1646.

14. J. L. Ortiz, D. J, A. Baeza, G. I, R. Sanabria, and R. Miranda, *Journal of Electroanalytical Chemistry*, 1996, **411**, 103.

15. M. Aguilar-Martínez, J. A. Bautista-Martínez, N. Macías-Ruvalcaba, I. González, E. Tovar, T. Marín del Alizal, O. Collera, and G. Cuevas, *The Journal of Organic Chemistry*, 2001, **66**, 8349–63.

16. G. Oriji, Y. Katayama, and T. Miura, *Journal of Power Sources*, 2005, **139**, 321–324.

Chapter 7: Electron Transfer Kinetics of Quinones

7.1 Introduction

Quinone ET kinetics play a crucial role in many biological, physical and chemical systems, and understanding ET phenomena for quinones can contribute to a better understanding of some important electrochemical processes which are of potential interest for use in energy storage devices such as batteries and supercapacitors.

Quinone moieties that undergo reversible redox reactions have been employed as anode active materials for rechargeable polymer-air batteries[1] and electrolyte active materials for supercapacitors[2]. Determination of heterogeneous ET rate constants for quinones plays a critical role in terms of device energy efficiency. Therefore, kinetic studies in aprotic media give valuable information about the stability and energetics of semiquinones, since these radicalic intermediates are formed and stabilized in non-aqueous media. Aprotic media permit the study of single-step one-electron transfer of quinones and this kinetic information can be used for protic media in which two-electron transfers occur in a one-step reaction.

In this part of the doctoral study, kinetic properties of quinones were studied to further understand the ET kinetics of different compounds which can serve as promising materials either as a pseudocapacitive sources or redox active species for electrochemical energy storage devices. Accordingly, numerical calculation of rate constants gives valuable information to evaluate the molecules of interest for this purpose. Interpretation of the rate constant is quite straightforward i.e. high values of the standard rate constant (k^0) indicate fast ET kinetics, whereas a low k^0 value applies to a more sluggish process. Nevertheless, we cannot say the same for the experimental measurement of rate constants, which is much more challenging. Although several different techniques exist for the true measurement of rate constants, there are still many discrepancies in the reported literature values. Table 7.1 is a striking illustration of experimentally measured k^0 values for quinonoid species in which reported rate constants span a wide range, even for the same

compound on the same type of electrode material. The direction of errors in reported k^0 values is towards smaller values than the actual ones. So a series of experimental factors should be taken into consideration, such as compensation of solution resistance. Microelectrodes appear highly advantageous for eliminating such errors in voltammetry and considerably higher rate constants are reported so far by employing microelectrodes [3].

	k^0(cms^{-1})[4]	k^0(cms^{-1})[5]	k^0(cms^{-1})[6]	k^0(cms^{-1})[6]	k^0(cms^{-1})[7]	k^0(cms^{-1})[7]	k^0(cms^{-1})[7]	k^0(cms^{-1})[8]	k^0(cms^{-1})[9]	k^0(cms^{-1})[10]
Electrolyte	MeCN/TBAP	(C_2mim)(NTF_2)	MeCN/TBAP	MeCN/TBAP	MeCN/TEAB	MeCN/TEAB	MeCN/TEAB	DMF/TBAP	DMF/TEAB	DMF/TEAB
Electrode	Ptmicroband	Au microdisk	Au microdisk	CF microdisk	Pt	Au	Graphite	Au	Au	Au/Hg
Size	40.5 μm	10 μm	10 μm	10 μm	Macro	Macro	Macro	Macro	Macro	Macro
p-BQ	0.130	≥0.03	0.051	0.067	0.63	0.66	0.45	0.065	0.0053	0.18
AQ	0.097	-	0.19	0.45	0.92	0.83	0.56	0.018	-	0.23
NQ	0.100	-	-	-	0.83	0.71	0.51	0.023	-	0.35

Table 7.3 A comparison of literature standard rate constants values for different quinones in aprotic electrolytes.

*NQ: Naphthaquinone, TBAP: Tetrabutylammonium phosphate, TEAB: Tetraethylammonium bromide

In this chapter, kinetic properties of a group of quinones will be presented in detail and calculated parameters will be compared to the literature values. A special emphasis has been made to investigate and eliminate the surface blocking processes of quinone electrochemistry at different electrode materials and their influence on measured kinetics will be discussed in detail.

7.2 Materials and Techniques

7.2.1 Compounds

In this chapter a family of quinone derivatives were studied for calculations of ET rate: p-benzoquinone (p-BQ); naphthaquinone (NQ); anthraquinone (AQ) and 2-(p-tolysulfinyl)cyclohexane-2,5-diene-1,4-dione in two different optical isomeric forms (enantiomer/- (E-), enantiomer/+(E+) and racemic mixture+/- (R)). Their molecular structures are displayed in Figure 7.1.

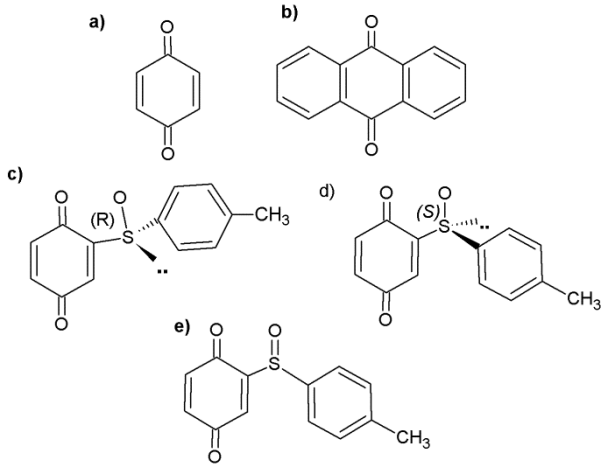

Figure 7.1 Molecular structures of p-benzoquinone (a), anthraquinone (b), Enantiomer /- (c), Enantiomer /+ (d) and racemic mixture /R (e).

7.2.2 Electrode Materials

Gold (Au) and carbon fiber (CF) electrodes were used for this study, and both serve as common electrode materials due to their unique properties. The former is an inert and very stable noble metal and the latter serves for a broad range of applications because of its wide potential window, low background currents, rich surface chemistry, chemical inertness and low cost [11].

7.2.3 Measurement techniques

Electrochemical experiments were performed on CF and Au microelectrodes, by performing cyclic voltammograms (CVs) using *Scanning Electrochemical Microscopy* (SECM), operated in the feedback mode, and *Non-Steady-State Cyclic Voltammetry* (NSS-CV).

7.2.3.1 Scanning electrochemical microscopy

SECM is a scanning probe technique which emerged as a useful tool for studying structures and processes on the micrometer- and submicrometer scale. Since its inception, it has been widely used to probe a variety of electrochemical processes due to its high spatial resolution for both quantitative and qualitative investigations [12]. The technique involves scanning an ultramicroelectrode (UME) tip over a surface, the electrochemical response of which provides information on local properties such as topography or electroactivity [13].

Here, SECM in the feedback mode was employed, using positive feedback of the Au substrate to measure quinone kinetics. In this mode, depicted in Figure 7.2, for a reduction reaction at the tip, when the tip is placed close to the conductive substrate surface, the reduced species (R) generated at the tip can diffuse to the substrate where it is reoxidized, resulting in an additional flux of oxidized species (O) to the tip. This process, known as positive feedback, occurs only if the substrate is electrically conducting. In negative feedback mode, diffusion of O is hindered by the insulating substrate so a decrease in tip current is observed when the tip is brought close to the substrate.

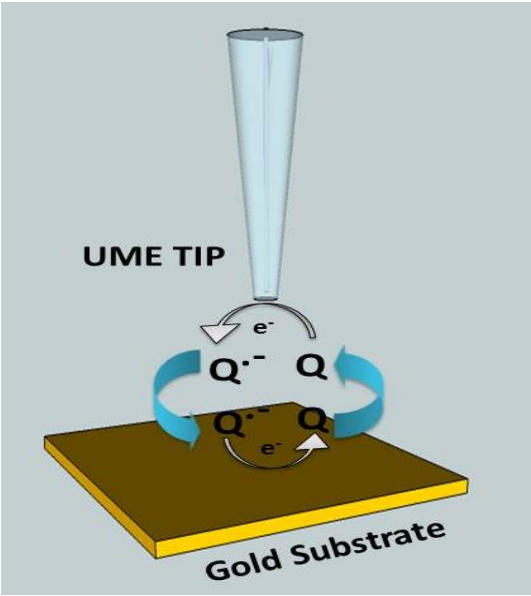

Figure 7.2 A schematic for SECM in feedback mode showing a quinone, Q, reduced at the tip to a semiquinone, $Q^{\bullet -}$.

An SECM approach curve is performed by approaching the tip towards and normal to the surface, whilst applying a potential to the tip that gives a steady-state limiting current. As the tip gets within a few electrode radii from the surface, feedback effects of the substrate are observed. If the electrode fouls during the approach, or the activity of the substrate is not known, there is not a reliable way to determining tip-substrate distance. This is a problem if the topography and electroactivity of the substrate need to be determined independently for a scan, or if the approach is to be halted before the tip crashes into the surface. Here, a non-electrochemical tip-positioning method was used to place the electrode close to the surface. The tip is oscillated in the *z*-direction, and the amplitude of this oscillation is damped as the tip makes intermittent contact (IC) with the surface. Since this technique, IC-SECM[14], relies on physical contact between the tip and substrate, the approach can be performed without applying a potential to the tip, thus preventing tip fouling whilst the tip is positioned at a well-defined distance to the substrate[15].

SECM is a very advantageous technique for studying fast heterogeneous ET kinetics since mass-transport of electroactive species significantly increases when the tip approaches close enough to

the substrate surface. The usage of SECM also eliminates some common experimental errors such as the solution ohmic drop[16].

7.2.3.2 Non-steady-state cyclic voltammetry

Electrode fouling turned out to be a substantial concern for the CV measurements performed at low scan rates in bulk solution (i.e. not close to any underlying substrate), and also for the experiments performed with IC-SECM technique. This surface blocking issue was successfully eliminated for the Au electrode by simple modifications in experimental conditions. However it remained a significant issue in measurements performed by CF electrode at low scan rates. Therefore, NSS-CV was employed by increasing the potential scan up to 1 Vs^{-1} in order to eliminate the error arising from the carbon surface blocking processes impeding accurate evaluation of kinetic parameters.

7.3 Analysis of Electrode Surface Blocking Processes

In this part of the chapter, the kinetic properties of a quasi-reversible electrochemical reduction of semiquinone radical formation were studied. The following one-electron transfer process describes the transformation of a quinone unit to a radicalic species in aprotic media:

$$Q + e^- \underset{k_r}{\overset{k_f}{\rightleftharpoons}} Q^{\bullet -}$$

Here Q and $Q^{\bullet -}$ represent the quinone and semiquinone (radical anion) species, respectively. Although strong adsorption is described to occur more likely in aqueous than in aprotic media[18], strong electrode fouling was detected for almost all compounds in acetonitrile. Different degrees of surface fouling were observed depending both on the electrode material and the compound studied.

Preliminary experiments on the Au electrode were performed in a 2 mM quinone concentration solution, at which electrode surface fouling was observed upon repetitive cycling, as shown in Figure 7.3a. Figure 7.3b demonstrates how surface blockage was eliminated on the Au electrode by decreasing the concentration of active species from 2 mM to 0.2 mM. The lower concentration

means that fewer quinone species are present in solution to passivate the surface during the course of the measurement.

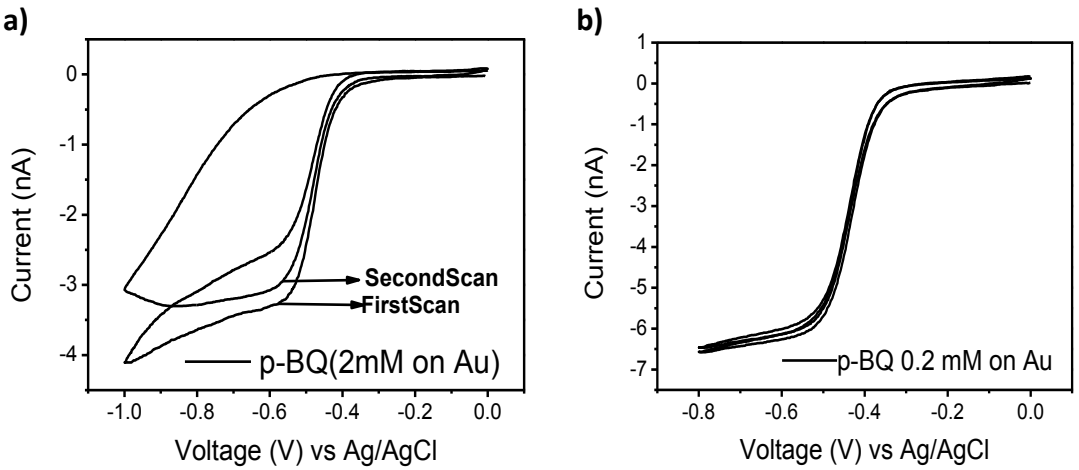

Figure 7.3 Two consecutive cyclic voltammograms of 2 mM (a) and 0.2 mM (b) of p-BQ solutions on Au microelectrode at 25 mVs^{-1}.

In the case of the CF electrode, electrochemical analysis was found to be very challenging because of the strong adsorption of quinonoid molecules to the electrode surface. Only the forward scans, and only the first scan, of voltammetric analyses (i.e. linear sweep voltammetry (LSV)) were shown in reported measurements by Compton *et al*. at Au and CF microelectrodes, in which fouling cannot be observed effectively[6]. A typical example of a voltammetric response is represented in Figure 7.4 for AQ at two different concentrations. Electrode fouling clearly appears during the first cycle and the electrode surface is partially recoverable upon resting the UME in electrolyte solution without applying a potential. However, complete removal of surface fouling was not possible even after sweeping the potential through highly positive values.

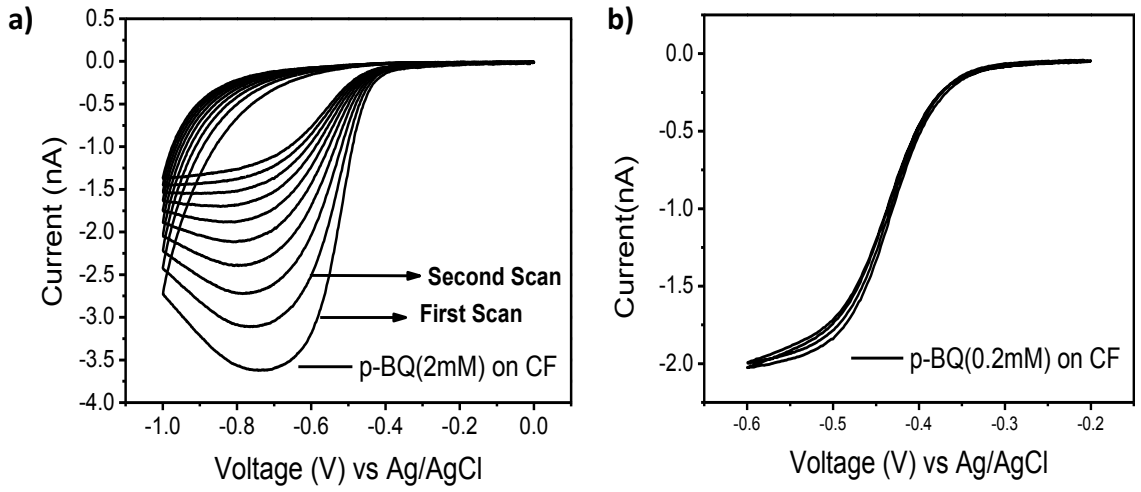

Figure 7.4 Cyclic voltammograms of 2 mM (10 cycles) (a) and 0.2 mM (2 cycles) (b) of AQ solutions on a CF microelectrode at 25mVs^{-1}.

Comparing the CVs for Au, Figure 7.3, and CF, Figure 7.4, it is easily noticeable that the surface fouling occurs more quickly on CF than on Au. On CF, a state-state current is not observed, rather the current magnitude decreases at the most negative potentials. This behaviour can be associated with carbon's intrinsic properties, for example it may arise from a carbon-quinone interaction. Quinone π-electrons in a cyclic arrangement most probably interact with the carbon sp^2 domain, giving rise to relatively strong π-π interactions. This type of interaction was previously reported for *pyrene* derivatives giving rise to non-covalent functionalization of carbon nanotubes with aromatic units [19]. As for the Au case, the degree of fouling on CF decreases by reducing the solution concentration from 2 mM to 0.2 mM, but it cannot be eliminated completely, even at the lowest solution concentration. After each consecutive cycle, fouling is noticeable and the apparent steady-state diffusion-limited current decreases.

Another interesting aspect about electrode fouling is that fouling was not observed on a glassy carbon macro electrode (3 mm in diameter) under exactly the same experimental conditions with conventional three-electrode electrochemical cell. Hence, we can deduce that the electrode fouling might become more favourable as the mass-transport of the active species increases due to the hemi-spherical diffusion profile exhibited by microelectrodes.

7.4 Measurements of Fast Heterogeneous Kinetics by Analysing Steady-State Cycling Voltammetries and SECM

Reduction of quinone species is best described as a heterogeneous outer sphere ET mechanism [20]. For this type of process, the total rate of transformation depends on the rate constants of both the forward/reduction (k_f) and reverse/oxidation (k_b) processes. In the present section of this chapter, a comparative ET kinetic study for a series of quinones at both Au and CF ultramicroelectrodes (UMEs) is presented by measuring kinetic parameters of a quasi-reversible quinone-semiquinone transformation. The application of SECM for steady state measurements of electrode kinetics is also described for both electrode materials.

Table 7.2 is given to present the results of the kinetic parameters which were extracted from the CVs of five different compounds (0.2 mM) on a Au (25 μm) electrode in MeCN/$TBAPF_6$ medium at 25 mV s^{-1} scan rate. CVs are represented in Figure 7.5, performed in the bulk solution for voltammetric analysis. To determine the kinetic parameters at microdisk electrodes, the following parameters were calculated; $E_{3/4}$ - $E_{1/4}$ (ΔE), $E_{1/4}$ - $E_{1/2}$ ($\Delta E_{1/4}$) and $E_{1/2}$ - $E_{3/4}$ ($\Delta E_{3/4}$) where $E_{1/2}$ is the half wave potential and $E_{1/4}$ and $E_{3/4}$ are voltammetric quartile potentials. Then, the values of kinetic parameters, i.e. the transfer coefficient (α) and formal potentials ($\Delta E^{o'}$) were calculated from Table II in ref. 21 at the intersection of $\Delta E_{3/4}$ and $\Delta E_{1/4}$ values.

Compound	ΔE mV	$\Delta E_{3/4}$ mV	$\Delta E_{1/4}$ mV	α	$\Delta E^{o'}$ mV	λ	k^0 / cm s^{-1}
p-BQ	71.00	35.25	32.75	0.35±0.08	9.18±1.25	4.62±0.82	0.098±0.017
AQ	68.35	34.00	31.75	0.36±0.06	7.65±1.55	6.14± 2.66	0.106±0.045
R	69.30	38.75	33.75	0.25±0.02	7.79±0.10	5.88±0.10	0.067±0.001
E(+)	69.95	35.50	33.25	0.25±0.05	8.25±2.60	5.13±1.68	0.058±0.001
E(-)	75.15	40.00	35.00	0.26±0.06	12.30±0.75	3.60±0.32	0.041±0.003

Table 7.4 Kinetic parameters extracted from steady-state voltammetric analysis of compounds studied at an Au microdisk electrode.

In the case of micro-disk electrodes, whose surface is not uniformly accessible, the theory describing quasi-reversible steady-state voltamograms on non-uniformly accessible electrodes was implemented where standard rate constant (k^0) is represented by equation (7.1)[21];

$$K'_{1/2} = \pi d k^0 / 8 D_0 \exp[-\alpha n f \left(E_{1/2} - E_0'\right)] \qquad \textbf{(7.1)}$$

Equation (7.1) assumes Butler-Volmer kinetics of electrode reaction where

$$f = \frac{F}{RT} \qquad \textbf{(7.2)}$$

(F is Faraday's constant, R is the universal gas constant and T is the temperature) and $E_{1/2}$ is the half-wave potential of the electrode.

Standard rate constants in table 7.2 illustrate fast ET kinetics of all type of quinones studied. Values presented here seem well-correlated with some of the results reported for quinone kinetics with microelectrode systems. The observed standard rate constant for anthraquinone was found higher than other type of quinones investigated. As previously discussed, the rate of reaction increases as the charge on the anion radical becomes more delocalized.[22] This effect was demonstrated in the electroreduction of a series of quinones, in which higher standard rate constants were obtained with the increasing number of benzene rings, in the series benzoquinone < naphthoquinone < anthraquinone [23]. The greater degree of charge delocalization in the radical anions of the larger molecules results in the decreased interactions with the solvent environment which lower the activation energies for charge transfer and therefore, higher charge-transfer rate constants are expected.[7] Additionally, the calculated rate constants for the enantiomers and racemic mixture are relatively smaller than those for AQ and p-BQ. Again, compound nature and their interaction with solvent molecules might influence the ET kinetics and thereby, the rate constant.

Herein, the application of the scanning electrochemical microscope (SECM) for steady-state measurements of fast heterogeneous quinone kinetics was demonstrated. The method is practically based on the determination of the current vs potential curve for an electrode reaction through cyclic voltammetric measurements at an ultramicroelectrode (radius, *a*). For CV measurements, a Au microelectrode, 25 µm diameter, acts as a working electrode. This tip was held in close proximity (distance, *d*) to a conductive gold substrate biased at 0.0 V, which served to regenerate the quinone from the semiquinone. This technique can be used to study very fast electrode reactions and permits calculation of more accurate rate constant values due to very high mass transport rates. This technique allows the elimination of some complications in the measurements associated with solution resistance and charging current, which are usual for relaxation techniques.[24]

In order to study fast ET kinetics, the mass transfer of the electroactive material should be higher compared to the heterogeneous ET rate. Rapid steady-state mass-transfer rates can be achieved by using UMEs with sufficiently small electrode radius (*a*). Even higher mass transport rate with the UME can be obtained by using the SECM technique, so long as the tip gets in close proximity with substrate such a distance at $d < a$.

In aprotic solvents, the first reduction step of a quinonoid species (Q) is known to generate the quinone radical anion ($Q^{\bullet -}$). Figure 7.5 depicts bulk and surface CVs of each compound at 0.2 mM concentration. Analysis was done at a 25 µm diameter gold disk electrode above a flat gold substrate in acetonitrile (0.1 M $TBAPF_6$ as a supporting electrolyte), at a potential sweep rate of 25 mV s^{-1}.

a)(i)

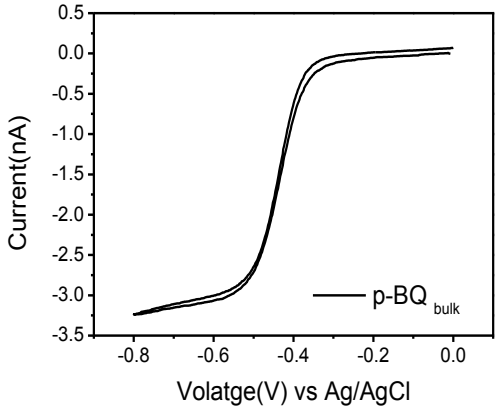

(ii)

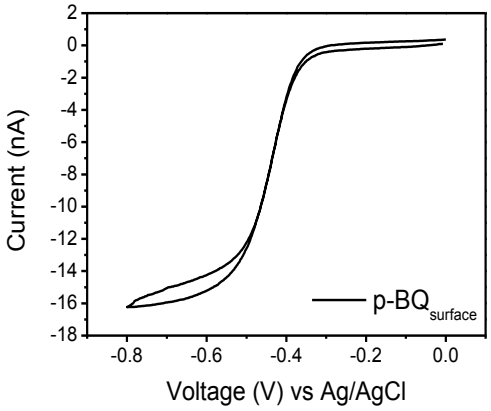

b)(i)

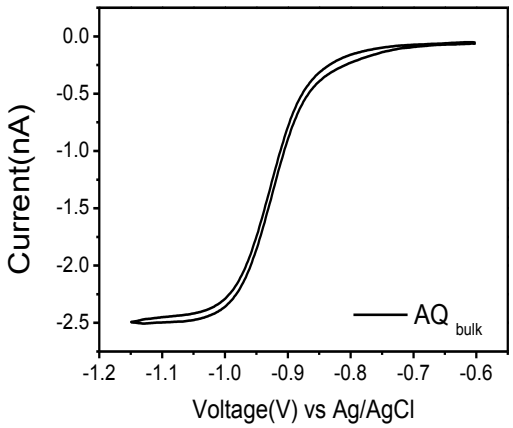

(ii)

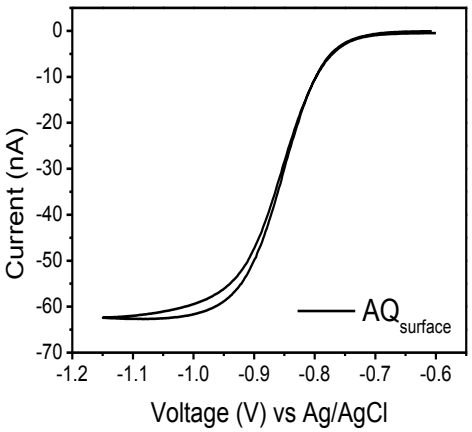

c)(i)

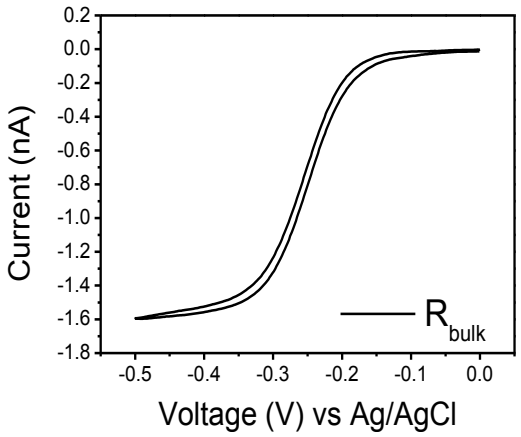

(ii)

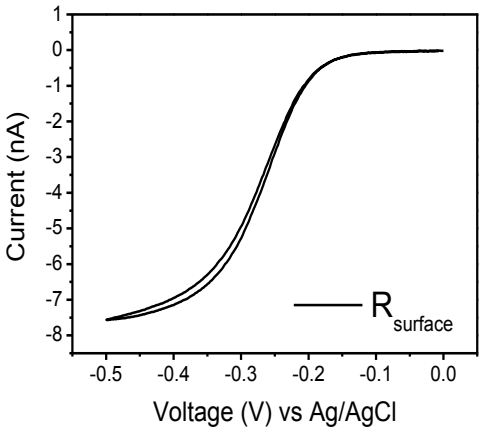

d)(i)

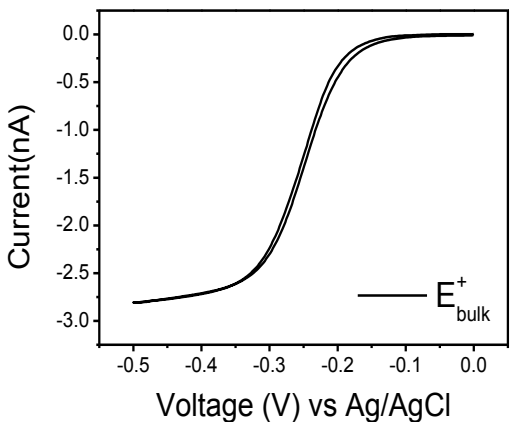

(ii)

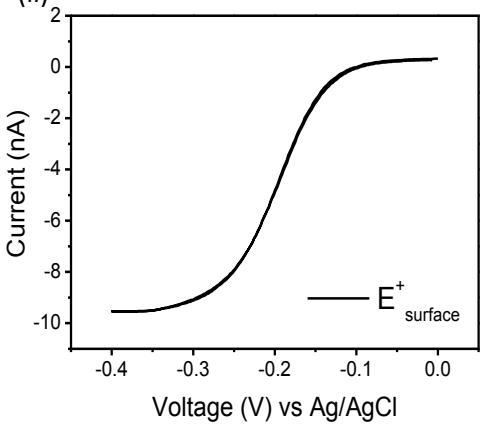

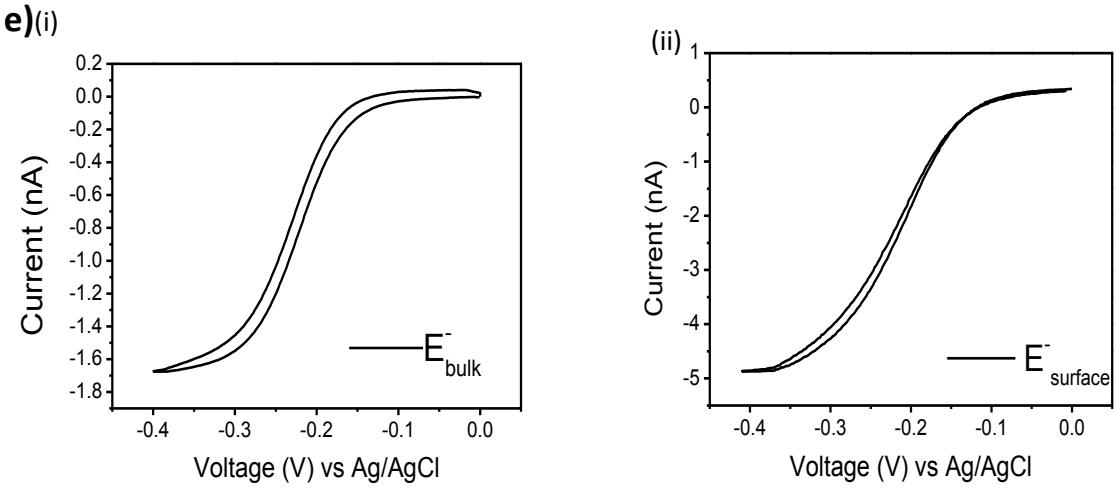

Figure 7.5 Cyclic voltammograms for the first reduction step of 0.2 mM p-BQ (a), AQ (b), R (c), E^+ (d) and E^- (e) in bulk (i) and on the substrate surface (ii) at gold microdisk electrode at a scan rate of 25 mV s^{-1}.

Cyclic voltammetries performed on the surface of the flat Au substrates were analysed in order to calculate kinetic parameters (Figure 7.5 surface CV analysis).

Substrate-tip distance was calculated from equation 7.3. Analytical approximation for diffusion controlled steady state current for a conducting substrate can be obtained from following equation;

$$I_T(L) = i_T/i_{T,\infty} = 0.78377/L + 0.3315 \exp(-1.0672/L) + 0.68 \qquad \textbf{(7.3)}$$

where L = d/a, is the normalized tip/substrate distance, and $I_T(L)$ is the normalized tip current. Based on the above equation, the tip-substrate distance was calculated, and the numerical values obtained were 11.8, 0.7, 4.0, 3.4 and 3.9 µm for p-BQ, AQ, E(+), E(-) and R, respectively.

Kinetic parameters such as $\Lambda = k^o / m_o$, α and ΔE^0 were determined from CVs at the surface, using three quartile potentials, $E_{1/2}$, $E_{1/4}$ and $E_{3/4}$.

A single table containing the above parameters for all possible pairs of $\Delta E_{1/4} = E_{1/4} - E_{l/2}$ and $\Delta E_{3/4} = E_{l/2} - E_{3/4}$ is available (see Table I in ref 21) for all parameters. Each parameter was determined from this table and represented in table 7.3.

After determination of such parameters, the effective mass transfer coefficient for SECM (m_o) was calculated from following equation;

m_o= 4Do(0.68+0.78377/L+0.3315exp(-1.0672/L))/πa =I_T(L)/πa^2nf ^oC **(7.4)**

Consequently, the standard rate constant , k^o was determined from $k^o=\lambda m_o$ *(Table 3)*[24].

Compound	ΔE mV	$\Delta E_{3/4}$ mV	$\Delta E_{1/4}$ mV	m_o cms^{-1}	α	$\Delta E^{o'}$ mV	λ	k^o cms^{-1}
p-BQ	85.00	47.50	35.00	0.065	0.27±0.03	19.85±5.85	3.63±0.32	0.23±0.02
AQ	76.10	39.50	33.00	0.320	0.41±0.02	10.75±4.80	3.98±0.45	1.26±0.46
R	83.00	51.55	35.00	0.046	0.27±0.06	11.30±6.46	4.14±0.19	0.19±0.05
E(+)	70.50	38.50	32.05	0.052	0.34±0.05	7.76±7.47	6.47±2.04	0.28±0.06
E(-)	90.00	55.00	37.50	0.046	0.23±0.06	17.05±8.53	3.06±0.28	0.12±0.06

Table 7.5 Kinetic parameters extracted from SECM steady-state voltammetric analysis of compounds studied at an Au microdisk electrode.

In accordance with the results in table 7.3, k^0 values obtained by the SECM technique were approximately 2-4 times higher than the values determined by CVs obtained in bulk solution, since the SECM technique enable much higher rates of mass transfer of active species, since the UME tip is held close to the substrate surface which is able to regenerate the quinone species. Despite careful IR compensations by using the UME, the values obtained in bulk solution cannot always guarantee the accuracy of the analysis especially when the ET kinetics are too fast. The much higher value of the rate constant for AQ (k^o= 1.26±0.46 cms^{-1}), determined by positive feedback method, which is roughly 12 times higher than the value calculated in the bulk CV analysis (k^o= 0.106±0.045 cms^{-1}). The high ET kinetics were determined due to the small distance between the tip and the substrate surface (0.7 μm). As discussed before, mass transport increases dramatically at very close substrate-tip separations. Therefore, the mass transfer coefficient (m_o) for AQ is much higher compared to the values obtained for the other compounds, which were within the range of 0.046-0.065 cms^{-1}. The main difficulty with obtaining a very small tip-substrate separation is most probably the surface blocking processes that prevents an effective approach of the UME tip to the substrate surface. This phenomenon was extensively explained at both Au and CF electrodes in section 7.3.

7.5 Non-steady-state voltammetry

Non-steady-state voltammetric analysis was performed to increase the accuracy of kinetic parameters on the CF microelectrode at relatively faster scan rates. As previously discussed, quinone adsorption is stronger on carbon-type electrodes, which blocks the surface of electrode and prevents the accurate measurements of kinetics. Thus, increasing the scan rate above the values which were used for the measurements at the Au electrode is advantageous in preventing strong electrode fouling.

Here, CVs were performed for each compound (2 mM) by increasing the potential scan rate up to 1 Vs^{-1} (Fig.7.5).

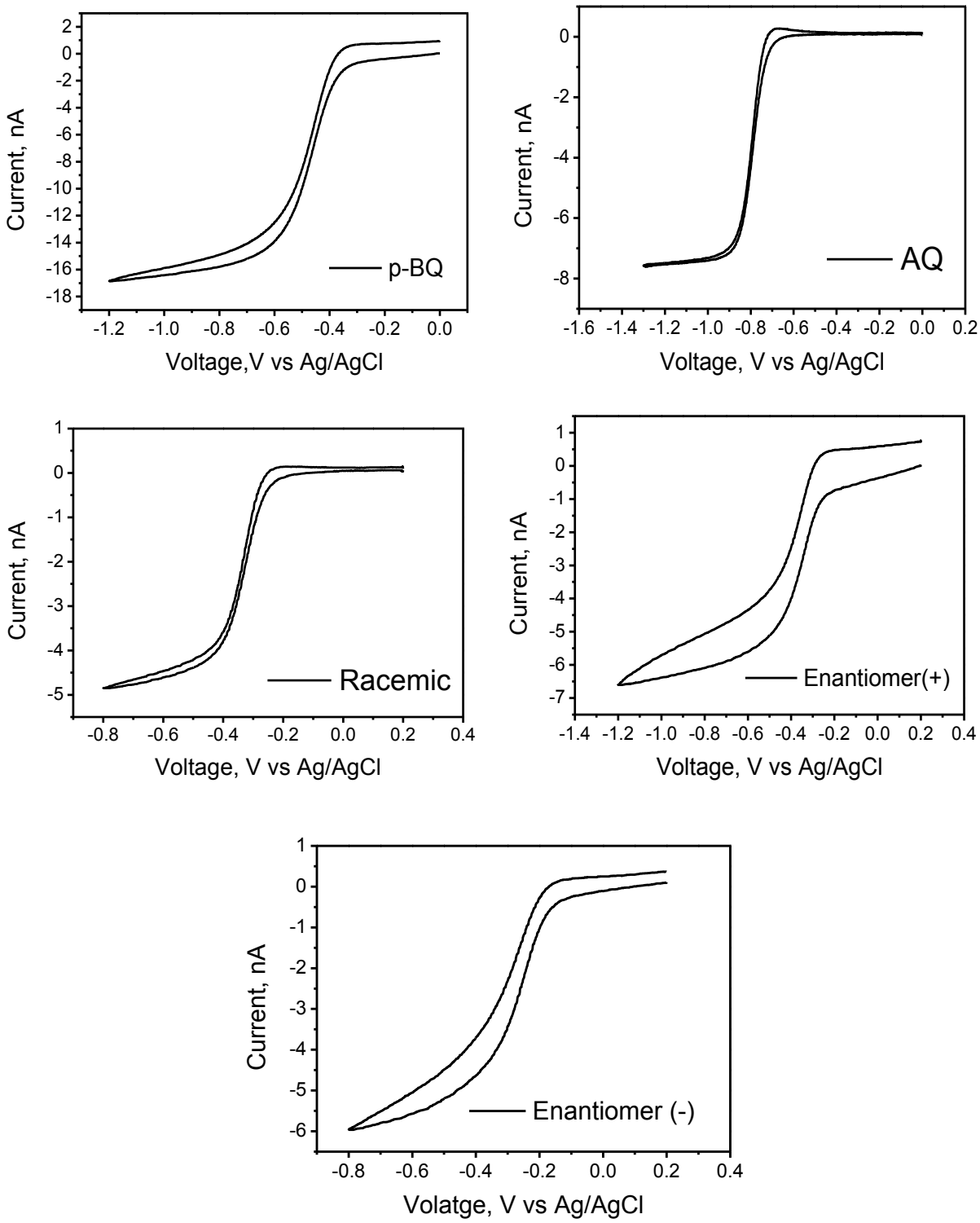

Figure 7.6 Non-steady-state CV analysis of all compounds (2 mM) studied at 1 Vs^{-1} scan rate.

Accurate analysis of the rate constant is rather complicated for this technique, since there are no redox peaks due to the employment of UME. Therefore this particular analysis requires special simulations techniques for numerical evaluation of rate constants.

It is previously demonstrated that the use of the Nicholson method [28] to analyse CVs obtained at a microdisk electrode at intermediate scan rates without accounting for non-linear diffusion leads to an underestimation of k^o. A more sophisticated analysis is necessary to reduce this difference.[29]

7.6 Adiabaticity of Quinone Reactions

Theories of ET kinetics based on macroscopic concepts simply involve parameters like α and k^0. On the other hand, such theories can no longer be effective once the structural modifications and environmental factors start to influence the rate of electrochemical processes. Therefore, Marcus-Hush theory can be considered as an appropriate microscopic approach since it involves a reorganization energy term which covers the influence of solvent dynamics and structural changes of both reactants and products on the ET mechanism (*vide supra*).

Equation (7.7) is based on a transition-state formalism of heterogeneous ET kinetics that Marcus-Hush theory explains;

$$k^0 = K_p v_n \ \kappa \exp\left(-\Delta G^* / RT\right) \qquad \textbf{(7.7)}$$

where k^0 represents the standard rate constant for the outer sphere electrode reaction, K_p is the equilibrium constant, v_n is the nuclear barrier crossing frequency, κ is the electronic transmission coefficient, and ΔG^* is the Gibbs energy of activation for the electrode reaction [20].

Marcus-Hush theory emerged as a significant contribution to the ET theory since it focuses on the effect of chemical properties of both reduced and oxidized species on ET kinetics. This approach has

been widely applied to electrochemical reactions in order to predict the influence of structural effects on kinetic properties [26].

One important contribution of the Marcus-Hush theory is that it proposed that the Gibbs free energy of activation during the ET process ($\Delta G^{\ddagger}$), is dependent on a parameter (λ) which accounts on the effects of the structural reorganization processes occurring during the ET. $\Delta G^{\ddagger}$ is given in equation (7.8),

$$\Delta G^{\ddagger} = \frac{\lambda}{4}\left(1+\frac{F\left(E-E_0\right)}{\lambda}\right)^2 \qquad \textbf{(7.8)}$$

where E is the electrode potential and E_0 is the standard electrode potential.

The reorganization energy, λ, is the energy needed for all necessary structural adjustments of the reactants and the solvent to be converted to the state of the products. The reorganization term is composed of solvational and vibrational components.

The expression for the apparent rate constant (k_{et}) is given in the standard Arrhenius relationship, in equation (7.9),

$$k_{et} = A\exp\left[-\Delta G^{\ddagger} / k_B T\right] \qquad \textbf{(7.9)}$$

where A is the pre-exponentional factor and k_B is the Boltzmann constant.

In ET theory, adiabaticity generally refers to the extent of interaction or electronic coupling between a reactant and the electrode. If this interaction is strong, which occurs when a sufficiently close distance is achieved, the transmission coefficient (κ) approaches to unity and the process is called adiabatic. If this reaction is weak, the process is said to be non-adiabatic and κ becomes smaller than unity.

A recent study by Compton *et al*.[6] demonstrates a valuable discussion by comparing the reaction kinetics of a family of quinones on CF and Au UMEs. So it is useful to discuss their finding to clarify concepts of adiabaticity of quinone reactions. ET processes on carbon electrodes were considered as non-adiabatic and the rate of ET was associated with the variation in redox potential since the density of states (DOS) was expected to vary with potential. On the other hand, electrochemical reactions on Au were assumed to be adiabatic and DOS for Au was considered as constant, which is indeed the case for adiabatic processes.

In non-adiabatic systems the rate depends strongly on the strength of the interaction. In Compton's work, the coupling strength (*V*) was considered as constant, so the rate and the DOS of the electrode were said to be directly proportional. Table 1 includes a comparison of kinetic parameters extracted from their work. Based on results presented, faster ET kinetics for quinones were confirmed for the CF electrode. Therefore, electronic coupling of quinone species to the electrode surface was reported to be greater for carbon than for gold electrodes[6].

Schmickler's short discussion[30] on adiabaticity of quinone ET on graphite electrode is highly relevant and important for the discussion presented in this chapter. Most of the outer sphere ET kinetics on metals is assumed to be adiabatic, yet there is some doubt about the likelihood of an adiabatic process on semimetals like graphite. Therefore, their work mainly argues about whether quinone electroreduction on graphite is adiabatic by re-examining the experimental data presented by Compton *et al*.[6]

Their density functional theory (DFT) calculations reveal that non-adiabatic reactions should be slower on graphite since the DOSs of graphite is smaller than the one of gold, which is contrary to what Compton reported [6]. Their reasoning for the gold case, which is truly adiabatic**,** enlightens why the overall rate constant is independent of electronic properties of the electrode material. In the adiabatic case, the energy of reorganization is much greater than the interaction constant; therefore

the overall rate depends solely on solvent dynamics. They reported all these reactions to be fast and adiabatic.

As detailed in an early study by Kojima and Bard[31], electrochemical kinetics of most aromatic compounds were assumed to be adiabatic, in which variation of the rate constant was directly related to changes in the reorganization energy. ET reactions of all quinones are fast and adiabatic on a Au electrode. In this particular case, reorganization energy and so the rate constant is governed by solvent dynamics (outer component) since neither reactants nor products change their configuration during actual ET.

Formation of an adsorption layer on the surface of carbon might highly influence the electrode-compound interaction. The electronic transmission coefficient (κ) which participates in the rate equation (equation (7.7)) is directly related to this interaction, and if this interaction weakens by an adsorption barrier, the rate constant rapidly falls off. As discussed before, if κ declines beyond unity, the reaction is no longer adiabatic.

7.7 Kinetics of Optical Isomers

Intrinsic ET kinetics were reported to be exceptionally sensitive to molecular structure [32]. Kinetic differences have been confirmed previously for structural isomers. A study of Frontana *et al*. explains the differences in ET kinetics by comparing structural isomers of p-BQ. Their findings point out the differences in the stability of the quinone radical formed during the first reduction reaction and the observed differences were associated with changes in the inner component of reorganization energy of each structural isomer [33]. On the other hand, differences in ET kinetics for optical isomers have not been demonstrated previously. Optical isomers (enantiomers) are molecules with a chiral centre and they are non-superimposable mirror images of each other [34].

In this study, we tried to answer the question whether chirality may cause differences in heterogeneous ET kinetics. The data obtained from CVs reveals some differences between

enantiomers in terms of ET rate at both the Au and CF electrode. Now the question turns to whether such differences are caused by distinct orientation of each enantiomer on carbon type electrode. As explained previously, quinone derivatives may undertake strong interactions with carbon. The strength of this interaction highly depends upon the distance of the molecule from the electrode surface and its orientation, in agreement with the fact that such chiral discrimination in the homogenous ET step was earlier demonstrated and the rate constant of such processes was found to be highly sensitive to the orientation and separation of the interacting species. Outer sphere reorganization energy was pointed out as a major determinant for such differences[35]. Variations in solvational energies should therefore be the main reason of different kinetics for optical isomers. However supplementary work might be needed to further explain this phenomenon since the stability of the electrogenerated semiquinone (radical anion) is highly influenced by these reorganization processes.

References

1. W. Choi, D. Harada, K. Oyaizu, and H. Nishide, *Journal of the American Chemical Society*, 2011, **133**, 19839–43.

2. S. Roldán, C. Blanco, M. Granda, R. Menéndez, and R. Santamaría, *Angewandte Chemie International Edition*, 2011, **50**, 1699–701.

3. D. H. Evans, *Chemical Reviews*, 2008, **108**, 2113–2144.

4. N. V Rees, A. D. Clegg, O. V Klymenko, B. A. Coles, and R. G. Compton, *Journal of Physical Chemistry, B*, 2004, 13047–13051.

5. Y. Wang, E. I. Rogers, S. R. Belding, and R. G. Compton, *Journal of Electroanalytical Chemistry*, 2010, **648**, 134–142.

6. R. Nissim, C. Batchelor-McAuley, M. C. Henstridge, and R. G. Compton, *Chemical Communications*, 2012, **48**, 3294–3296.

7. R. Samuelsson and M. Sharp, *Electrochimica Acta*, 1978, **23**, 315–317.

8. C. Russel and W. Jaenicke, *Journal of Electroanalytical Chemistry*, 1986, **200**, 249–260.

9. A. Capon and R. Parsons, *Electroanalytical Chemistry and Interfacial Electrochemistry*, 1973, **46**, 215–222.

10. D. H. E. Thomas W. Rosanske, *Journal of Electroanalytical Chemistry*, 1975, **72**, 277–285.

11. B. Uslu and S. a Ozkan, *Combinatorial Chemistry & High Throughput Screening*, 2007, **10**, 495–513.

12. O. Bard, A.J. , Fan, F.R.F , Kwak, J. , Lev, *Analytical Chemistry*, 1989, **61**, 132.

13. S. C. S. Lai, J. V. Macpherson, and P. R. Unwin, *MRS Bulletin*, 2012, **37**, 668–674.

14. K. M. Kelvey, M. A. Edwards, and P. R. Unwin, *Letters to Analytical Chemistry*, 2010, **82**, 6334–6337.

15. C.-A. McGeouch, M. Peruffo, M. a. Edwards, L. a. Bindley, R. a. Lazenby, M. M. Mbogoro, K. McKelvey, and P. R. Unwin, *The Journal of Physical Chemistry C*, 2012, **116**, 14892–14899.

16. M. V. Mirkin and B. R. Horrocks, *Analytica Chimica Acta*, 2000, **406**, 119–146.

17. R. M. Robinson, D. L.; Wightman, *In Electrochemical Methods for Neuroscience; Michael, A. C., Borland, L. M.Robinson, D. L.; Wightman, R. M. 2007;pp 17-36*.

18. C. Batchelor-McAuley, L. M. Gonçalves, L. Xiong, A. a Barros, and R. G. Compton, *Chemical Communications*, 2010, **46**, 9037–9.

19. C. Ehli, G. M. A. Rahman, N. Jux, D. Balbinot, D. M. Guldi, F. Paolucci, M. Marcaccio, D. Paolucci, M. Melle-Franco, F. Zerbetto, S. Campidelli, and M. Prato, *Journal of the American Chemical Society*, 2006, **128**, 11222–31.

20. J. K. Hubig, Stephan M.; Kochi, *Journal of American Chemical Society*, 1999, **121**, 1688–1694.

21. M. V Mirkin and A. J. Bard, *Analytical Chemistry*, 1992, **18**, 2293–2302.

22. W. R. Fawcett and M. Opallo, *Angewandte Chemie*, 1994, **33**, 2131–2143.

23. R. M. W. Howell, *Analytical Chemistry*, 1984, **56**, 524.

24. M. V Mirkin, T. C. Richards, and A. J. Bard, *Journal of Physical Chemistry*, 1993, **97**, 7672–7677.

25. R. S. Nicholson, *Analytical Chemistry*, 2002, **37**, 1351–1355.

26. A. J. Bard, L. R. Faulkner, E. Swain, and C. Robey, *Electrocehmical Methods:Fundamentals and Applications*, John Wiley & Sons, United States, 2nd edn.

27. S. W. Feldberg, *Analytical Chemistry*, 2010, **82**, 5176–83.

28. R. S. Nicholson, *Analytical Chemistry*, 2002, **37**, 1351–1355.

29. I. Lavagnini, P. Pastore, and F. Magno, *Journal of Electroanalytical Chemistry*, 1992, **333**, 1–10.

30. N. B. Luque and W. Schmickler, *Electrochimica Acta*, 2013, **88**, 892–894.

31. Hiroyuki Kojima and Allen J. Bard, *Journal of American Chemical Society*, 1975, **97**, 6317–6324.

32. S. F. Nelsen, M. N. Weaver, Y. Luo, J. R. Pladziewicz, L. K. Ausman, T. L. Jentzsch, and J. J. O'Konek, *Journal of Physical Chemistry. A*, 2006, **110**, 11665–76.

33. C. Frontana and I. González, *Jounal of the Mexican Chemical Society*, 2008, **52**, 11–18.

34. V. Duyne, *Nature*, 2003, **425**, 3–6.

35. B. Pispisa, A. Palleschi, M. Barteri, and S. Nardini, *Journal of Physical Chemistry*, 1985, **89**, 1767–1775.

CHAPTER 8: Conclusions and Future Perspectives

The main objective of this doctoral study was to propose alternative redox materials and novel strategies for the integration of such redox compounds into electrochemical storage devices such as supercapacitors (SC) and redox flow batteries (RFBs). Research results presented here include physical, structural and electrochemical characterization methods to evaluate the resultant compound as the electrode or electrolyte active material.

Particular attention has been drawn to highly reversible quinone redox system in many fields. Their application areas have been recently broaden to different fields such as energy storage systems due to their attractive redox properties, low cost, variety, ease of accessibility and low toxicity. Therefore, in this doctoral work, our research efforts have been focused on the integration of quinone based active materials as electrode materials for SCs and electrolyte redox couples for RFBs, together with a detailed kinetic analysis of their electron transfer reactions. In the following parts, a detailed summary of the conclusions and future perspective of our approach will be given.

8.1 General Conclusions

8.1.1 Supercapacitors

A physical adsorption technique and a covalent strategy were successfully established in order to fabricate composite carbon-quinone electrode materials for the SCs applications.

As the first approach, anthracenetetraone (AT) and p-benzoquinone (p-BQ) were physically impregnated on the surface of different carbon electrodes. Adsorption of AT molecules on high surface area Pica carbon (0.75 wt.% loading) and low surface area Vulcan carbon (0.55wt.% loading) electrodes were achieved. The influence of the substrate type on the electrochemical properties of AT and accordingly, on the electrochemical performance of SC device was successfully analysed.

By means of AT modification, a substantial improvement of the specific capacitance was reported for both Pica (40%) and Vulcan (80%) modified electrodes based on 3-electrode cyclic voltammetry (CV)

measurements at slow scans. Consecutive charge-discharge analysis was performed to test the stability of grafting. Capacity fades were of 10% and 40% for modified Pica and Vulcan carbon respectively after 1000 cycles at 200 mAg^{-1} which are much higher compared to a 3% (Pica) and 7% (Vulcan) loss of unmodified carbons in the same conditions. These findings were explained by means of structural differences of the carbon substrates. A stable grafting was detected for Pica carbon, whereas Vulcan carbon gives rise to unstable grafting due to its mesoporous structure and non-functionalized surface.

In a parallel study, Pica activated carbon electrodes were modified with p-BQ by the adsorption technique likewise in the previous case. In this case, p-BQ loading was achieved up to 55 wt.% or higher according to p-BQ high solubility in impregnation media(1.5 M). However, at very high loadings levels, lower specific capacity was reported due to the resistive nature of adsorbed p-BQ. The maximum capacitance (350 Fg^{-1} at 10 mVs^{-1}) was accomplished for an optimum loading of 30 wt.% of active material.

Cycling test verified very highly stable electrodes modified with adsorbed p-BQ moieties: after 5000 consecutive cycles at 2 Ag^{-1}, a loss of only 6.5% of total capacity for modified Pica was determined, which is actually very close to the reported values for unmodified Pica carbon electrodes.

Briefly, physical adsorption of quinone species can be used as a promising approach to greatly increase the energy densities of supercapacitor electrodes. This strategy offers very attractive advantages such as simplicity and low cost over other covalent modification techniques. However, low power density at high current loadings remains as a problematic issue to resolve which led us to study a covalent grafting approach.

Our second approach for modification of carbon substrate is the direct covalent attachment of quinone species to the carbon structure which we successfully demonstrated via Friedel-Crafts reaction. This highly effective C-C bond-forming electrophilic aromatic substitution reaction has

taken place between the aromatic rings of Pica carbon and benzoquinone which acts as the electrophile, in the presence of catalyst. This reaction leads to direct attachment of hydroquinone fragments into the Pica carbon through a 1,4-addition/enolization process, occurring at the conjugated benzoquinone system. Followed to the first reaction step, oxidation of hydroquinone to p-BQ was performed. Characterization techniques including FTIR and Solid State NMR spectroscopies effectively confirmed the covalent bond formation between carbon particles and p-BQ units with some amount of non-oxidized hydroquinone species. Quantification of these grafted species was done by thermogravimetric analysis (TGA) coupled to mass spectroscopy and the total amount of grafted molecules was calculated as 7.72wt.% from TGA. This data was combined with the mass fraction analysis of CO_2, and 6.57 wt.% of p-BQ was approximated as the grafted amount, which is 85% of the total weight loss in TGA. Physico-chemical properties of modified and unmodified carbons were compared by BET and DFT surface area analysis. The most striking finding regarding this grafting technique is the anomalous increase of the micropore volume and surface ratio to total volume or surface despite an overall decrease in pore volume and surface. Micro-pore size reduced from 1.4 nm to 0.86 nm homogenously after grafting.

Electrochemical characterization points out a substantial increase in specific capacitance with respect to unmodified electrodes. This important increment in gravimetric capacitance, which is maintained even after many cycles, is not only due to the redox reactions of p-BQ, but also arises from an increased double layer capacitance after p-BQ modification. A correlation between the pore size distribution and the BET surface area shows that the increased double layer capacitance comes from a better matching of newly created carbon pore size with the size of electrolyte ions (the size of SO_4^{2-} ions). The amount of p-BQ grafted was also quantified from the area of CV curves, where a total mass of 4.16% is associated with redox active units, coming from both the added p-BQ and unoxidized hydroquinone. The difference between the values calculated by TGA and CV represents the electrochemically inactive amounts due to the limited electrolyte access within sub-nanometer sized pores.

This novel strategy, which also preserves the power density and cycling life of unmodified carbon, can serve as an alternative strategy for the grafting of quinones on carbon particles for high energy SCs electrodes, combining pseudocapacitive reactions and increased double layer capacitance due to ion-pore size matching.

8.1.2 Redox Flow Batteries

In this doctoral study, the use of quinones is also presented as electrolyte active materials for aqueous RFB applications.

Since very high soluble concentration of redox species are required for high energy density RFB, and low cost, availability and less environmental impact are the critical requirements to meet from a practical point of view, quinones are potentially interesting redox couples in this respect.

Quinone species were studied in terms of their key electrochemical properties and water solubility. It is proved that these important features can be modified by simple modification techniques. Quinones are generally partially soluble or non-soluble in aqueous media. In this sense, we try to compare the water solubility of simple quinones such as tetrahydroxy-1,4-benzoquinone (THBQ) and Chloroanilic acid (CAA) and try to explain the importance of functionality of the compound. THBQ demonstrated an important degree of water solubility, especially when the solution pH increases, however electrochemical properties are not proper due to the strong electron donating nature of the OH substituents. That explains why replacing two of the OH groups with electron withdrawing units, such as Cl in CAA case, enhances electrochemical response. However, it is concluded that the water solubility decreases by decreasing the number of –OH substituents.

Previous preliminary results led us to study the polyhydroxylated quinones as water soluble redox species. The novel organic synthesis technique proposed for the enhancement of water solubility is the covalent attachment of polyhydroxylated compounds to the quinonoid structures. The target molecule was successfully synthesized through the polyhdroxylation of Juglone molecule. Juglone

molecule was determined as the base quinone compound due to reversible kinetics which was attributed to the position of the –OH substituent. Modified juglone showed 200-fold better water solubility with respect to unmodified one. Water solubility of functionalized quinones was highly affected by both quinonoid base and the type of polyhydroxylated unit. Another important outcome regarding final molecule was its electrochemical features, which were conserved as good as juglone molecule after polyhydroxylation. This strategy was further extended to the selection of natural quinones whose characteristics were pretty much similar to the synthesized model compound.

8.1.3 Kinetic Studies

Kinetic properties of redox species have a direct influence on the electrochemical performance of both SC and RFBs. Quinone electron transfer reaction was successfully studied in an aprotic media since this media permits calculation of a single-step electron transfer (ET) kinetics of quinones due to the stabilization of the radicalic intermediates. Experiments were performed for a family of quinones at gold (Au) and carbon fibre(CF) ultramicro-electrodes (UMEs).

Electrode surface fouling was confirmed for the first time in an aprotic media for almost all compounds. Different degrees of surface fouling were observed depending both on the electrode material and the compound studied. Fouling issue was minimized on Au electrode surface by simple modification of reaction conditions. However, surface blocking processes could not be eliminated for CF material due to strong quinone-carbon interaction.

Steady-state analysis for the selected quinones and organically synthesized enantiomeric couples are studied at Au electrode for semiquinone formation. Rate constants calculated via steady state CVs are well correlated with some of the literature results. The observed standard rate constant for anthraquinone was found higher than other type of quinones investigated regarding the more delocalized charge on this conjugated system.

Scanning electrochemical microscopy (SECM) technique was successfully employed for Au UME on flat gold substrate. Higher rate constants were reported by implementation of SECM technique comparing to steady-state analysis due to higher mass transport rates.

Non-steady-state CV analysis was performed for kinetic studies of compounds at CF micro-electrode. However, numerical evaluation of rate constant requires a special simulation technique for this approach.

Kinetic data obtained from different methods reveals some differences between enantiomers in terms of ET rate at both Au and CF electrode. These differences were attributed to the distinct orientation of each enantiomer on the electrode surface.

8.2 Future Perspectives

Further studies investigating detailed quinone-carbon interaction may give additional strength to the non-covalent physical impregnation technique and performance evaluation of SC device. Also, different organic and electrochemical grafting strategies can be proposed for carbon modification with quinones for applications in SCs. Pore size and ion size matching studies can be extended by using other types of electrolytes such as organic electrolytes and ionic liquids. Finally, the methods presented in this thesis including non-covalent and covalent strategies for the modified carbon can be extended to the use of other type of multi-electron transfer redox species.

Preliminary results reported for RFBs provide useful method to design a model compound. This information, together with the information on the influence of the molecular structure on the electron transfer kinetics, can be applied for the selection and preparation of environmentally friendly, cheap and abundant materials such as natural compounds for aqueous organic RFB applications. Finally, electron transfer kinetic studies can also be of use for the optimization of other quinone-based electrochemical energy storage devices, such as SCs and RFBs.